Comparison Between Gradients and Parcellations for Functional Connectivity Prediction of Behavior

Ru Kong[1,2,3,4], Yan Rui Tan[2], Naren Wulan[1,2,3,4], Leon Qi Rong Ooi[1,2,3,4], Seyedeh-Rezvan Farahibozorg[5], Samuel Harrison[5], Janine D. Bijsterbosch[6], Boris C. Bernhardt[7], Simon Eickhoff[8,9], B.T. Thomas Yeo[1,2,3,4,10]

[1]Centre for Sleep and Cognition (CSC) & Centre for Translational Magnetic Resonance Research (TMR), Yong Loo Lin School of Medicine, National University of Singapore, Singapore [2]Department of Electrical and Computer Engineering, National University of Singapore, Singapore [3]N.1 Institute for Health and Institute for Digital Medicine (WisDM), National University of Singapore, Singapore [4]Integrative Sciences and Engineering Programme (ISEP), National University of Singapore, Singapore [5]Wellcome Centre for Integrative Neuroimaging, FMRIB, Nuffield Department of Clinical Neurosciences, University of Oxford, Oxford, United Kingdom [6]Department of Radiology, Washington University School of Medicine, St Louis, MO, USA [7]McConnell Brain Imaging Centre, Montreal Neurological Institute and Hospital, McGill University, Montreal, QC, Canada [8]Institute for Systems Neuroscience, Medical Faculty, Heinrich-Heine University Düsseldorf, Düsseldorf, Germany [9]Institute of Neuroscience and Medicine, Brain & Behaviour (INM-7), Research Center Jülich, Jülich, Germany [10]Martinos Center for Biomedical Imaging, Massachusetts General Hospital, Charlestown, MA, USA

Address correspondence to:

B.T. Thomas Yeo

CSC, TMR, ECE, N.1 & WisDM

National University of Singapore

Email: thomas.yeo@nus.edu.sg

Abstract

Resting-state functional connectivity (RSFC) has been widely used to predict behavioral measures. To predict behavioral measures, there are different approaches for representing RSFC with parcellations and gradients being the two most popular approaches. There is limited comparison between parcellation and gradient approaches in the literature. Here, we compared different parcellation and gradient approaches for RSFC-based prediction of a broad range of behavioral measures in the Human Connectome Project (HCP) and Adolescent Brain Cognitive Development (ABCD) datasets. Among the parcellation approaches, we considered group-average "hard" parcellations (Schaefer et al., 2018), individual-specific "hard" parcellations (Kong et al., 2021a), and an individual-specific "soft" parcellation (spatial independent component analysis with dual regression; Beckmann et al., 2009). For gradient approaches, we considered the well-known principal gradients derived from diffusion embedding (Margulies et al., 2016), and the local gradient approach that detects local changes in RSFC across the cortex (Laumann et al., 2015). Across two regression algorithms (linear ridge regression and kernel ridge regression), we found that individual-specific hard-parcellation performed the best in the HCP dataset, while the principal gradients, spatial independent component analysis and group-average "hard" parcellations exhibited similar performance. On the other hand, principal gradients and all parcellation approaches performed similarly in the ABCD dataset. Across both datasets, local gradients performed the worst. Finally, we found that the principal gradient approach required at least 40 to 60 gradients in order to perform as well as parcellation approaches. While most principal gradient studies utilize a single gradient, our results suggest that incorporating higher order gradients could provide significant behaviorally relevant information.

Introduction

Resting-state functional connectivity (RSFC) reflects the synchrony of fMRI signals between brain regions, while a subject is lying at rest without performing any explicit task (Biswal et al., 1995; Greicius et al., 2003; Fox and Raichle, 2007). There is significant interest in using RSFC for predicting individual differences in behavior (Hampson et al., 2006; van den Heuvel et al., 2009; Finn et al., 2015; Smith et al., 2015; Dubois et al., 2018a). To predict behavioral measures, there are different approaches for representing RSFC data (Bijsterbosch et al., 2020) with the two most popular approaches being parcellations (Smith et al., 2009; Power et al., 2011; Yeo et al., 2011; Glasser et al., 2016) and gradients (Cohen et al., 2008; Margulies et al., 2016; Haak et al., 2018; Tian et al., 2020). Since different parcellation and gradient approaches might capture different aspects of brain organization, we compared different parcellation and gradient approaches for RSFC-based behavioral prediction.

Example parcellation approaches include hard-parcellation approaches that estimate non-overlapping regions of interest (ROIs) (Shen et al., 2013; Glasser et al., 2016; Schaefer et al., 2018), and soft-parcellation approaches that estimate overlapping ROIs (Calhoun et al., 2001; Beckmann et al., 2005; Smith et al., 2009; Zuo et al., 2010; Lee et al., 2012; Harrison et al., 2015; Farahibozorg et al., 2021). Most studies have utilized RSFC from population-average brain parcellations to predict behavior measures. Recent studies have shown that individual-specific parcellation topography is behaviorally relevant (Bijsterbosch et al., 2018; Kong et al., 2019; Cui et al., 2020). Functional connectivity derived from individual-specific parcellations could further improve the prediction performance compared with population-average parcellations (Li et al., 2019b; Farahibozorg et al., 2021; Kong et al., 2021a).

Besides parcellation approaches, many studies have also utilized gradient techniques to characterize brain organization(Huntenburg et al., 2018; Bernhardt et al., 2022). For example, the local gradient approach detects local changes (i.e., gradients) in RSFC across the cortex (Cohen et al., 2008; Wig et al., 2014; Laumann et al., 2015; Gordon et al., 2016). On the other hand, gradients have also been derived using manifold learning algorithms, such as diffusion embedding (also referred to as principal gradients; Margulies et al., 2016), principal component analysis (PCA; Hong et al. 2020) and Laplacian eigenmaps (LE) (Haak et al., 2018; Tian et al., 2020).

There have been previous comparisons of various parcellations approaches for predicting behavioral measures (Dadi et al., 2019; Pervaiz et al., 2020; Farahibozorg et al., 2021). These studies typically found that soft parcellations (e.g., ICA dual regression) performed better than group-level hard parcellations. However, these studies did not consider the use of individual-specific hard parcellation approaches (e.g., Kong et al., 2021). Furthermore, these studies found that RSFC computed using full correlation (Pearson's correlation) performed worse than partial correlation. Given the increased popularity of gradient approaches, there is a need to compare prediction performance between parcellation and gradient approaches.

One recent study has suggested that RSFC gradients (based on PCA, diffusion embedding and Laplacian eigenmaps) resulted in better prediction performance than parcellation-based RSFC (Hong et al., 2020). However, prediction with parcellation-based RSFC was performed using connectome predictive modeling (Shen et al., 2017), while prediction with gradient approaches was performed using canonical correlation analysis (Smith et al., 2015), so it is somewhat challenging to directly compare the two results were actually not comparable. Furthermore, their prediction analyses were performed only in the Human Connectome Project (HCP) dataset, which is one of the most widely used dataset for investigating individual differences in behaviors. Repeated reuse of the same dataset by multiple researchers can lead to inflated error rates (Thompson et al., 2020). Additionally, repeatedly using the same dataset for training and testing yield less generalizable models to new datasets (Recht et al., 2019; Beyer et al., 2020). This emphasizes the importance of replicating analyses using less commonly used datasets.

In this study, we compared different parcellation and gradient approaches for RSFC prediction of behavioral measures across a wide range of behavioral measures in two different datasets using two different prediction models. We considered a group-level hard-parcellation approach (Schaefer et al., 2018), an individual-specific hard-parcellation approach (Kong et al., 2021a), an individual-specific soft-parcellation approach based on ICA dual regression (Calhoun et al., 2001; Beckmann et al., 2005; Smith et al., 2009; Zuo et al., 2010; Nickerson et al., 2017), the principal gradients (Margulies et al., 2016), and the local gradient approach (Wig et al., 2014; Laumann et al., 2015; Gordon et al., 2016). Furthermore, we considered different resolutions (i.e., number of ROIs or gradients) for each approach. To compare the prediction performance across different approaches, the resolution was optimized as a hyperparameter in the prediction

model. In a separate analysis, we investigated prediction performance as a function of the number of ROIs or gradients.

Methods

Datasets

We considered two publicly available datasets: the Human Connectome Project (HCP) S1200 release (Van Essen et al., 2012a; Smith et al., 2013) and the Adolescent Brain Cognitive Development (ABCD) 2.0.1 release. Both datasets contained structural MRI, resting-state fMRI (rs-fMRI), and multiple behavioral measures for each subject. After strict pre-processing quality control of the HCP and ABCD datasets based on our previous studies (Li et al., 2019a; Kong et al., 2021a; Chen et al., 2022), we considered participants with all four rs-fMRI scans remaining as well as all behavioral scores of interest. Our main analysis comprised 746 participants from HCP and 1476 participants from ABCD.

Preprocessing

Details of the HCP preprocessing can be found elsewhere (Van Essen et al., 2012a; Glasser et al., 2013; Smith et al., 2013). The HCP rs-fMRI data has been projected to the fs_LR32k space (Van Essen et al., 2012b), denoised with ICA-FIX (Griffanti et al., 2014; Salimi-Khorshidi et al., 2014) and aligned with MSMAll (Robinson et al., 2014). Consistent with our previous studies (Li et al., 2019a; He et al., 2020), we further applied global signal regression (GSR) and censoring to eliminate global and head motion related artifacts. More details of the processing can be found elsewhere (Li et al., 2019a). Runs with more than 50% censored frames were removed. Participants with all four rs-fMRI runs remaining (N = 835) were considered.

Details of the ABCD preprocessing can be found elsewhere (Casey et al., 2018; Hagler et al., 2019). We utilized the minimally preprocessed functional data with additional processing steps including T1-T2* registration, respiratory pseudomotion motion filtering, nuisance regression, censoring and bandpass filtering. Nuisance regressors comprised global signal, ventricular signal, white matter signal, and six motion parameters, as well as their temporal derivatives. The data was then projected to the FreeSurfer fsaverage6 surface space and smoothed using a 6 mm full-width half maximum kernel. More details of the processing can be found elsewhere (Chen et al., 2022). Of the 2264 unrelated participants considered in our previous study (Chen et al., 2022), 1476 subjects had four runs of rs-fMRI data.

Functional connectivity features for behavioral prediction

Here, we compared functional connectivity behavioral prediction across different parcellation and gradient approaches, including a group-level hard-parcellation approach (Schaefer et al., 2018), an individual-specific hard-parcellation approach (Kong et al., 2021a), a individual-specific soft-parcellation approach (Calhoun et al., 2001; Beckmann et al., 2005; Smith et al., 2009; Zuo et al., 2010; Nickerson et al., 2017), the principal gradient (Margulies et al., 2016), and the local gradient (Wig et al., 2014; Laumann et al., 2015; Gordon et al., 2016).

The different parcellation and gradient approaches were applied to each participant from the HCP and ABCD datasets using all rs-fMRI scans. We then estimated the functional connectivity features for each participant based on the derived parcellations and gradients (Figure 1):

1. *Group-level hard-parcellation Schaefer2018*. Group-level hard-parcellations are estimated by averaging or concatenating data across many individuals, where each vertex is assigned to one region of interest (ROI). In our previous work, we developed a set of high-quality group-level hard-parcellations of the cerebral cortex with multiple resolutions from 100 to 1000 ROIs (Schaefer et al., 2018), which we will refer to as "Schaefer2018". For each parcellation resolution, the Schaefer2018 parcellation was applied to all rs-fMRI scans of each participant to generate a resting-state functional connectivity (RSFC) matrix. The RSFC matrix was generated by Tikhonov-regularized partial correlation using nets_netmats.m from FSLNets (Smith et al., 2011; Pervaiz et al., 2020). The lower triangular portion of each RSFC matrix was vectorized for each participant to serve as the individual functional connectivity features (Figure 1 top row).

2. *Individual-specific hard-parcellation Kong2021*. Individual-specific hard-parcellations are estimated for each participant, where each vertex is only assigned to one ROI. We have previously developed a multi-session hierarchical Bayesian model (MS-HBM) of individual-specific hard-parcellation that accounted for both between-subject and within-subject variability (Kong et al., 2021a), which we will refer to as "Kong2021". For each participant, we generated individual-specific Kong2021 parcellations with 100 to 1000 ROIs using all rs-fMRI scans. For each parcellation resolution, the Kong2021 parcellation was applied to all rs-fMRI scans of each

participant to generate a RSFC matrix. The RSFC matrix was generated by Tikhonov-regularized partial correlation using nets_netmats.m from FSLNets (Smith et al., 2011; Pervaiz et al., 2020). The lower triangular portion of each RSFC matrix was vectorized for each participant to serve as the individual functional connectivity features (Figure 1 second row).

3. *Individual-specific soft-parcellation sICA*. Individual-specific soft-parcellations are estimated in the cerebral cortex of each participant, where each vertex could be involved in multiple ROIs. Spatial independent component analysis (ICA) is one of the most popular soft-parcellation approaches (Calhoun et al., 2001; Beckmann et al., 2005; Smith et al., 2009; Zuo et al., 2010; Nickerson et al., 2017). The individual-specific soft-parcellations could be estimated by spatial ICA followed by dual regression (Beckmann et al., 2009; Nickerson et al., 2017), which we will refer to as "sICA". For each HCP and ABCD participant, we obtained the individual-specific sICA parcellations with 50, 100, 200, 300 components using all rs-fMRI scans. For each resolution and each participant, the RSFC matrix was generated by Tikhonov-regularized partial correlation using nets_netmats.m from FSLNets (Smith et al., 2011; Pervaiz et al., 2020). The lower triangular part of each RSFC matrix was vectorized for each participant to serve as the individual functional connectivity features (Figure 1 third row).

4. *Principal gradients (PrincipalGrad)*. Resting-state functional connectivity can be decomposed into multiple principal gradients using dimension reduction techniques, such as the non-linear diffusion embedding (Margulies et al., 2016), which we will refer to as "PrincipalGrad". We first generated group-level principal gradients for the HCP and ABCD datasets separately using rs-fMRI scans of all participants (Margulies et al., 2016). For each dataset, we then generated the principal gradients separately for each participant using all rs-fMRI scans of this participant. The Procrustes alignment was used to align individual principal gradient maps to the group-level principal gradients (Hong et al., 2020; Vos de Wael et al., 2020). We considered different number of principal gradients. The top 1, 5, 10, 20, 40, 60, 80 or 100 principal gradients were concatenated as the individual functional connectivity features (Figure 1 fourth row).

5. *Local gradient (LocalGrad)*. The local gradient approach detects local abrupt changes in resting-state functional connectivity across the cortex (Cohen et al., 2008; Wig et al., 2014;

Laumann et al., 2015; Gordon et al., 2016), which we will refer to as "LocalGrad". For each participant in the HCP and ABCD datasets, we estimated the local gradient map using all rs-fMRI scans (Laumann et al., 2015; Gordon et al., 2016). Unlike the principal gradient approach (Margulies et al., 2016), the local gradient approach has a single gradient map, which was used as the individual functional connectivity features (Figure 1 last row).

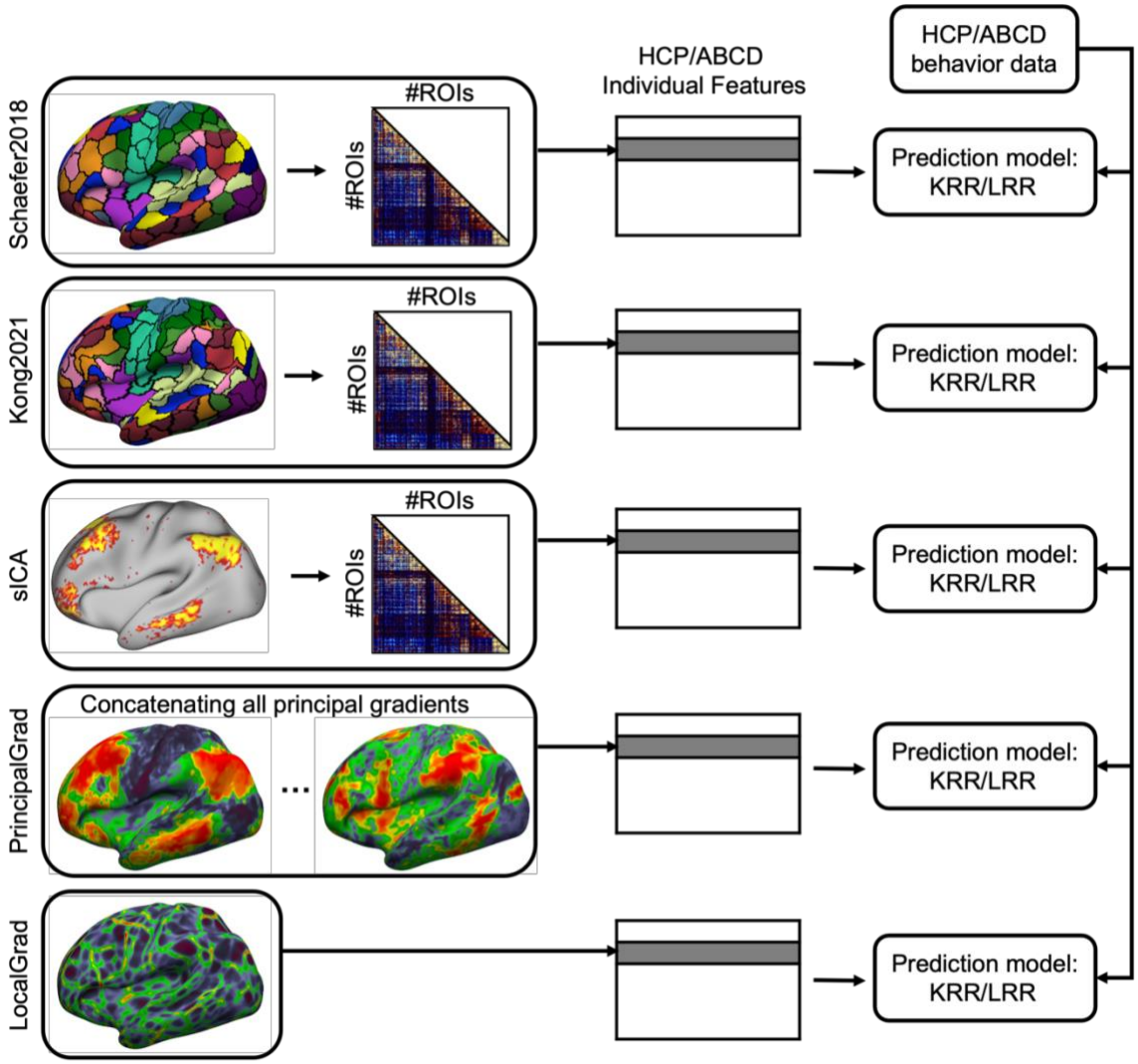

Figure 1. Flowchart across different parcellation and gradient approaches for RSFC-based behavioral prediction. For three parcellation approaches Schaefer2018, Kong2021 and sICA, the lower triangular part of the RSFC matrix was vectorized for each participant to serve as the individual-level RSFC features. For the principal gradient approach PrincipalGrad, the principal gradients for each participant were concatenated together to serve as the individual-level RSFC features. For the local gradient approach LocalGrad, the local gradient map was used as the individual-level RSFC features. For each approach, we performed behavioral prediction for HCP and ABCD datasets separately using two different prediction models KRR and LRR.

Behavioral data

Consistent with our previous work, we considered 58 behavioral measures from the HCP dataset (Kong et al., 2019; Li et al., 2019a; Kong et al., 2021a), and 36 behavioral measures from the ABCD dataset (Chen et al., 2022). We also included three behavioral components derived by a factor analysis from our previous work (Ooi et al., 2022). These three components for HCP dataset were interpreted to be related to cognition, life dissatisfaction, and emotional recognition, which we will refer to as "cognition", "dissatisfaction", and "emotion". These three components for ABCD dataset were interpreted to be related to cognition, mental health, and personality, which we will refer to as "cognition", "mental", and "personality".

Of the 835 HCP participants with 4 runs, only 746 have all 58 behavioral measures, who were used in the current study. Of the 1476 ABCD participants with 4 runs, all have the 36 behavioral measures, who were used in the current study.

RSFC-Based Behavioral Prediction

Consistent with our previous work (Kong et al., 2019; Li et al., 2019a; He et al., 2020; Kong et al., 2021a), kernel ridge regression (KRR) was used to predict behavioral measures in our main analysis. Given parcellations and gradients derived from different approaches (Schaefer2018, Kong2021, sICA, PrincipalGrad, LocalGrad), KRR performs predictions based on the similarity between functional connectivity features. Suppose y is the behavioral measure (e.g., fluid intelligence) and FC is the functional connectivity features of a test participant. In addition, suppose y_i is the behavioral measure (e.g., fluid intelligence) and FC_i is the individual-specific functional connectivity matrix of the i-th training participant. Then kernel regression would predict the behavior of the test participant as the weighted average of the behavioral measures of the training participants: $y \approx \sum_{i \in \text{training set}} \text{Similarity}(\mathrm{FC}_i, \mathrm{FC}) y_i$. Here, $\text{Similarity}(\mathrm{FC}_i, \mathrm{FC})$ is the Pearson's correlation between the functional connectivity features of the i-th training participant and the test participant. A L2-regularization term was used in the model to reduce overfitting.

To compare the prediction performance across different parcellation and gradient approaches, we treated the resolution (i.e., number of parcels or gradients) as a hyperparameter

for approaches with multiple resolutions (i.e. Schaefer2018, Kong2021, sICA, and PrincipalGrad). This hyperparameter is estimated via a nested cross-validation procedure (see below). As a separate analysis, we also compared the prediction performance across different resolutions for Schaefer2018, Kong2021, sICA, and PrincipalGrad, where the prediction was performed using RSFC features from different number of ROIs/gradients.

A nested cross-validation procedure was performed to train predictive models. In the HCP dataset, we performed 100 random replications of 20-fold nested cross-validation. Family structure was taken into account by ensuring participants from the same family were kept within the same fold and not split across folds. In the ABCD dataset, as before (Chen et al., 2022), we combined participants across the 19 imaging sites, yielding 9 "site-clusters". Each site-cluster comprised at least 124 participants. We performed a leave-3-site-clusters out nested cross-validation. For each fold, 6 random site-clusters were used for training while the remaining 3 site-clusters were used for testing. The prediction was performed for every possible split of the site clusters, resulting in 84 replications (9 choose 3 = 84).

As certain behavioral measures are known to correlate with motion (Siegel et al., 2017), we regressed out age, sex, framewise displacement, and DVARS from the behavioral data before kernel ridge regression for both HCP and ABCD datasets. To prevent any information leak from the training data to test data, the regression was performed on the training data and the estimated nuisance regression coefficients were applied to the test fold.

Accuracy was measured by correlating the predicted and actual behavioral measure across all participants within the test fold (Finn et al., 2015; Kong et al., 2019; Li et al., 2019a; Kong et al., 2021a), and then averaged across test folds and replications. When comparing between approaches, a corrected resampled t-test for repeated k-fold cross-validation was performed (Bouckaert and Frank, 2004). To control for multiple comparisons, we performed a false discovery rate (FDR) (Benjamini and Hochberg, 1995)correction with $q < 0.05$ for all p-values reported in this paper.

To ensure our conclusions are robust across different regression approaches, we also considered linear ridge regression (LRR) as the predictive model, which has been widely used in many studies (Siegel et al., 2016; Cui et al., 2020; Rapuano et al., 2020).

Code and data availability

Code for this work is freely available at the GitHub repository maintained by the Computational Brain Imaging Group (https:// github.com/ThomasYeoLab/CBIG). The kernel ridge regression and linear ridge regression model used in this paper are available in this Github repository (GITHUB_LINK). Code specific to the regression models and analyses in this study can be found here (GITHUB_LINK). The HCP data are publicly available in this Github repository (GITHUB_LINK). The ABCD data are publicly available via the NIMH Data Archive (NDA) website (NDA_LINK).

Results

Kong2021 compared favorably with other approaches in the HCP dataset

The RSFC features of different gradient and parcellation approaches with optimal resolutions (estimated from inner-loop nested cross-validation) were used for predicting behavioral measures in the HCP dataset. For the HCP dataset, we trained a separate KRR model for each approach to predict three behavioral components ("cognition", "dissatisfaction", and "emotion") and 58 behavioral measures.

Figure 2A shows the average prediction accuracies of all 58 behavioral measures, task performance measures, and self-reported measures from the HCP dataset across different gradient and parcellation approaches. Figure 2B shows the prediction accuracies of three behavioral components from the HCP dataset across different gradient and parcellation approaches.

To compare the prediction accuracies across different approaches, p values were computed between each pair of approaches. Figure 3 shows the p values of comparing prediction accuracies between each pair of approaches in the HCP dataset. P values that remained significant after correcting for multiple comparisons (FDR $q < 0.05$) were colored based on -log10(p). Therefore, bright color indicates small p values, while dark color indicates large p values. The black color indicates non-significant p values after FDR correction. The warm colors represent higher prediction accuracies of the "row" approach compared with the "column" approach.

The individual-specific hard-parcellation approach Kong2021 compared favorably with the other approaches, as can be seen from warm colors along the rows corresponding to Kong2021 in Figure 3. This is especially the case for average prediction accuracies across all 58 behavioral measures (p=4.4e-3, p=2.9e-5, p=2.4e-3, and p=5.3e-25 with respect to Schaefer2018, sICA, PrincipalGrad, and LocalGrad, respectively) and self-reported measures (p=7.7e-3, p=2.9e-2, p=7.6e-3, and p=1.5e-8 with respect to Schaefer2018, sICA, PrincipalGrad, and LocalGrad, respectively). The principal gradient approach PincipalGrad, sICA, and Schaefer2018 peformed similarly. The local gradient approach LocalGrad performed the worst, as can be seen by cool colors along the rows corresponding to LocalGrad in Figure 3.

Similar results were obtained with LRR (Figures S1 and S2).

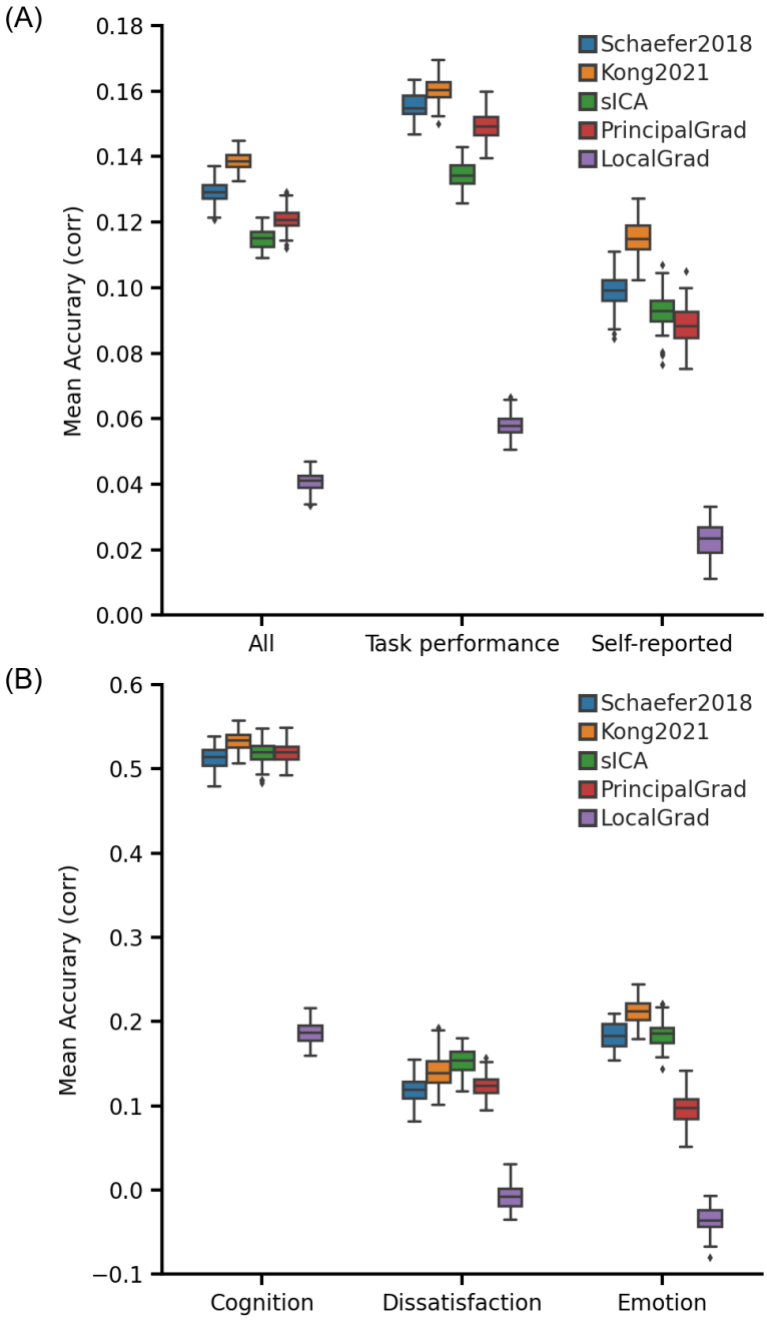

Figure 2. Individual-specific hard-parcellation approach Kong2021 compared favorably with other approaches for kernel ridge regression (KRR) in the HCP dataset. (A) Average prediction accuracies (Pearson's correlation) of all 58 behavioral measures, task performance measures, and self-reported measures. (B) Prediction accuracies (Pearson's correlation) of three behavioral components: cognition, dissatisfaction, and emotion. Boxplots utilized default Python seaborn

parameters, that is, box shows median and interquartile range (IQR). Whiskers indicate 1.5 IQR. Designation of behavioral measures into "self-reported" and "task-performance" measures followed previous studies (Li et al., 2019a; Liégeois et al., 2019; Kong et al., 2021a). The RSFC features of different gradient and parcellation approaches with optimal resolutions (estimated from inner-loop nested cross-validation) were used for predicting behavioral measures. LRR results are shown in Figure S1.

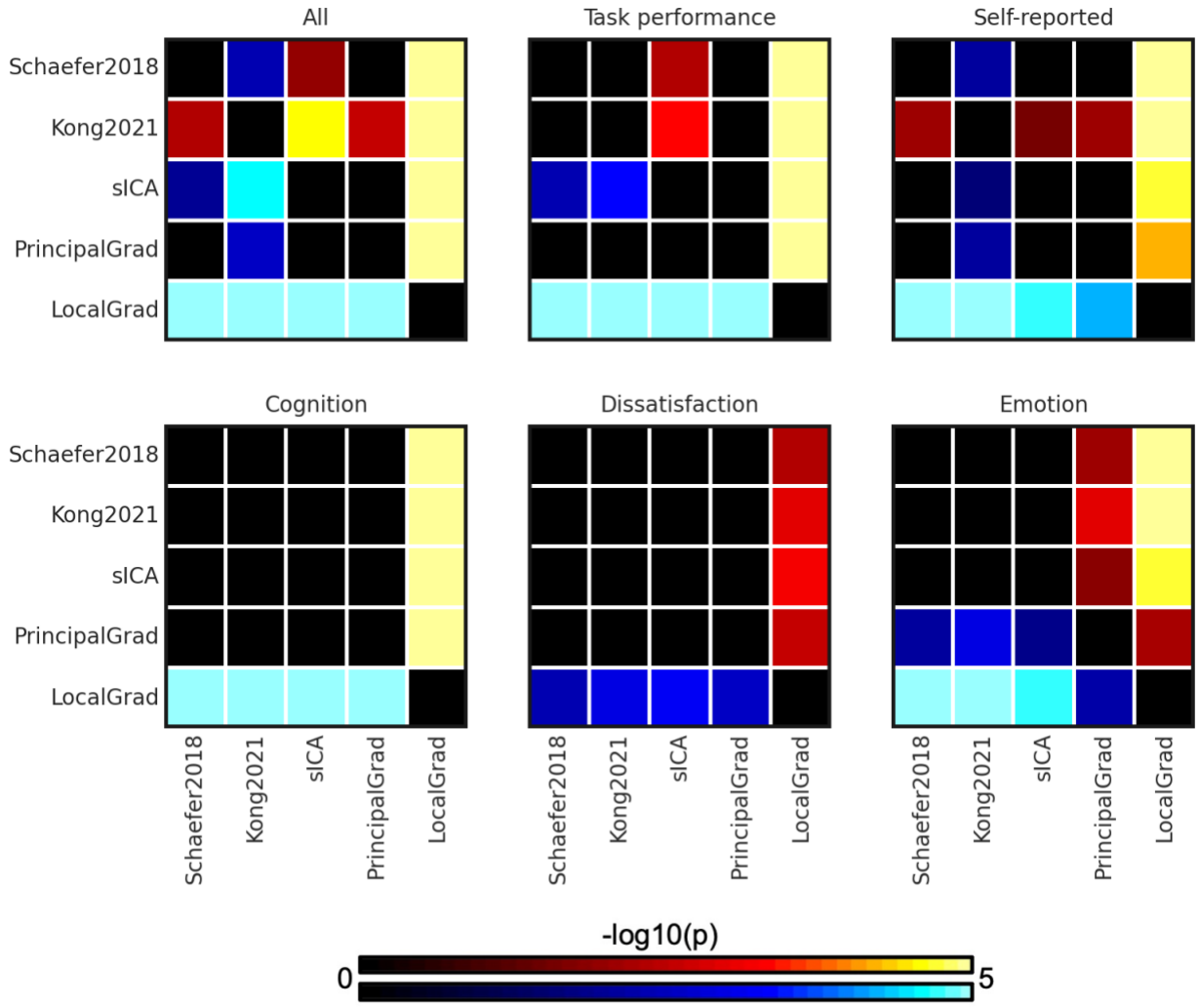

Figure 3. P values (-log10(p)) of comparing prediction accuracies between each pair of approaches for kernel ridge regression (KRR) in the HCP dataset. Non-black colors denote significantly different prediction performances after correcting for multiple comparisons with FDR $q < 0.05$. Bright colors indicate small p values, dark colors indicate large p values. For each pair of comparisons, warm colors represent higher prediction accuracies of the "row" approach than the "column" approach. Individual-specific hard-parcellation approach Kong2021 compared favorably with the other approaches, as can be seen from warm colors along the rows corresponding to Kong2021. LRR results are shown in Figure S2.

Parcellation and principal gradients exhibit similar performance in the ABCD dataset

The RSFC features of different gradient and parcellation approaches with optimal resolutions (estimated from inner-loop nested cross-validation) were used for predicting behavioral measures in the ABCD dataset. For the ABCD dataset, we trained a separate KRR model for each approach to predict three behavioral components ("cognition", "mental", and "personality") and 36 behavioral measures. For both datasets, we categorized the behavioral measures into "task performance" and "self-reported" measures.

Figure 4A shows the average prediction accuracies of all 36 behavioral measures, task performance measures, and self-reported measures from the ABCD dataset across different gradient and parcellation approaches. Figure 4B shows the prediction accuracies of three behavioral components from the ABCD dataset across different gradient and parcellation approaches.

In the ABCD dataset, the principal gradient approach PrincipalGrad was numerically the best for most cases, but there was largely no statistical difference among the approaches. More specifically, PrincipalGrad was significantly better than Kong2021, sICA and LocalGrad in the case of the average prediction accuracies across task performance measures ($p=3.3e-2$, $p=7.6e-5$, and $p=5.8e-29$ with respect to Kong2021, sICA, and LocalGrad, respectively), while Kong2021 was significantly better than sICA and PrincipalGrad in the case of the mental health component ($p=3.7e-2$, $p=2.0e-2$ with respect to sICA and PrincipalGrad respectively).

Similar results were obtained with LRR (Figures S3 and S4).

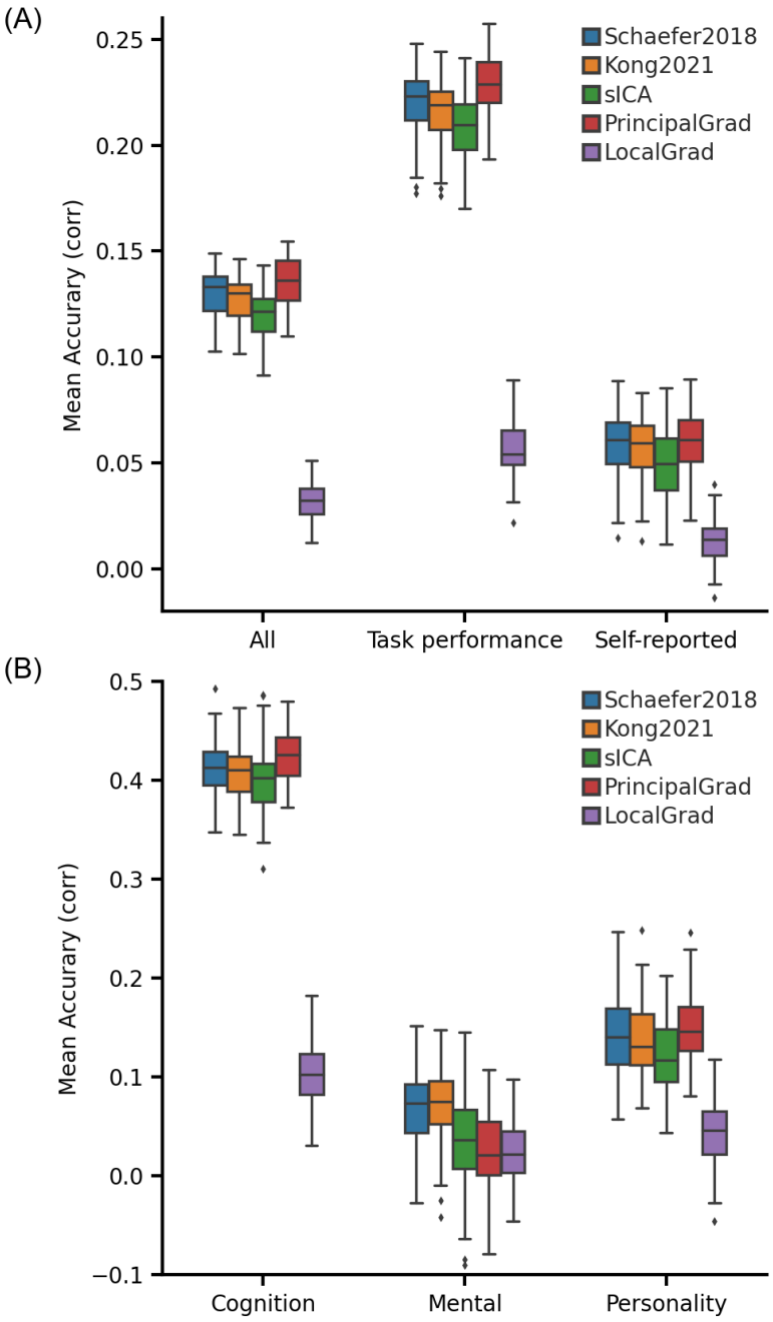

Figure 4. Principal gradient approach achieves comparable behavioral prediction performance as parcellation approaches for kernel ridge regression (KRR) in the ABCD dataset. (A) Average prediction accuracies (Pearson's correlation) of all 36 behavioral measures, task performance measures, and self-reported measures. (B) Prediction accuracies (Pearson's correlation) of three behavioral components: cognition, mental health, and personality. Boxplots utilized default Python seaborn parameters, that is, box shows median and interquartile range (IQR). Whiskers indicate 1.5 IQR. Designation of behavioral measures into "self-reported" and "task-performance" measures followed previous studies (Li et al., 2019a; Liégeois et al., 2019; Kong et al., 2021a). The RSFC features of different gradient and parcellation approaches with optimal resolutions (estimated from inner-loop nested cross-validation) were used for predicting

behavioral measures. LRR results are shown in Figure S3. The principal gradient approach PrincipalGrad was numerically the best for most cases, but there was largely no statistical difference among the approaches.

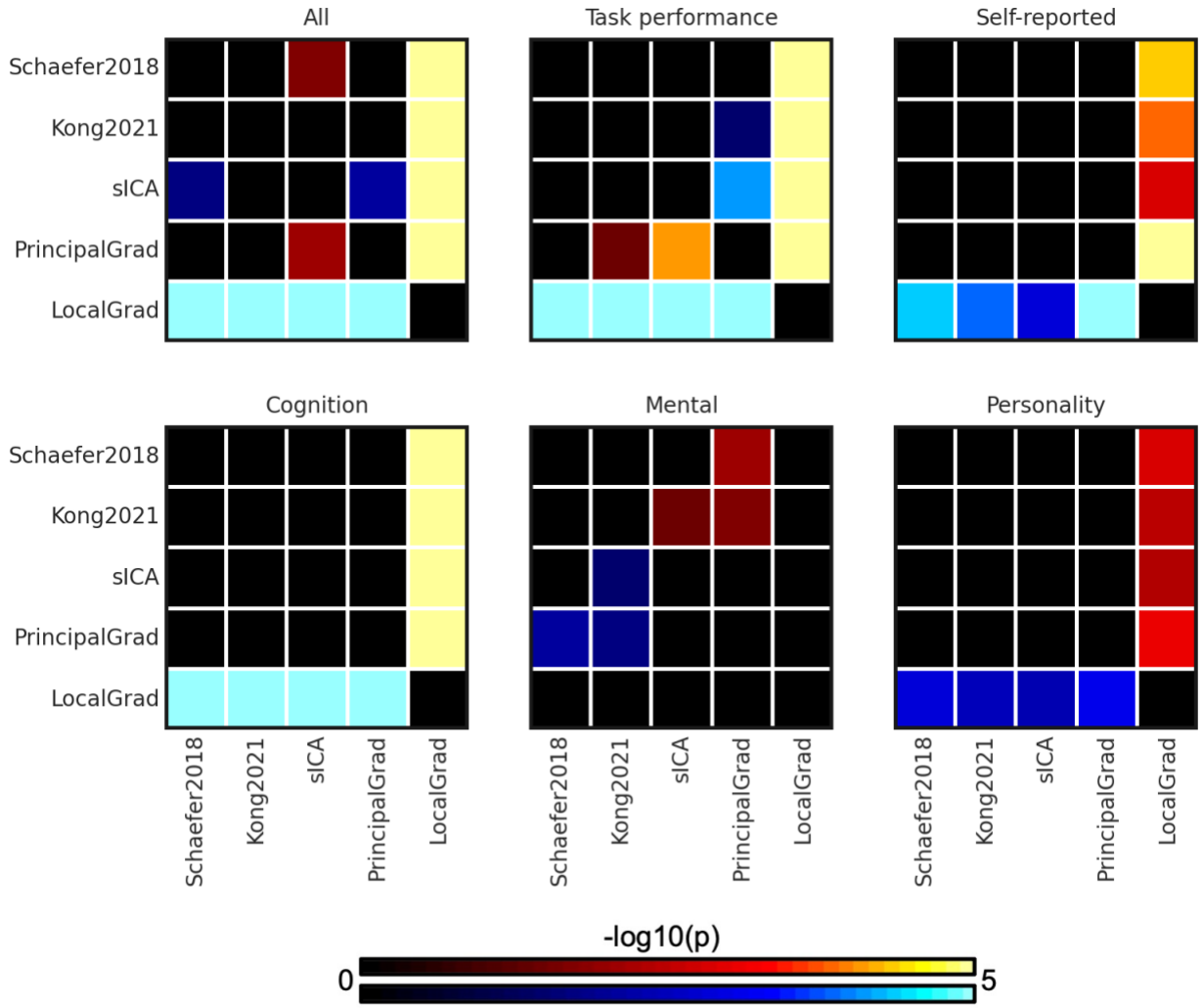

Figure 3. P values (-log10(p)) of comparing prediction accuracies between each pair of approaches for kernel ridge regression (KRR) in the ABCD dataset. Non-black colors denote significantly different prediction performances after correcting for multiple comparisons with FDR $q < 0.05$. Bright colors indicate small p values, dark colors indicate large p values. For each pair of comparisons, warm colors represent higher prediction accuracies of the "row" approach than the "column" approach. There was no statistical difference among most approaches. LRR results are shown in Figure S4.

Task performance measures are more predictable than self-reported measures for all approaches

To explore which behavioral measures can be consistently predicted well regardless of gradient and parcellation approaches, we ordered the behavioral measures based on averaged prediction accuracies (Pearson's correlation) across different approaches with the optimized resolutions for KRR in the HCP (Figure 6) and ABCD (Figure 7) datasets. Our previous studies have suggested that self-reported and task performance measures might be differentially predicted under different conditions (Li et al., 2019a; Liégeois et al., 2019; Kong et al., 2021a). For example, the task performance measures were more predictable than self-reported measures based on functional connectivity of hard-parcellation approaches (Kong et al., 2021a).

In the HCP dataset, we found the average prediction accuracies of task performance measures were r = 0.156 ± 0.004 (mean ± std), r = 0.160 ± 0.004, r = 0.135 ± 0.004, r = 0.149 ± 0.004, and r = 0.058 ± 0.003 for Schaefer2018, Kong2021, sICA, PrincipalGrad, and LocalGrad, respectively (Figure 2A), while the prediction accuracies of self-reported measures were r = 0.099 ± 0.005, r = 0.115 ± 0.005, r = 0.093 ± 0.005, r = 0.089 ± 0.006, and r = 0.023 ± 0.005 for Schaefer2018, Kong2021, sICA, PrincipalGrad, and LocalGrad, respectively (Figure 2A).

In the ABCD dataset, we found the average prediction accuracies of task performance measures were r = 0.220 ± 0.016 (mean ± std), r = 0.216 ± 0.015, r = 0.209 ± 0.016, r = 0.229 ± 0.014, and r = 0.056 ± 0.013 for Schaefer2018, Kong2021, sICA, PrincipalGrad, and LocalGrad, respectively (Figure 4A), while the prediction accuracies of self-reported measures were r = 0.059 ± 0.015, r = 0.058 ± 0.015, r = 0.049 ± 0.016, r = 0.061 ± 0.0140, and r = 0.014 ± 0.010 for Schaefer2018, Kong2021, sICA, PrincipalGrad, and LocalGrad, respectively (Figure 4A).

These results suggested that on average, task performance measures were more predictable than self-reported measures across all gradient and parcellation approaches (p = 4.0e-4, p = 2.6e-3, p = 7.2e-3, p = 2.6e-4, and p = 3.5e-2 for Schaefer2018, Kong2021, sICA, PrincipalGrad, and LocalGrad, respectively). Similar results were obtained with LRR (Figures S5 and S6). P values remained significant after correcting for multiple comparisons with FDR $q < 0.05$.

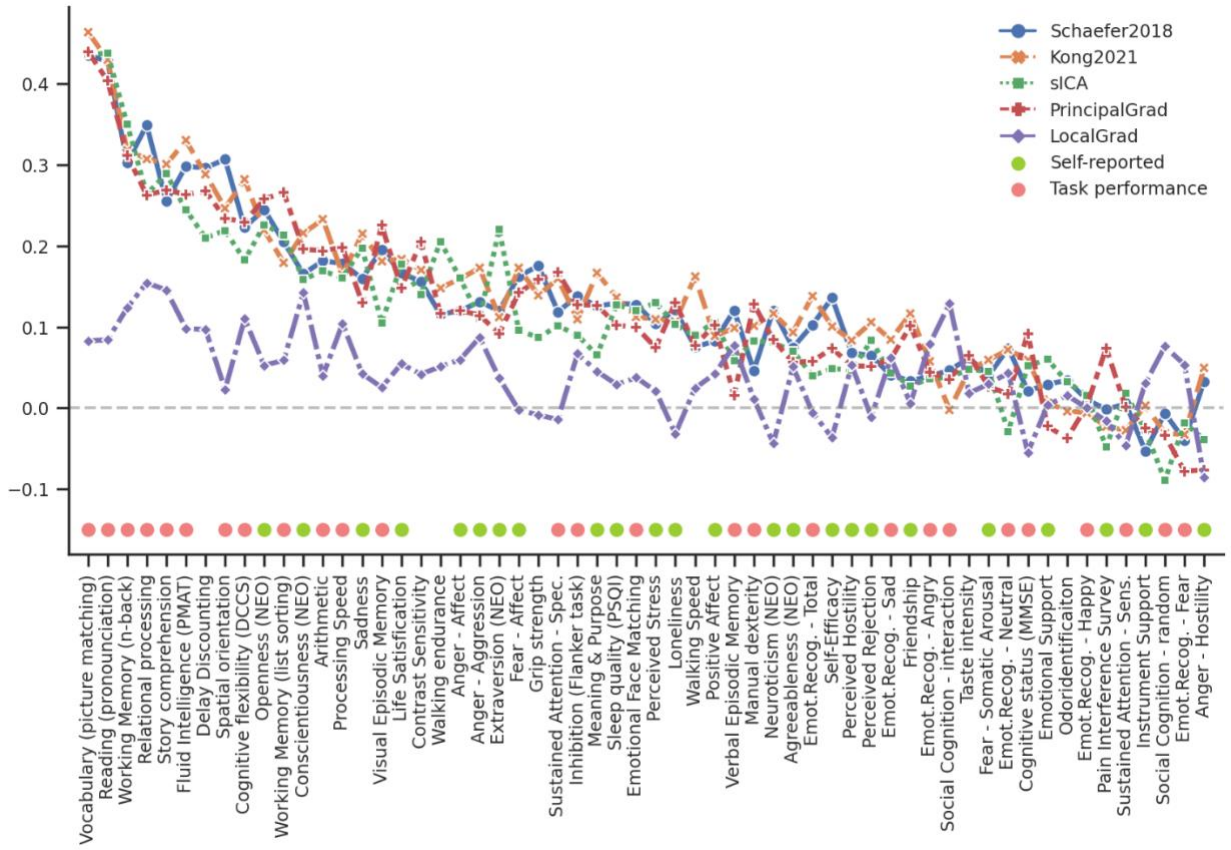

Figure 4. Task performance measures were predicted better than self-reported measures across different gradient and parcellation approaches with optimized resolutions for KRR in the HCP dataset. 58 behavioral measures were ordered based on average prediction accuracies across Schaefer2018, Kong2021, sICA, PrincipalGrad, and LocalGrad. Pink circles indicate task performance measures. Green circles indicate self-reported measures. Boxplots utilized default Python seaborn parameters, that is, box shows median and interquartile range (IQR). Whiskers indicate 1.5 IQR. Designation of behavioral measures into "self-reported" and "task-performance" measures followed previous studies (Li et al., 2019a; Liégeois et al., 2019; Kong et al., 2021a). LRR results are shown in Figure S5.

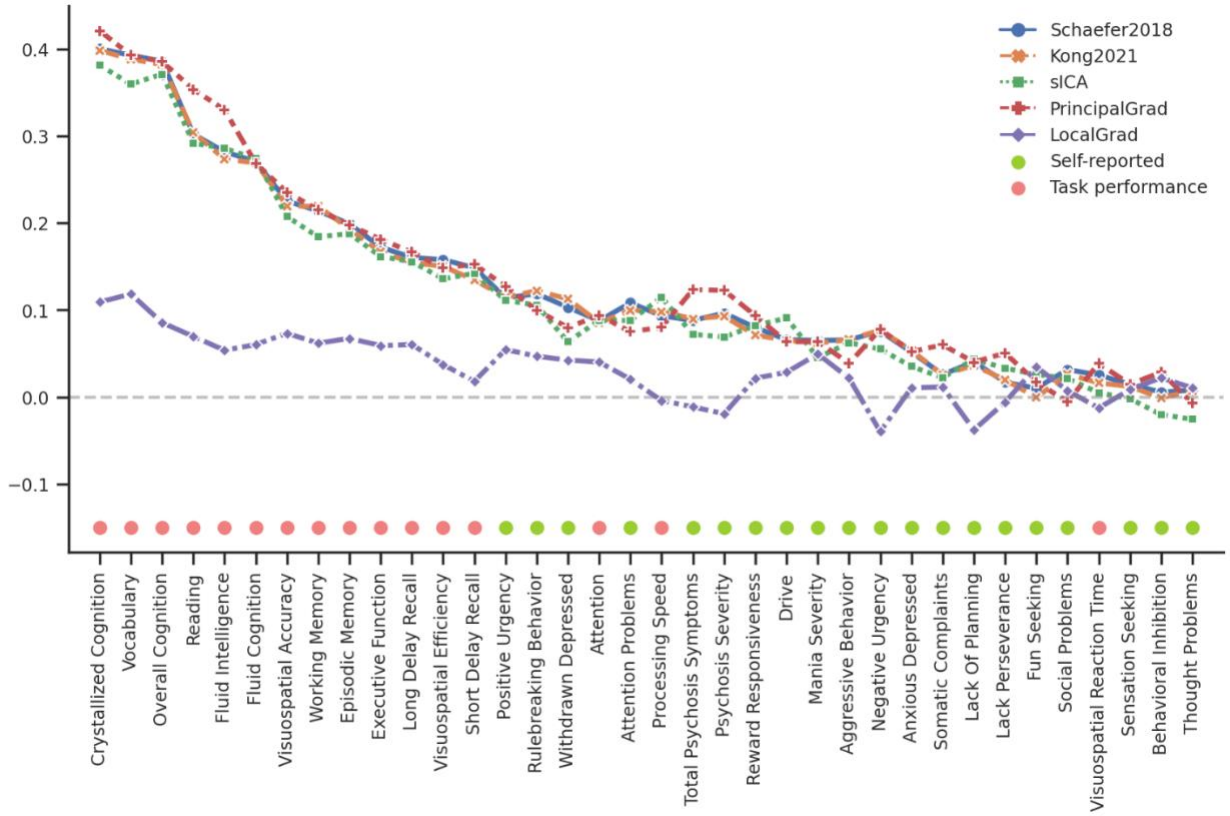

Figure 5. Task performance measures were predicted better than self-reported measures across different gradient and parcellation approaches with optimized resolutions for KRR in the ABCD dataset. 36 behavioral measures were ordered based on average prediction accuracies across Schaefer2018, Kong2021, sICA, PrincipalGrad, and LocalGrad. Pink circles indicate task performance measures. Green circles indicate self-reported measures. Boxplots utilized default Python seaborn parameters, that is, box shows median and interquartile range (IQR). Whiskers indicate 1.5 IQR. Designation of behavioral measures into "self-reported" and "task-performance" measures based on ABCD behavioral measures description (Li et al., 2019a; Liégeois et al., 2019; Kong et al., 2021a). LRR results are shown in Figure S6.

Prediction performances vary across resolutions for both gradient and parcellation approaches

To explore the impact of the number of gradients and parcels, we performed behavioral prediction for each approach using different resolutions in the HCP and ABCD datasets. The left column of Figure 8 and 9 show the KRR prediction accuracies (Pearson's correlation) of the average prediction accuracies of all behavioral measures for Schaefer2018, Kong2021, sICA, and PrincipalGrad in the HCP and ABCD datasets with different resolutions. The local gradient approach LocalGrad was not included here because this approach did not have different resolutions.

To compare the prediction accuracies across different resolutions for each approach, p values were computed between each pair of resolutions. The right column of Figure 8 and 9 show the p values of comparing prediction accuracies between each pair of approaches in the HCP and ABCD datasets. P values remained significant after correcting for multiple comparisons with FDR $q < 0.05$ were colored based on -log10(p). The bright colors indicate small p values, while the dark colors indicate large p values. The warm colors represent higher prediction accuracies of the "row" resolution than the "column" column resolution.

In the HCP dataset, the hard-parcellation approaches Schaefer2018 and Kong2021with low resolutions generally predicted behavioral measures worse than high resolutions, especially in the case of 100 ROIs (Figures 8A and 8B). The prediction accuracies plateaued around 300 ROIs for Schaefer2018 and 200 ROIs for Kong2021. Compared with other resolutions, Schaefer2018 and Kong2021 with 100 ROIs yielded significantly worse prediction accuracies of all 58 behavioral measures with $p < 2.6e\text{-}7$ and $p < 8.3e\text{-}5$, respectively. Similarly, the principal gradient approach PrincipalGrad with low resolutions also predicted behavioral measures worse than high resolutions (Figure 8D). The prediction accuracies kept increasing and plateaued around 40 gradients. Compared with using more than 40 gradients, PrincipalGrad with less than 40 gradients yielded significantly worse prediction accuracies of all 58 behavioral measures with $p < 5.2e\text{-}5$. By contrast, the soft-parcellation approach sICA with high resolutions predicted behavioral measures worse than low resolutions, especially in the case of 300 components (Figure 8C). Compared with other resolutions, sICA with 300 components yielded significantly worse prediction accuracies with $p < 3.8e\text{-}3$.

Intriguingly, in the ABCD dataset, the prediction accuracies of all parcellation approaches Schaefer2018, Kong2021, and sICA exhibited no obvious difference across resolutions (Figure 9A to 9C). The principal gradient approach PrincipalGrad with low resolutions generally predicted behavioral measures worse than high resolutions. The prediction accuracies plateaued around 60 gradients (Figure 9D). Compared with less than 40 gradients, PrincipalGrad with more than 60 gradients yielded significantly higher prediction accuracies with $p < 9.8e\text{-}3$.

Similar results were obtained with LRR (Figures S7 and S8). Prediction results of task performance measures, self-reported measures, and three behavioral components are shown in Figures S9 to S28, yielding similar conclusions. Figure S29 to S32 show the prediction results across different resolutions for all approaches in the same plot.

(A) Schaefer2018

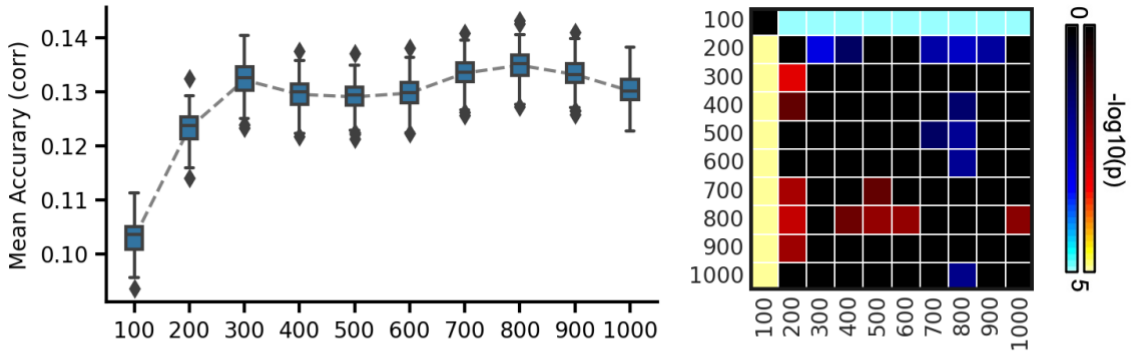

(B) Kong2021

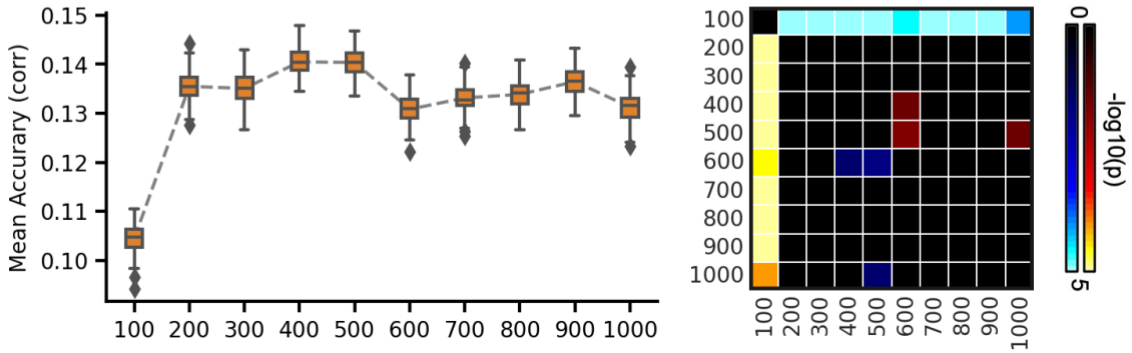

(C) sICA

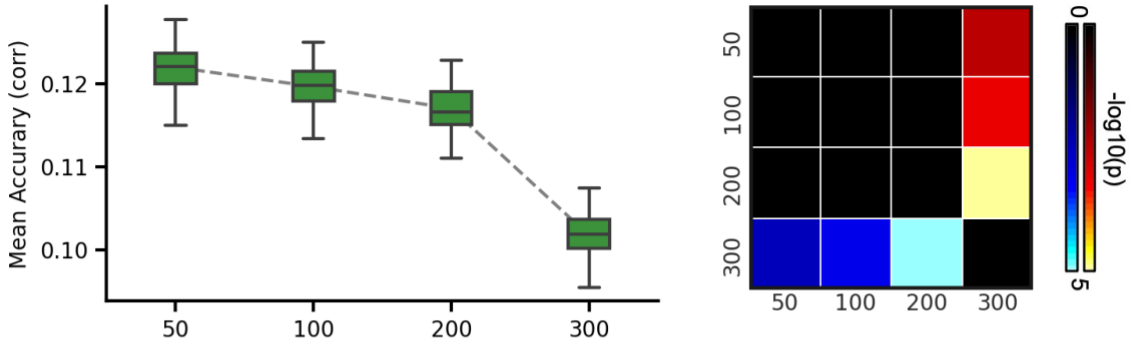

(D) PrincipalGrad

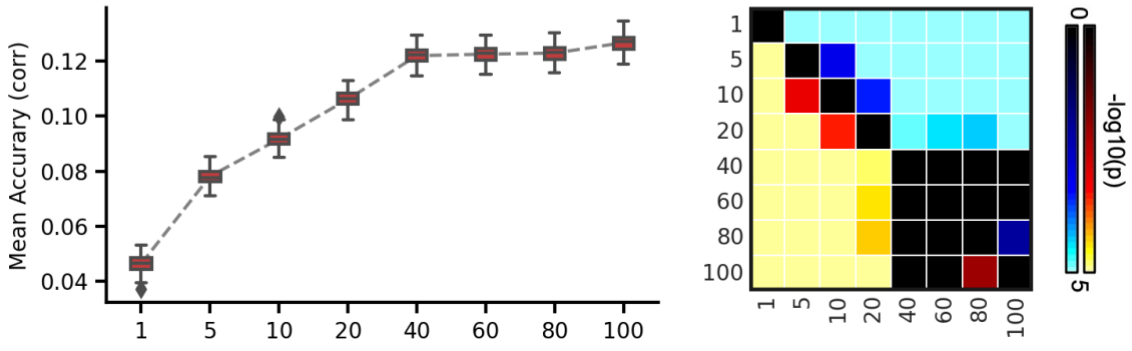

Figure 6. Average prediction accuracies (Pearson's correlation) of all 58 behavioral measures vary across resolutions for gradient and parcellation approaches using KRR in the HCP dataset. (A) Prediction accuracies and p values of the hard-parcellation Schaefer2018 with 100 to 1000 ROIs. (B) Prediction accuracies and p values of the hard-parcellation Kong2021 with 100 to 1000 ROIs. (C) Prediction accuracies and p values of the soft-parcellation sICA with 50 to 300 components. (D) Prediction accuracies and p values of the principal gradient PrincipalGrad with 1 to 100 gradients. Boxplots utilized default Python seaborn parameters, that is, box shows median and interquartile range (IQR). Whiskers indicate 1.5 IQR. P values (-log10(p)) were computed between prediction accuracies of each pair of resolutions. Non-black colors denote significantly different prediction performances after correcting for multiple comparisons with FDR $q < 0.05$. Bright colors indicate small p values, dark colors indicate large p values. For each pair of comparisons, warm colors represent higher prediction accuracies of the "row" resolution than the "column" resolution.

(A) Schaefer2018

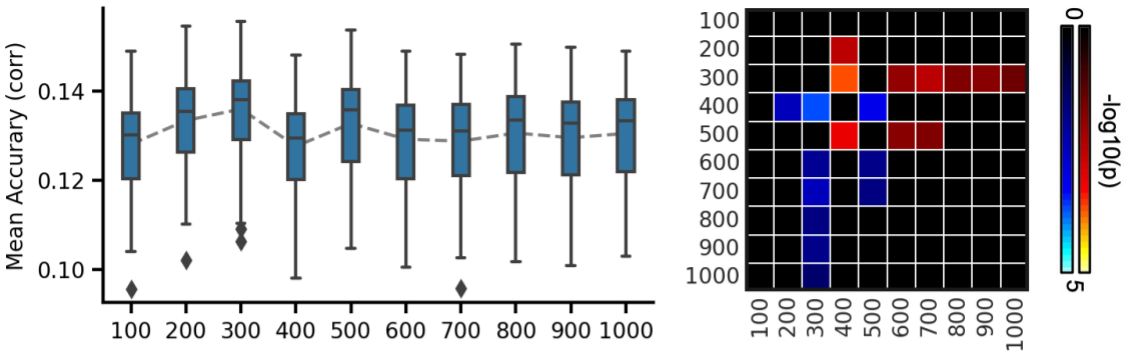

(B) Kong2021

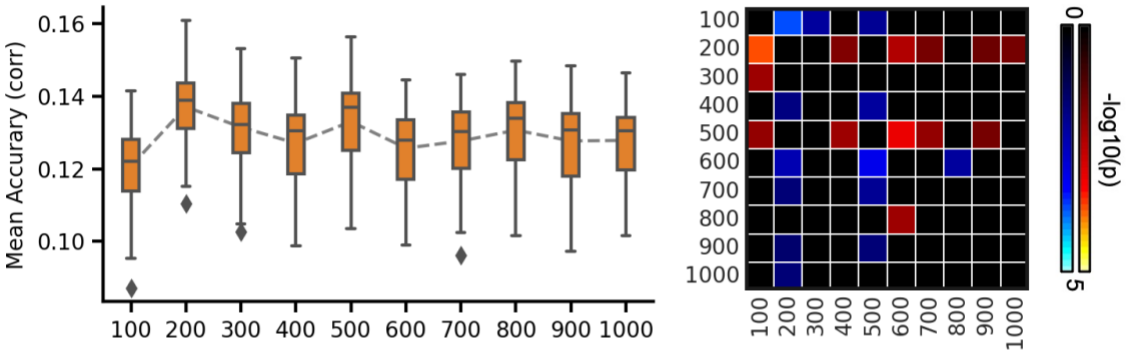

(C) sICA

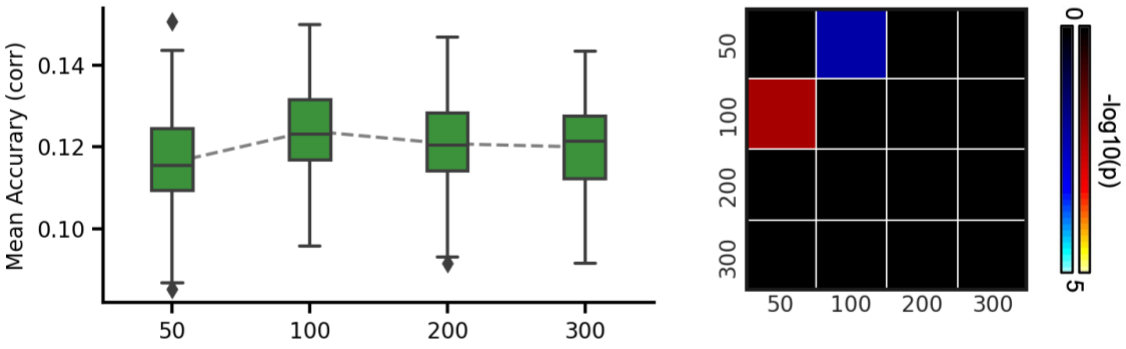

(D) PrincipalGrad

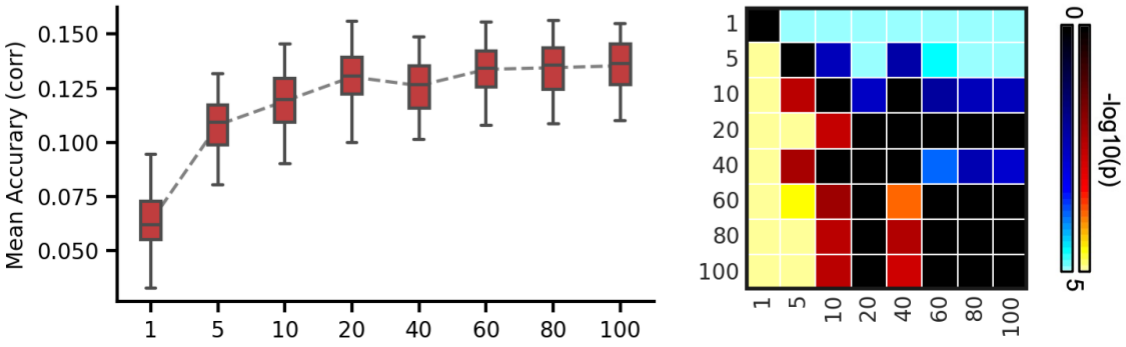

Figure 7. Average prediction accuracies (Pearson's correlation) of all 36 behavioral measures vary across resolutions for gradient and parcellation approaches using KRR in the ABCD dataset. (A) Prediction accuracies and p values of the hard-parcellation Schaefer2018 with 100 to 1000 ROIs. (B) Prediction accuracies and p values of the hard-parcellation Kong2021 with 100 to 1000 ROIs. (C) Prediction accuracies and p values of the soft-parcellation sICA with 50 to 300 components. (D) Prediction accuracies and p values of the principal gradient PrincipalGrad with 1 to 100 gradients. Boxplots utilized default Python seaborn parameters, that is, box shows median and interquartile range (IQR). Whiskers indicate 1.5 IQR. P values (-log10(p)) were computed between prediction accuracies of each pair of resolutions. Non-black colors denote significantly different prediction performances after correcting for multiple comparisons with FDR $q < 0.05$. Bright colors indicate small p values, dark colors indicate large p values. For each pair of comparisons, warm colors represent higher prediction accuracies of the "row" resolution than the "column" resolution.

Discussion

Overview

In this manuscript, we demonstrated that RSFC principal gradients at sufficiently high resolution (e.g. more than 40 or 60 gradients) exhibited similar behavioral prediction performance as parcellation-based RSFC. More specifically, individual-specific hard-parcellation Kong2021 compared favorably with other approaches in the HCP dataset, while principal gradient and parcellation approaches performed similarly in the ABCD dataset. We found that for all parcellation and gradient approaches, task performance measures were more predictable than self-reported measures. We showed that prediction performances varied across resolutions for all gradient and parcellation approaches. These findings were replicated in both HCP and ABCD datasets using two prediction models KRR and LRR.

Functional connectivity behavioral prediction using parcellation versus gradients

There has been great interest in functional connectivity prediction of behavioral measures. While most previous studies utilized RSFC from hard- or soft-parcellations, few studies have focused on gradient techniques for behavioral prediction. One recent study showed that principal gradients were behaviorally meaningful (Hong et al., 2020). Hong and colleagues further compared the prediction performance between principal gradients and RSFC from the Schaefer2018 group-level hard-parcellation with 1000 ROIs. They found that 100 principal gradients outperformed Schaefer2018 1000-ROI hard-parcellation in predicting general cognition in HCP dataset.

In our study, instead of only focusing one specific resolution, we considered multiple resolutions for each approach and optimized the resolution as a hyperparameter in the prediction models. We compared the prediction performance between parcellation and gradient approaches using the same prediction framework with two different prediction models. We performed prediction for a wide range of behavioral measures across different domains and three behavioral components derived from a factor analysis. The prediction analyses were done in the HCP healthy young adult dataset, and the ABCD healthy children dataset.

Similarly, we also found that principal gradients could predict behavioral measures as well as RSFC from parcellations in HCP dataset using both KRR and LRR. However, unlike

Hong and colleagues (Hong et al., 2020), we found that principal gradients achieved similar level of prediction accuracy as the Schaefer2018 group-level hard-parcellation in HCP dataset. Furthermore, the individual-specific hard-parcellation Kong2021 achieved the best prediction results. More specifically, Hong and colleagues showed that combining 100 principal gradients was able to predict general cognition with a $r = 0.405$, while RSFC from Schaefer2018 1000-ROI group-level hard-parcellation only achieved an accuracy of $r = 0.181$. In our study, we found that principal gradients could predict cognition with a $r = 0.520 \pm 0.011$ using KRR and $r = 0.487 \pm 0.011$ using LRR, while RSFC from Schaefer2018 group-level hard-parcellation could achieve an accuracy of $r = 0.513 \pm 0.013$ using KRR and $r = 0.514 \pm 0.008$ using LRR. Therefore, our principal gradient prediction performance was comparable to Hong and colleagues, but our parcellation-based RSFC prediction performance was significantly better. We replicated similar results in a children dataset (ABCD).

The main reason for this discrepancy might be due to different prediction models being utilized for principal gradient and parcellation approaches in Hong and colleagues (2020). In their behavioral prediction framework, they utilized the canonical correlation analysis (CCA) for principal gradients, but utilized the connectome-based predictive modeling approach (Shen et al., 2017) for Schaefer2018. Therefore, the prediction results were not comparable between approaches.

Interestingly, the local gradient approach performed much worse than parcellation approaches and principal gradients. The local gradient approach has been widely used as a tool to derive hard-parcellation (Laumann et al., 2015; Gordon et al., 2016). Specifically, an edge detection approach (i.e. watershed algorithm) was applied on the gradient map to generate the binarized boundary map, which could be used to define non-overlapping ROIs (Laumann et al., 2015; Gordon et al., 2016). In this paper, instead of using the hard-parcellation from the local gradient approach to predict behavioral measures, we used the individual-specific gradient maps. However, a single gradient map might lose too much information from the original RSFC, yielding poor prediction performance.

Prediction of task performance measures is better than self-reported measures

Our results suggested that the task performance measures were more predictable than self-reported measures for all parcellation and gradient approaches in both HCP and ABCD

datasets (Figures 6,7, S5 and S6). This distinction between task performance and self-reported measures echoed well with previous investigations of RSFC–behavior relationships. It has been shown that RSFC could predict cognition and task performance measures better than self-reported measures (Dubois et al., 2018a; Li et al., 2019a; Kong et al., 2021a). Dynamic functional connectivity is also more strongly associated with task performance measures than self-reported measures (Vidaurre et al., 2017; Liégeois et al., 2019; Ikeda et al., 2022). Furthermore, utilizing functional connectivity from task fMRI rather resting-state fMRI has been shown to improve the prediction of cognition more than personality and mental health (Chen et al., 2022).

One possible reason for better prediction accuracies in task performance measures might be a result of the subjective nature of self-reported measures. For example, the self-reported personality measures NEO-FFI could be influenced by an individual's insight, impression management, and reference group effects (Dubois et al., 2018b), leading to unreliable estimate of personality. We might be able to predict self-reported measures better with more accurate estimates of personality, emotion and mental health.

Impact of resolutions in connectivity prediction of behavioral measures

Previous studies have established that the optimal resolution for behavioral prediction varied across behavioral measures using RSFC from different soft- and hard-parcellation approaches (Dadi et al., 2019, 2020). Within a reasonable range, the impact of resolutions in prediction accuracy was small (Dadi et al., 2019). Pervaiz and colleagues also explored the impact of sICA resolution for predicting fluid intelligence(Pervaiz et al., 2020). They found that increasing dimensionality of sICA could lead to an increase in prediction accuracy. Furthermore, sICA outperformed the group-level hard-parcellation approach Schaefer2018 in predicting fluid intelligence (Pervaiz et al., 2020). One recent study compared cognition prediction accuracies of different resolutions of a new soft-parcellation approach (Farahibozorg et al., 2021). They focused on high-resolution soft-parcellations (i.e. 100, 150, 200 components) and found the prediction performance was generally similar across resolutions (Farahibozorg et al., 2021).

Consistent with previous studies, we found the optimal resolution in predicting behavioral measures varied across behavioral phenotypes for each parcellation approach. Within a range of high resolutions, the impact of resolutions in prediction performance were relatively

small for hard-parcellation approaches. We also found that increasing resolutions of different parcellation approaches might not yield better prediction performance. Specifically, the soft-parcellation approach sICA tended to have relatively lower prediction accuracy with very high resolution in the HCP dataset. For example, the average prediction accuracy of all 58 behavioral measures of HCP using sICA 200 components were significantly worse than lower resolutions 50, 100, and 150 (Figure 8C).

Intriguingly, we found that the prediction accuracies of soft- and hard-parcellation approaches had no obvious difference across resolutions in the ABCD children dataset. One possible reason for this might be due to discrepancy in brain organization between healthy young adults and young children. Specifically, the Schaefer2018 group-level hard-parcellations were derived by healthy young adults, which might not be optimal for representing RSFC of young children.

While there have been several studies focusing on the impact of different resolutions for soft- and hard-parcellation approaches in RSFC prediction of behavioral measures (Dadi et al., 2019; Pervaiz et al., 2020; Farahibozorg et al., 2021), few studies have looked into the gradient approach. A recent study (Hong et al., 2020) compared the prediction performances between using a single principal gradient versus combining 100 gradients. In our study, we considered a wide range of resolutions for principal gradients. With increased number of principal gradients, we found that the prediction performance increased in both HCP and ABCD dataset. Most studies have focused mainly on the first or first several principal gradients (Margulies et al., 2016; Paquola et al., 2019; Wang et al., 2019; Tian et al., 2020; Kong et al., 2021b), since these gradients captured the most variance in RSFC (Huntenburg et al., 2018). However, the first principal gradient alone predicted behavioral measures very poorly in both HCP and ABCD datasets. In fact, the prediction accuracy of principal gradients plateaued only after more than 40 gradients in the HCP dataset and 60 gradients in the ABCD dataset. The first few gradients are quite stable features of brain organization which might not vary much across individuals. As such, most literature interested in the group-level brain organization representation mainly focused on the first few principal gradients. However, the less widely studied higher order gradients captured more idiosyncrasies across participants. Principal gradients studies focusing on individual differences would need at least 40 to 60 gradients to not lose significant behaviorally relevant information.

Conclusions

We compared 3 different parcellation approaches (Schaefer2018, Kong2021 and sICA) and 2 different gradient techniques (PrincipalGrad and LocalGrad) for RSFC prediction of behavioral measures from HCP and ABCD datasets using KRR and LRR. We showed that functional connectivity principal gradients could predict behavioral measures similar to parcellation approaches with optimized resolutions. Comparing different approaches, individual-specific hard-parcellation approach performed the best in the HCP dataset, while principal gradient and parcellation approaches performed similarly in the ABCD dataset. In both datasets, we found that the task performance measures could be predicted better than self-reported measures for all parcellation and gradient approaches. Furthermore, hard-parcellations and principal gradients with very low resolutions performed worse than high resolutions, but this is not necessarily true for soft-parcellation approach sICA. Overall, our results suggested that principal gradients with relatively high resolution (> 40 or > 60 gradients) could predict behavioral measures no worse than parcellation approaches.

References

Beckmann, C., Mackay, C., Filippini, N., and Smith, S. (2009). Group comparison of resting-state FMRI data using multi-subject ICA and dual regression. NeuroImage *47*, S148.

Beckmann, C.F., DeLuca, M., Devlin, J.T., and Smith, S.M. (2005). Investigations into resting-state connectivity using independent component analysis. Philos. Trans. R. Soc. Lond., B, Biol. Sci. *360*, 1001–1013.

Benjamini, Y., and Hochberg, Y. (1995). Controlling the False Discovery Rate: A Practical and Powerful Approach to Multiple Testing. Journal of the Royal Statistical Society: Series B (Methodological) *57*, 289–300.

Bernhardt, B.C., Smallwood, J., Keilholz, S., and Margulies, D.S. (2022). Gradients in brain organization. NeuroImage *251*, 118987.

Beyer, L., Hénaff, O.J., Kolesnikov, A., Zhai, X., and Oord, A. van den (2020). Are we done with ImageNet? ArXiv:2006.07159 [Cs].

Bijsterbosch, J., Harrison, S.J., Jbabdi, S., Woolrich, M., Beckmann, C., Smith, S., and Duff, E.P. (2020). Challenges and future directions for representations of functional brain organization. Nat Neurosci *23*, 1484–1495.

Bijsterbosch, J.D., Woolrich, M.W., Glasser, M.F., Robinson, E.C., Beckmann, C.F., Van Essen, D.C., Harrison, S.J., and Smith, S.M. (2018). The relationship between spatial configuration and functional connectivity of brain regions. ELife *7*, e32992.

Biswal, B., Yetkin, F.Z., Haughton, V.M., and Hyde, J.S. (1995). Functional connectivity in the motor cortex of resting human brain using echo-planar mri. Magnetic Resonance in Medicine *34*, 537–541.

Bouckaert, R.R., and Frank, E. (2004). Evaluating the Replicability of Significance Tests for Comparing Learning Algorithms. In Advances in Knowledge Discovery and Data Mining, H. Dai, R. Srikant, and C. Zhang, eds. (Berlin, Heidelberg: Springer), pp. 3–12.

Calhoun, V. d., Adali, T., Pearlson, G. d., and Pekar, J. j. (2001). A method for making group inferences from functional MRI data using independent component analysis. Human Brain Mapping *14*, 140–151.

Casey, B.J., Cannonier, T., Conley, M.I., Cohen, A.O., Barch, D.M., Heitzeg, M.M., Soules, M.E., Teslovich, T., Dellarco, D.V., Garavan, H., et al. (2018). The Adolescent Brain Cognitive Development (ABCD) study: Imaging acquisition across 21 sites. Dev Cogn Neurosci *32*, 43–54.

Chen, J., Tam, A., Kebets, V., Orban, C., Ooi, L.Q.R., Asplund, C.L., Marek, S., Dosenbach, N.U.F., Eickhoff, S.B., Bzdok, D., et al. (2022). Shared and unique brain network features

predict cognitive, personality, and mental health scores in the ABCD study. Nat Commun *13*, 2217.

Cohen, A.L., Fair, D.A., Dosenbach, N.U.F., Miezin, F.M., Dierker, D., Van Essen, D.C., Schlaggar, B.L., and Petersen, S.E. (2008). Defining functional areas in individual human brains using resting functional connectivity MRI. Neuroimage *41*, 45–57.

Cui, Z., Li, H., Xia, C.H., Larsen, B., Adebimpe, A., Baum, G.L., Cieslak, M., Gur, R.E., Gur, R.C., Moore, T.M., et al. (2020). Individual Variation in Functional Topography of Association Networks in Youth. Neuron *106*, 340-353.e8.

Dadi, K., Rahim, M., Abraham, A., Chyzhyk, D., Milham, M., Thirion, B., and Varoquaux, G. (2019). Benchmarking functional connectome-based predictive models for resting-state fMRI. NeuroImage *192*, 115–134.

Dadi, K., Varoquaux, G., Machlouzarides-Shalit, A., Gorgolewski, K.J., Wassermann, D., Thirion, B., and Mensch, A. (2020). Fine-grain atlases of functional modes for fMRI analysis. NeuroImage *221*, 117126.

Dubois, J., Galdi, P., Paul, L.K., and Adolphs, R. (2018a). A distributed brain network predicts general intelligence from resting-state human neuroimaging data. Philos. Trans. R. Soc. Lond., B, Biol. Sci. *373*.

Dubois, J., Galdi, P., Han, Y., Paul, L.K., and Adolphs, R. (2018b). Resting-state functional brain connectivity best predicts the personality dimension of openness to experience. Personal Neurosci *1*, E6.

Farahibozorg, S.-R., Bijsterbosch, J.D., Gong, W., Jbabdi, S., Smith, S.M., Harrison, S.J., and Woolrich, M.W. (2021). Hierarchical modelling of functional brain networks in population and individuals from big fMRI data. NeuroImage *243*, 118513.

Finn, E.S., Shen, X., Scheinost, D., Rosenberg, M.D., Huang, J., Chun, M.M., Papademetris, X., and Constable, R.T. (2015). Functional connectome fingerprinting: identifying individuals using patterns of brain connectivity. Nat. Neurosci. *18*, 1664–1671.

Fox, M.D., and Raichle, M.E. (2007). Spontaneous fluctuations in brain activity observed with functional magnetic resonance imaging. Nature Reviews Neuroscience *8*, 700–711.

Glasser, M.F., Coalson, T.S., Robinson, E.C., Hacker, C.D., Harwell, J., Yacoub, E., Ugurbil, K., Andersson, J., Beckmann, C.F., Jenkinson, M., et al. (2016). A multi-modal parcellation of human cerebral cortex. Nature *536*, 171–178.

Glasser, M.F., Sotiropoulos, S.N., Wilson, J.A., Coalson, T.S., Fischl, B., Andersson, J.L., Xu, J., Jbabdi, S., Webster, M., Polimeni, J.R., et al. (2013). The minimal preprocessing pipelines for the Human Connectome Project. NeuroImage *80*, 105–124.

Gordon, E.M., Laumann, T.O., Adeyemo, B., Huckins, J.F., Kelley, W.M., and Petersen, S.E. (2016). Generation and Evaluation of a Cortical Area Parcellation from Resting-State Correlations. Cerebral Cortex *26*, 288–303.

Greicius, M.D., Krasnow, B., Reiss, A.L., and Menon, V. (2003). Functional connectivity in the resting brain: A network analysis of the default mode hypothesis. PNAS *100*, 253–258.

Griffanti, L., Salimi-Khorshidi, G., Beckmann, C.F., Auerbach, E.J., Douaud, G., Sexton, C.E., Zsoldos, E., Ebmeier, K.P., Filippini, N., Mackay, C.E., et al. (2014). ICA-based artefact removal and accelerated fMRI acquisition for improved resting state network imaging. Neuroimage *95*, 232–247.

Haak, K.V., Marquand, A.F., and Beckmann, C.F. (2018). Connectopic mapping with resting-state fMRI. NeuroImage *170*, 83–94.

Hagler, D.J., Hatton, SeanN., Cornejo, M.D., Makowski, C., Fair, D.A., Dick, A.S., Sutherland, M.T., Casey, B.J., Barch, D.M., Harms, M.P., et al. (2019). Image processing and analysis methods for the Adolescent Brain Cognitive Development Study. NeuroImage *202*, 116091.

Hampson, M., Driesen, N.R., Skudlarski, P., Gore, J.C., and Constable, R.T. (2006). Brain connectivity related to working memory performance. J. Neurosci. *26*, 13338–13343.

Harrison, S.J., Woolrich, M.W., Robinson, E.C., Glasser, M.F., Beckmann, C.F., Jenkinson, M., and Smith, S.M. (2015). Large-scale probabilistic functional modes from resting state fMRI. Neuroimage *109*, 217–231.

He, T., Kong, R., Holmes, A.J., Nguyen, M., Sabuncu, M.R., Eickhoff, S.B., Bzdok, D., Feng, J., and Yeo, B.T.T. (2020). Deep neural networks and kernel regression achieve comparable accuracies for functional connectivity prediction of behavior and demographics. NeuroImage *206*, 116276.

van den Heuvel, M.P., Stam, C.J., Kahn, R.S., and Hulshoff Pol, H.E. (2009). Efficiency of functional brain networks and intellectual performance. J. Neurosci. *29*, 7619–7624.

Hong, S.-J., Xu, T., Nikolaidis, A., Smallwood, J., Margulies, D.S., Bernhardt, B., Vogelstein, J., and Milham, M.P. (2020). Toward a connectivity gradient-based framework for reproducible biomarker discovery. NeuroImage *223*, 117322.

Huntenburg, J.M., Bazin, P.-L., and Margulies, D.S. (2018). Large-Scale Gradients in Human Cortical Organization. Trends in Cognitive Sciences *22*, 21–31.

Ikeda, S., Kawano, K., Watanabe, S., Yamashita, O., and Kawahara, Y. (2022). Predicting behavior through dynamic modes in resting-state fMRI data. NeuroImage *247*, 118801.

Kong, R., Yang, Q., Gordon, E., Xue, A., Yan, X., Orban, C., Zuo, X.-N., Spreng, N., Ge, T., Holmes, A., et al. (2021a). Individual-Specific Areal-Level Parcellations Improve Functional Connectivity Prediction of Behavior. Cereb Cortex *31*, 4477–4500.

Kong, R., Li, J., Orban, C., Sabuncu, M.R., Liu, H., Schaefer, A., Sun, N., Zuo, X.-N., Holmes, A.J., Eickhoff, S.B., et al. (2019). Spatial Topography of Individual-Specific Cortical Networks Predicts Human Cognition, Personality, and Emotion. Cereb. Cortex *29*, 2533–2551.

Kong, X., Kong, R., Orban, C., Wang, P., Zhang, S., Anderson, K., Holmes, A., Murray, J.D., Deco, G., van den Heuvel, M., et al. (2021b). Sensory-motor cortices shape functional connectivity dynamics in the human brain. Nat Commun *12*, 6373.

Laumann, T.O., Gordon, E.M., Adeyemo, B., Snyder, A.Z., Joo, S.J., Chen, M.-Y., Gilmore, A.W., McDermott, K.B., Nelson, S.M., Dosenbach, N.U.F., et al. (2015). Functional System and Areal Organization of a Highly Sampled Individual Human Brain. Neuron *87*, 657–670.

Lee, M.H., Hacker, C.D., Snyder, A.Z., Corbetta, M., Zhang, D., Leuthardt, E.C., and Shimony, J.S. (2012). Clustering of resting state networks. PLoS ONE *7*, e40370.

Li, J., Kong, R., Liégeois, R., Orban, C., Tan, Y., Sun, N., Holmes, A.J., Sabuncu, M.R., Ge, T., and Yeo, B.T.T. (2019a). Global signal regression strengthens association between resting-state functional connectivity and behavior. NeuroImage *196*, 126–141.

Li, M., Wang, D., Ren, J., Langs, G., Stoecklein, S., Brennan, B.P., Lu, J., Chen, H., and Liu, H. (2019b). Performing group-level functional image analyses based on homologous functional regions mapped in individuals. PLOS Biology *17*, e2007032.

Liégeois, R., Li, J., Kong, R., Orban, C., Van De Ville, D., Ge, T., Sabuncu, M.R., and Yeo, B.T.T. (2019). Resting brain dynamics at different timescales capture distinct aspects of human behavior. Nature Communications *10*, 2317.

Margulies, D.S., Ghosh, S.S., Goulas, A., Falkiewicz, M., Huntenburg, J.M., Langs, G., Bezgin, G., Eickhoff, S.B., Castellanos, F.X., Petrides, M., et al. (2016). Situating the default-mode network along a principal gradient of macroscale cortical organization. Proc. Natl. Acad. Sci. U.S.A. *113*, 12574–12579.

Nickerson, L.D., Smith, S.M., Öngür, D., and Beckmann, C.F. (2017). Using Dual Regression to Investigate Network Shape and Amplitude in Functional Connectivity Analyses. Frontiers in Neuroscience *11*, 115.

Ooi, L.Q.R., Chen, J., Shaoshi, Z., Kong, R., Tam, A., Li, J., Dhamala, E., Zhou, J.H., Holmes, A.J., and Yeo, B.T.T. (2022). Comparison of individualized behavioral predictions across anatomical, diffusion and functional connectivity MRI. NeuroImage 119636.

Paquola, C., Wael, R.V.D., Wagstyl, K., Bethlehem, R.A.I., Hong, S.-J., Seidlitz, J., Bullmore, E.T., Evans, A.C., Misic, B., Margulies, D.S., et al. (2019). Microstructural and functional gradients are increasingly dissociated in transmodal cortices. PLOS Biology *17*, e3000284.

Pervaiz, U., Vidaurre, D., Woolrich, M.W., and Smith, S.M. (2020). Optimising network modelling methods for fMRI. NeuroImage *211*, 116604.

Power, J.D., Cohen, A.L., Nelson, S.M., Wig, G.S., Barnes, K.A., Church, J.A., Vogel, A.C., Laumann, T.O., Miezin, F.M., Schlaggar, B.L., et al. (2011). Functional Network Organization of the Human Brain. Neuron *72*, 665–678.

Rapuano, K.M., Rosenberg, M.D., Maza, M.T., Dennis, N.J., Dorji, M., Greene, A.S., Horien, C., Scheinost, D., Todd Constable, R., and Casey, B.J. (2020). Behavioral and brain signatures of substance use vulnerability in childhood. Developmental Cognitive Neuroscience *46*, 100878.

Recht, B., Roelofs, R., Schmidt, L., and Shankar, V. (2019). Do ImageNet Classifiers Generalize to ImageNet? In Proceedings of the 36th International Conference on Machine Learning, (PMLR), pp. 5389–5400.

Robinson, E.C., Jbabdi, S., Glasser, M.F., Andersson, J., Burgess, G.C., Harms, M.P., Smith, S.M., Van Essen, D.C., and Jenkinson, M. (2014). MSM: a new flexible framework for Multimodal Surface Matching. Neuroimage *100*, 414–426.

Salimi-Khorshidi, G., Douaud, G., Beckmann, C.F., Glasser, M.F., Griffanti, L., and Smith, S.M. (2014). Automatic denoising of functional MRI data: combining independent component analysis and hierarchical fusion of classifiers. Neuroimage *90*, 449–468.

Schaefer, A., Kong, R., Gordon, E.M., Laumann, T.O., Zuo, X.-N., Holmes, A.J., Eickhoff, S.B., and Yeo, B.T.T. (2018). Local-Global Parcellation of the Human Cerebral Cortex from Intrinsic Functional Connectivity MRI. Cerebral Cortex *28*, 3095–3114.

Shen, X., Tokoglu, F., Papademetris, X., and Constable, R.T. (2013). Groupwise whole-brain parcellation from resting-state fMRI data for network node identification. NeuroImage *82*, 403–415.

Shen, X., Finn, E.S., Scheinost, D., Rosenberg, M.D., Chun, M.M., Papademetris, X., and Constable, R.T. (2017). Using connectome-based predictive modeling to predict individual behavior from brain connectivity. Nat Protoc *12*, 506–518.

Siegel, J.S., Mitra, A., Laumann, T.O., Seitzman, B.A., Raichle, M., Corbetta, M., and Snyder, A.Z. (2017). Data Quality Influences Observed Links Between Functional Connectivity and Behavior. Cerebral Cortex *27*, 4492–4502.

Siegel, J.S., Ramsey, L.E., Snyder, A.Z., Metcalf, N.V., Chacko, R.V., Weinberger, K., Baldassarre, A., Hacker, C.D., Shulman, G.L., and Corbetta, M. (2016). Disruptions of network connectivity predict impairment in multiple behavioral domains after stroke. Proceedings of the National Academy of Sciences *113*, E4367–E4376.

Smith, S.M., Nichols, T.E., Vidaurre, D., Winkler, A.M., Behrens, T.E.J., Glasser, M.F., Ugurbil, K., Barch, D.M., Van Essen, D.C., and Miller, K.L. (2015). A positive-negative mode of population covariation links brain connectivity, demographics and behavior. Nature Neuroscience *18*, 1565–1567.

Smith, S.M., Fox, P.T., Miller, K.L., Glahn, D.C., Fox, P.M., Mackay, C.E., Filippini, N., Watkins, K.E., Toro, R., Laird, A.R., et al. (2009). Correspondence of the brain's functional architecture during activation and rest. PNAS *106*, 13040–13045.

Smith, S.M., Beckmann, C.F., Andersson, J., Auerbach, E.J., Bijsterbosch, J., Douaud, G., Duff, E., Feinberg, D.A., Griffanti, L., Harms, M.P., et al. (2013). Resting-state fMRI in the Human Connectome Project. NeuroImage *80*, 144–168.

Smith, S.M., Miller, K.L., Salimi-Khorshidi, G., Webster, M., Beckmann, C.F., Nichols, T.E., Ramsey, J.D., and Woolrich, M.W. (2011). Network modelling methods for FMRI. NeuroImage *54*, 875–891.

Thompson, W.H., Wright, J., Bissett, P.G., and Poldrack, R.A. (2020). Dataset decay and the problem of sequential analyses on open datasets. ELife *9*, e53498.

Tian, Y., Margulies, D.S., Breakspear, M., and Zalesky, A. (2020). Topographic organization of the human subcortex unveiled with functional connectivity gradients. Nat Neurosci *23*, 1421–1432.

Van Essen, D.C., Ugurbil, K., Auerbach, E., Barch, D., Behrens, T.E.J., Bucholz, R., Chang, A., Chen, L., Corbetta, M., Curtiss, S.W., et al. (2012a). The Human Connectome Project: a data acquisition perspective. Neuroimage *62*, 2222–2231.

Van Essen, D.C., Glasser, M.F., Dierker, D.L., Harwell, J., and Coalson, T. (2012b). Parcellations and hemispheric asymmetries of human cerebral cortex analyzed on surface-based atlases. Cereb. Cortex *22*, 2241–2262.

Vidaurre, D., Smith, S.M., and Woolrich, M.W. (2017). Brain network dynamics are hierarchically organized in time. Proc Natl Acad Sci U S A *114*, 12827–12832.

Vos de Wael, R., Benkarim, O., Paquola, C., Lariviere, S., Royer, J., Tavakol, S., Xu, T., Hong, S.-J., Langs, G., Valk, S., et al. (2020). BrainSpace: a toolbox for the analysis of macroscale gradients in neuroimaging and connectomics datasets. Commun Biol *3*, 1–10.

Wang, P., Kong, R., Kong, X., Liégeois, R., Orban, C., Deco, G., van den Heuvel, M.P., and Thomas Yeo, B.T. (2019). Inversion of a large-scale circuit model reveals a cortical hierarchy in the dynamic resting human brain. Sci Adv *5*, eaat7854.

Wig, G.S., Laumann, T.O., and Petersen, S.E. (2014). An approach for parcellating human cortical areas using resting-state correlations. NeuroImage *93*, 276–291.

Yeo, B.T.T., Krienen, F.M., Sepulcre, J., Sabuncu, M.R., Lashkari, D., Hollinshead, M., Roffman, J.L., Smoller, J.W., Zöllei, L., Polimeni, J.R., et al. (2011). The organization of the human cerebral cortex estimated by intrinsic functional connectivity. Journal of Neurophysiology *106*, 1125–1165.

Zuo, X.-N., Kelly, C., Adelstein, J.S., Klein, D.F., Castellanos, F.X., and Milham, M.P. (2010). Reliable intrinsic connectivity networks: Test–retest evaluation using ICA and dual regression approach. NeuroImage *49*, 2163–2177.

Supplementary Figures

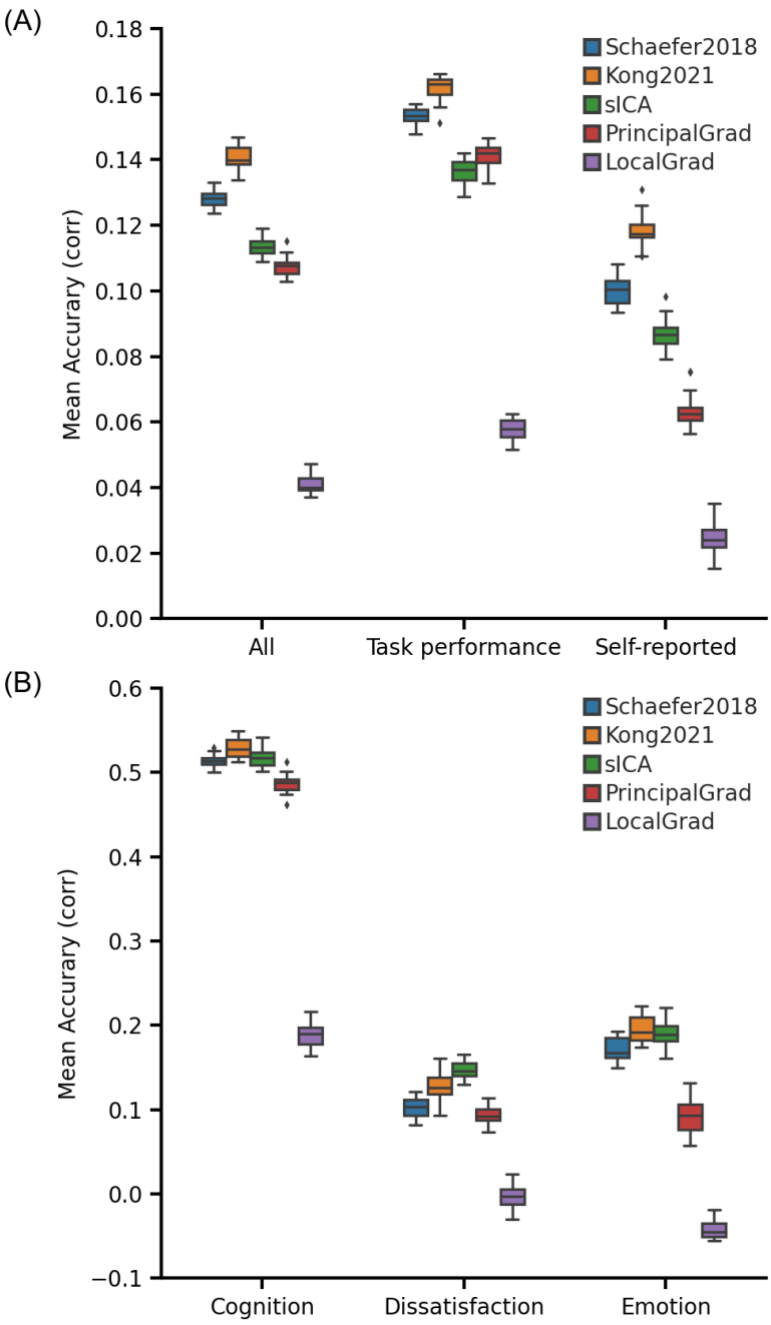

Figure S1. Individual-specific hard-parcellation approach Kong2021 compared favorably with other approaches for linear ridge regression (LRR) in the HCP dataset. (A) Average prediction accuracies (Pearson's correlation) of all 58 behavioral measures, task performance measures, and self-reported measures. (B) Prediction accuracies (Pearson's correlation) of three behavioral components: cognition, dissatisfaction, and emotion. Boxplots utilized default Python seaborn parameters, that is, box shows median and interquartile range (IQR). Whiskers indicate 1.5 IQR.

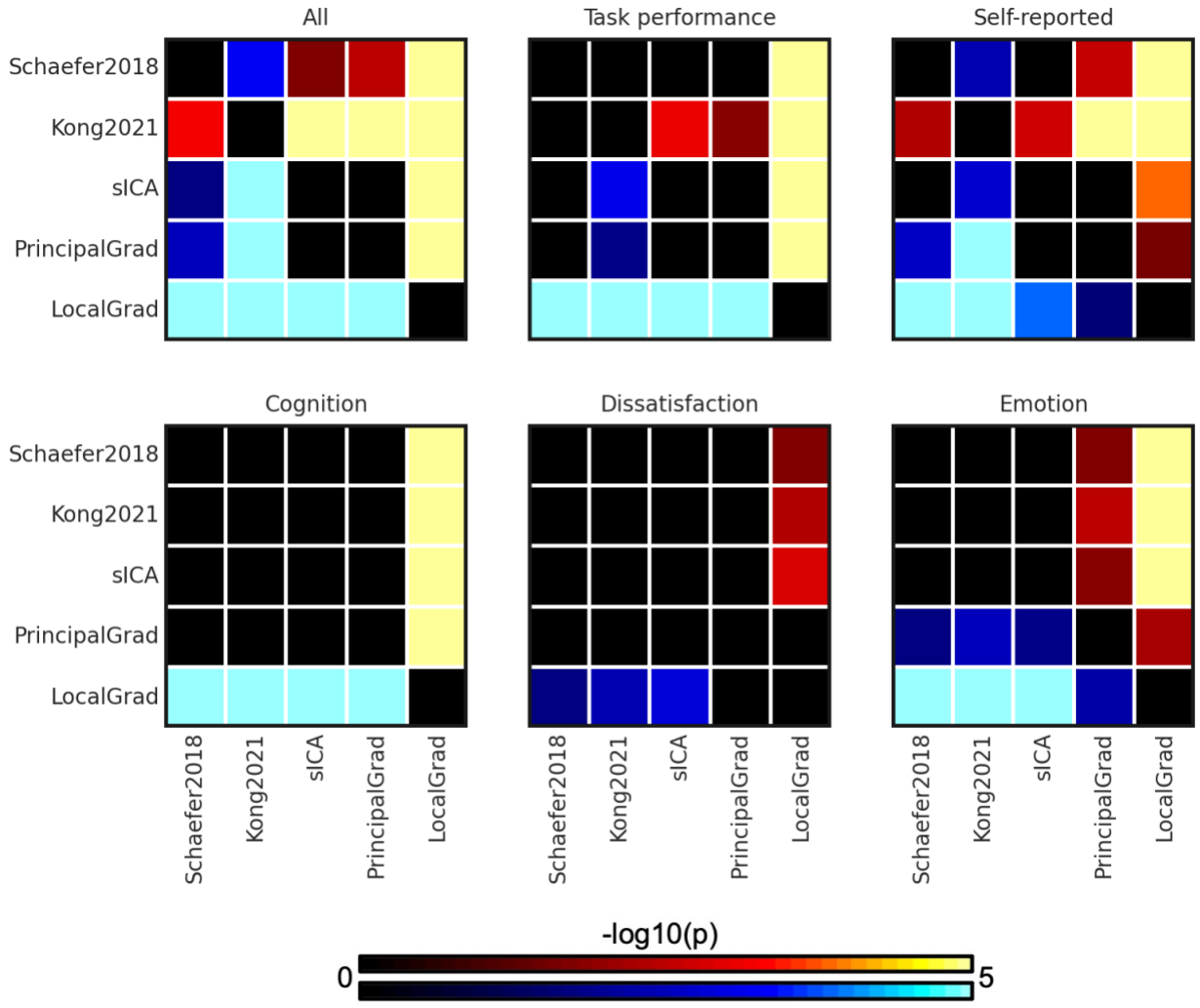

Figure S2. P values (-log10(p)) of comparing prediction accuracies between each pair of approaches for linear ridge regression (LRR) in the HCP dataset. Non-black colors denote significantly different prediction performances after correcting for multiple comparisons with FDR $q < 0.05$. Bright colors indicate small p values, dark colors indicate large p values. For each pair of comparisons, warm colors represent higher prediction accuracies of the "row" approach than the "column" approach. Individual-specific hard-parcellation approach Kong2021 compared favorably with the other approaches, as can be seen from warm colors along the rows corresponding to Kong2021.

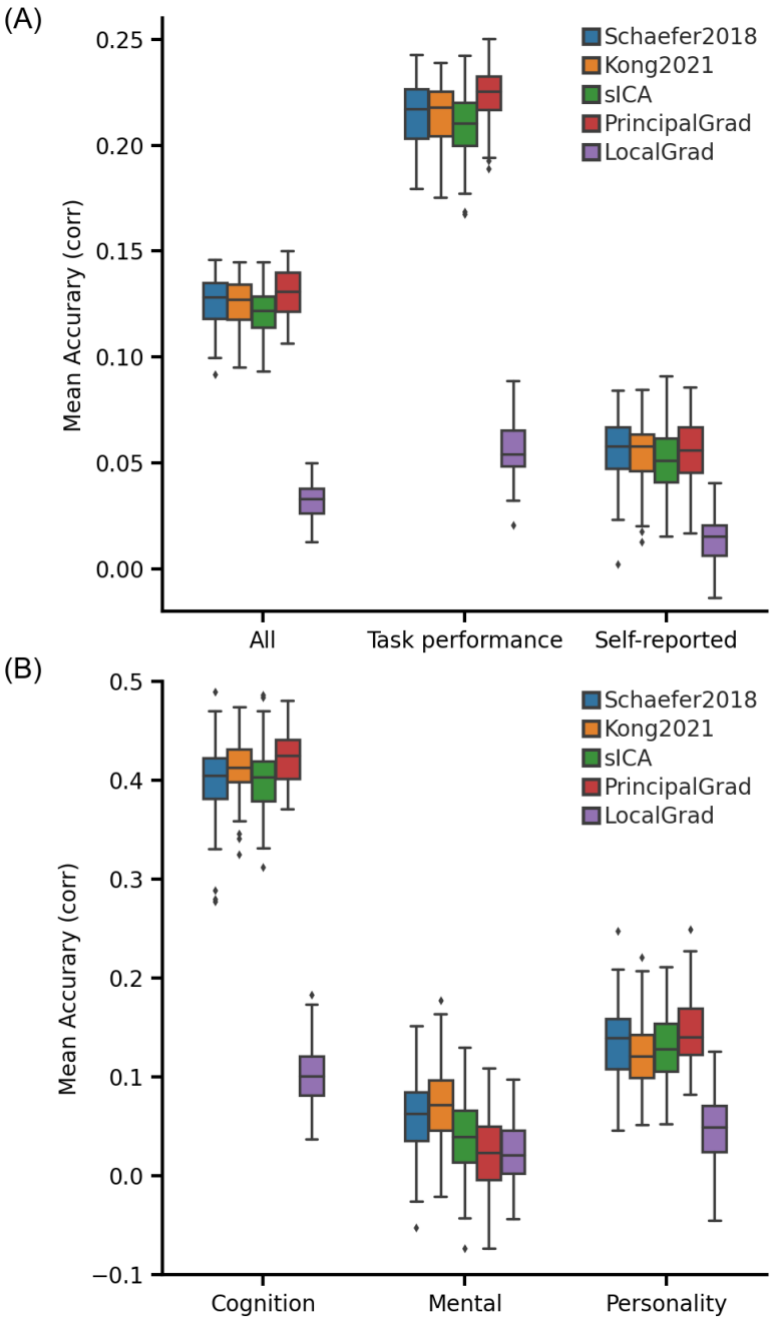

Figure S3. Principal gradient approach achieves comparable behavioral prediction performance as parcellation approaches for linear ridge regression (LRR) in the ABCD dataset. (A) Average prediction accuracies (Pearson's correlation) of all 36 behavioral measures, task performance measures, and self-reported measures. (B) Prediction accuracies (Pearson's correlation) of three behavioral components: cognition, mental health, and personality. Boxplots utilized default Python seaborn parameters, that is, box shows median and interquartile range (IQR). Whiskers indicate 1.5 IQR. The principal gradient approach PrincipalGrad was numerically the best for most cases, but there was largely no statistical difference among the approaches.

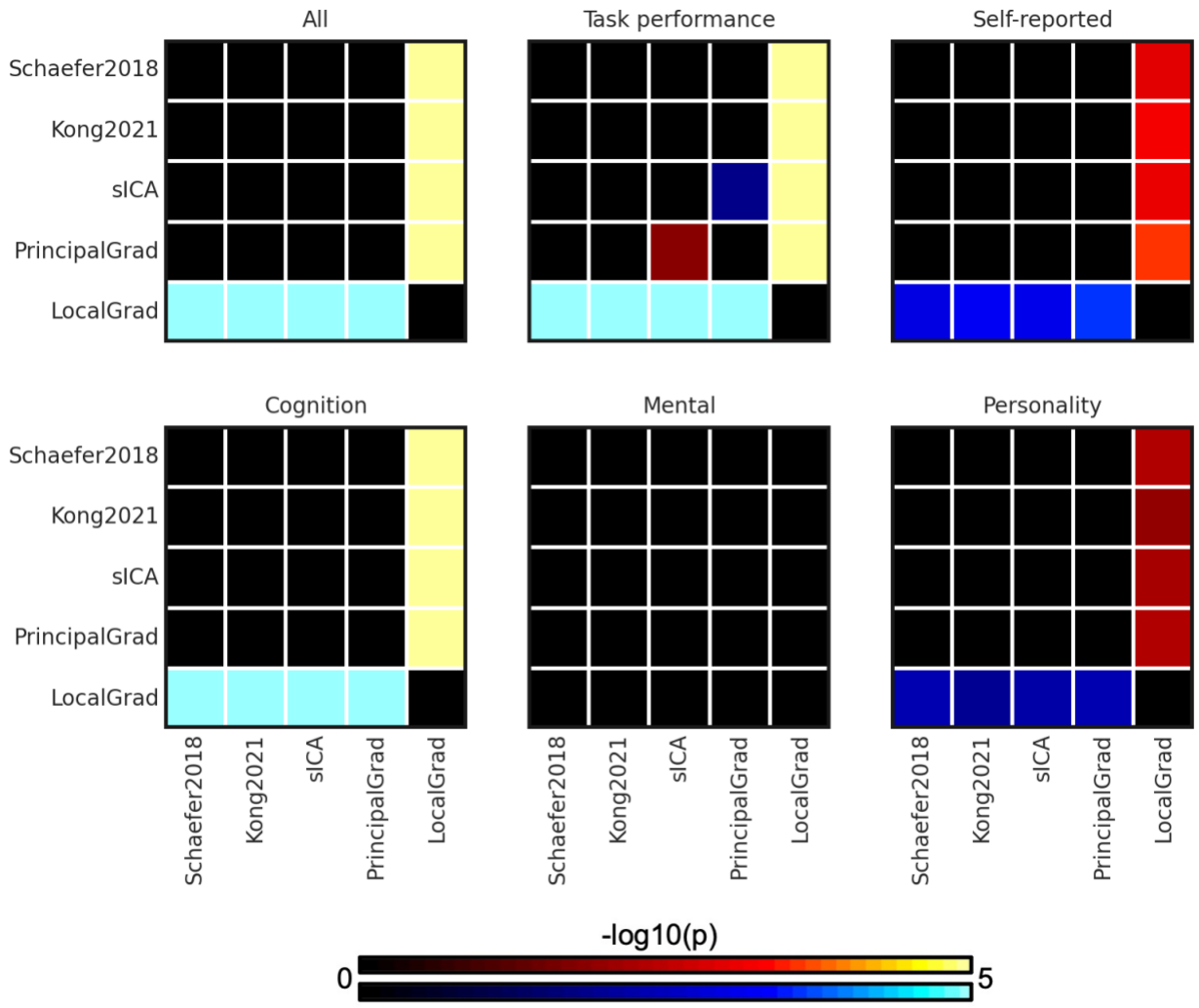

Figure S4. P values (-log10(p)) of comparing prediction accuracies between each pair of approaches for linear ridge regression (LRR) in the ABCD dataset. Non-black colors denote significantly different prediction performances after correcting for multiple comparisons with FDR $q < 0.05$. Bright colors indicate small p values, dark colors indicate large p values. For each pair of comparisons, warm colors represent higher prediction accuracies of the "row" approach than the "column" approach. There was no statistical difference among most approaches.

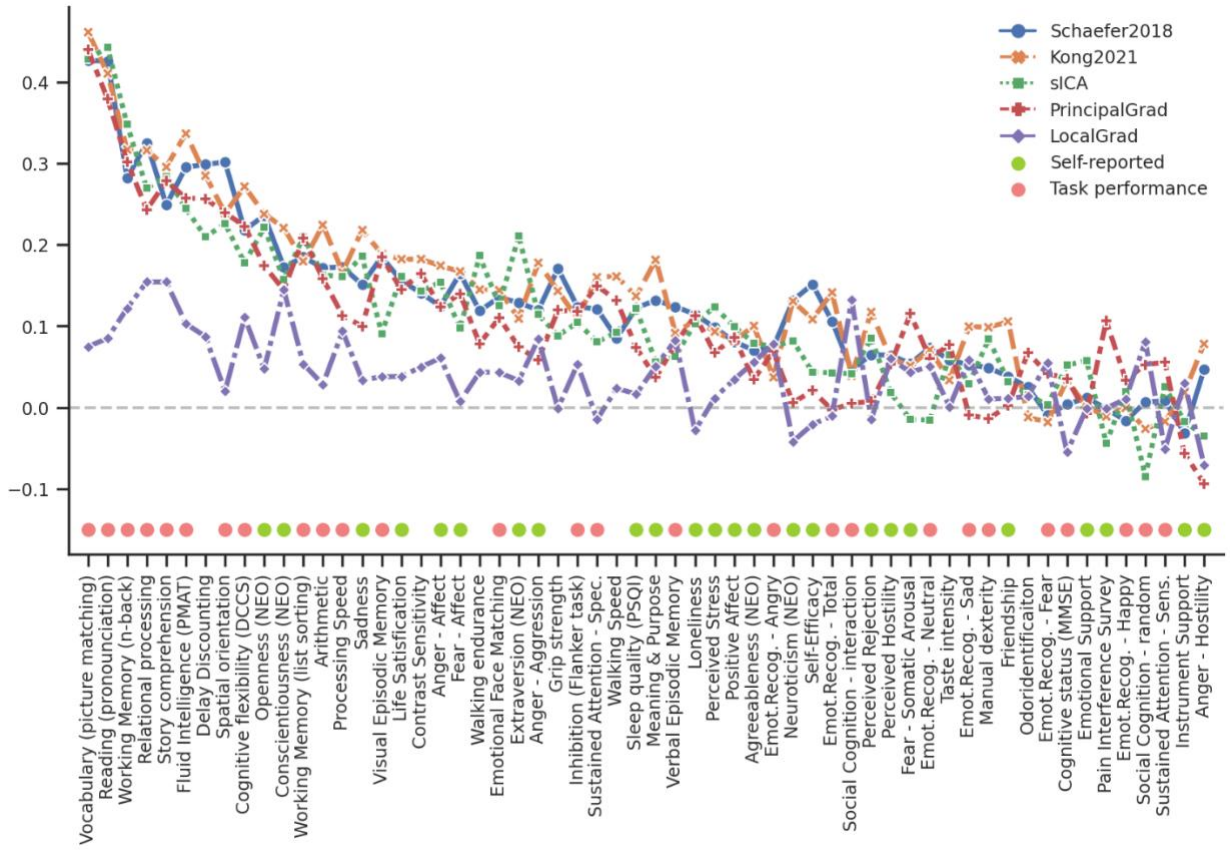

Figure S5. Task performance measures were predicted better than self-reported measures across different gradient and parcellation approaches with optimized resolutions for LRR in the HCP dataset. 58 behavioral measures were ordered based on average prediction accuracies across Schaefer2018, Kong2021, sICA, PrincipalGrad, and LocalGrad. Pink circles indicate task performance measures. Green circles indicate self-reported measures. Boxplots utilized default Python seaborn parameters, that is, box shows median and interquartile range (IQR). Whiskers indicate 1.5 IQR. Designation of behavioral measures into “self-reported” and “task-performance” measures followed previous studies (Li et al., 2019a; Liégeois et al., 2019; Kong et al., 2021a).

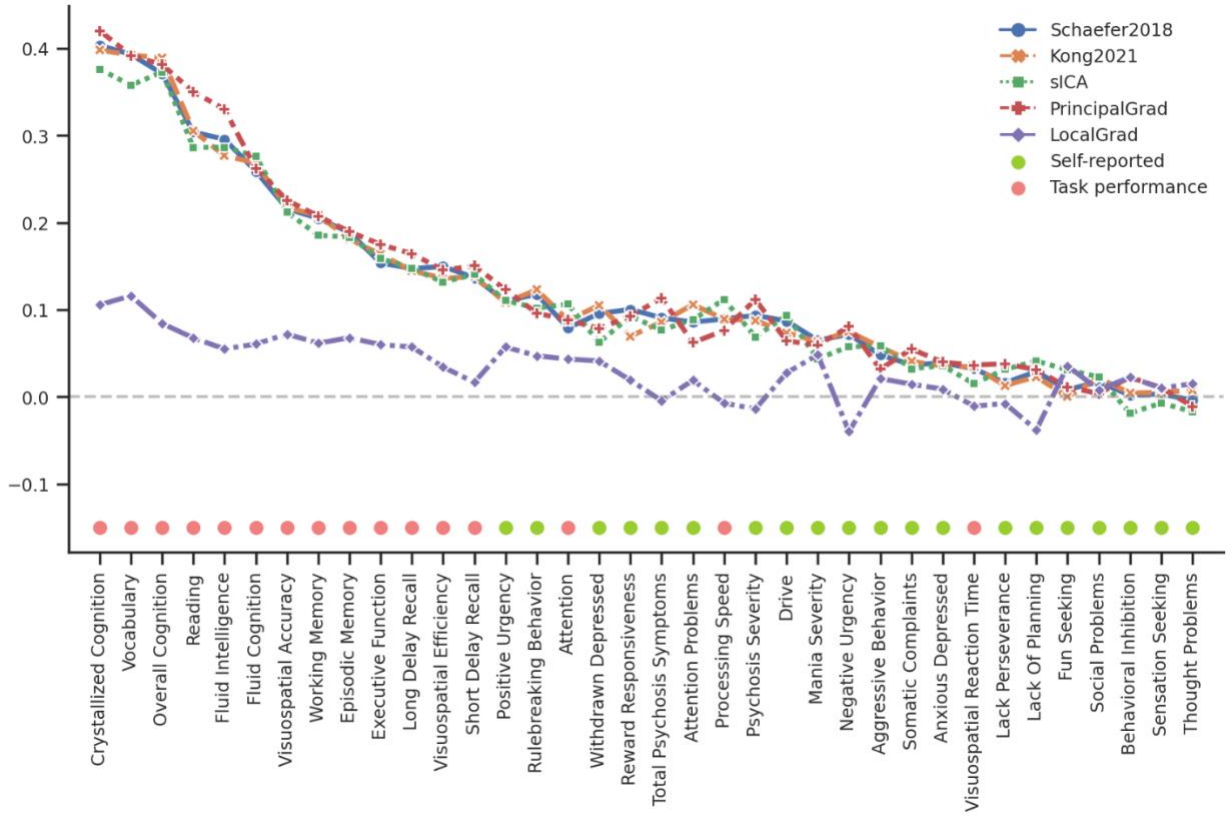

Figure S6. Task performance measures were predicted better than self-reported measures across different gradient and parcellation approaches with optimized resolutions for LRR in the ABCD dataset. 36 behavioral measures were ordered based on average prediction accuracies across Schaefer2018, Kong2021, sICA, PrincipalGrad, and LocalGrad. Pink circles indicate task performance measures. Green circles indicate self-reported measures. Boxplots utilized default Python seaborn parameters, that is, box shows median and interquartile range (IQR). Whiskers indicate 1.5 IQR. Designation of behavioral measures into "self-reported" and "task-performance" measures based on ABCD behavioral measures description (Li et al., 2019a; Liégeois et al., 2019; Kong et al., 2021a).

(A) Schaefer2018

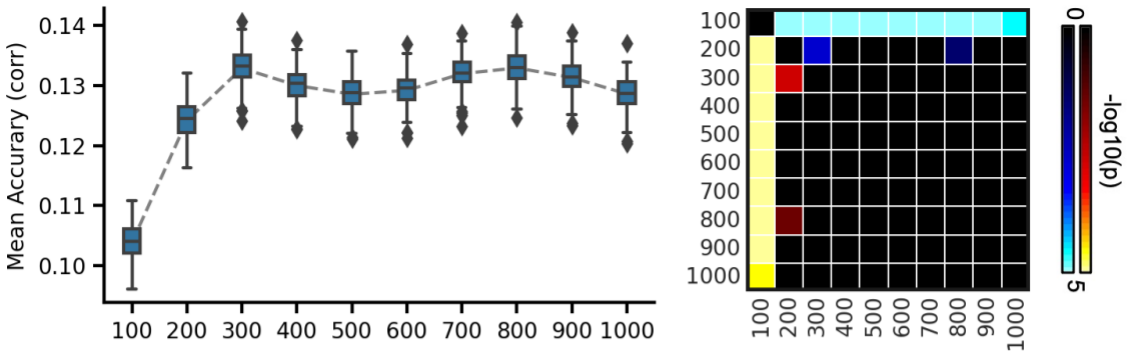

(B) Kong2021

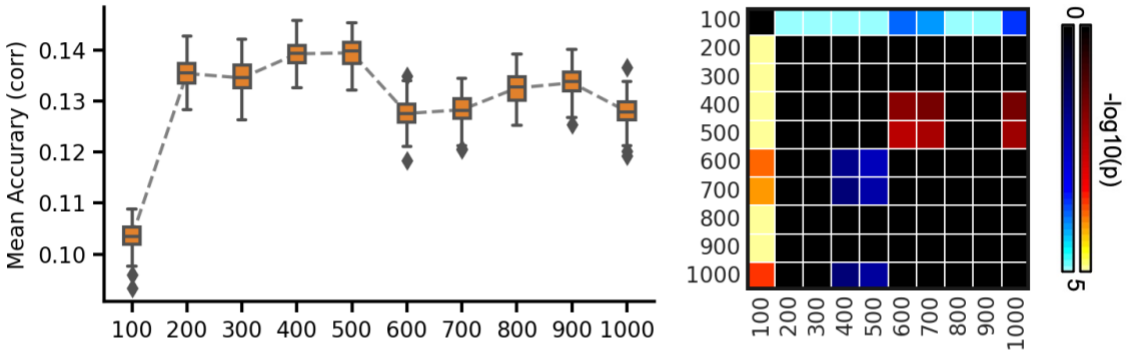

(C) sICA

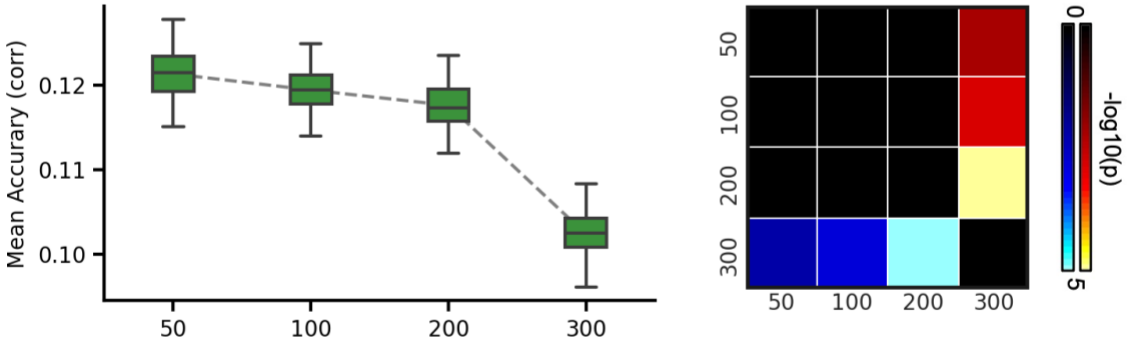

(D) PrincipalGrad

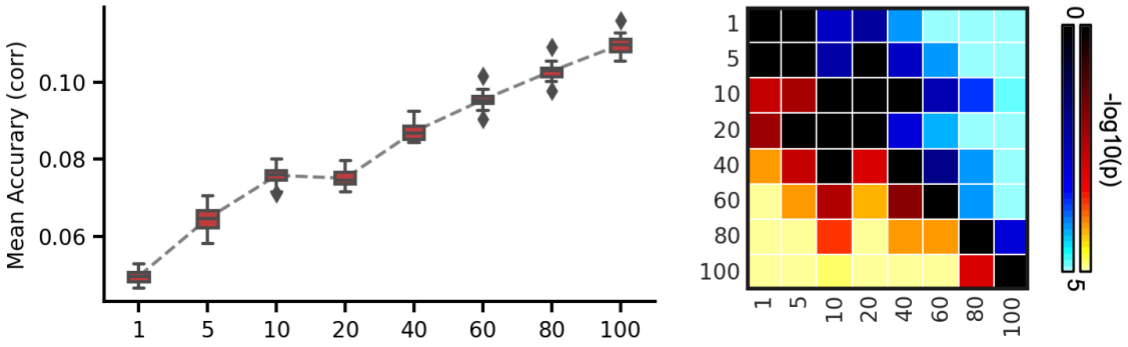

Figure S7. Average prediction accuracies (Pearson's correlation) of all 58 behavioral measures vary across resolutions for gradient and parcellation approaches using LRR in the HCP dataset. (A) Prediction accuracies and p values of the hard-parcellation Schaefer2018 with 100 to 1000 ROIs. (B) Prediction accuracies and p values of the hard-parcellation Kong2021 with 100 to 1000 ROIs. (C) Prediction accuracies and p values of the soft-parcellation sICA with 50 to 300 components. (D) Prediction accuracies and p values of the principal gradient PrincipalGrad with 1 to 100 gradients. Boxplots utilized default Python seaborn parameters, that is, box shows median and interquartile range (IQR). Whiskers indicate 1.5 IQR. P values (-log10(p)) were computed between prediction accuracies of each pair of resolutions. Non-black colors denote significantly different prediction performances after correcting for multiple comparisons with FDR $q < 0.05$. Bright colors indicate small p values, dark colors indicate large p values. For each pair of comparisons, warm colors represent higher prediction accuracies of the "row" resolution than the "column" resolution.

(A) Schaefer2018

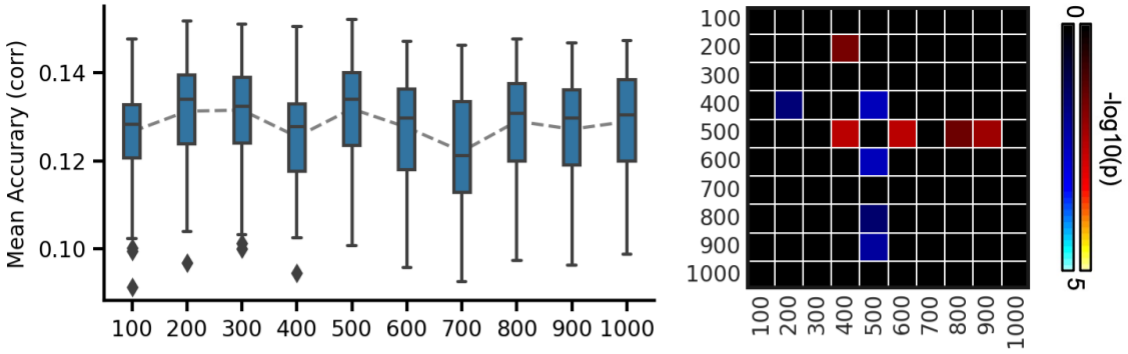

(B) Kong2021

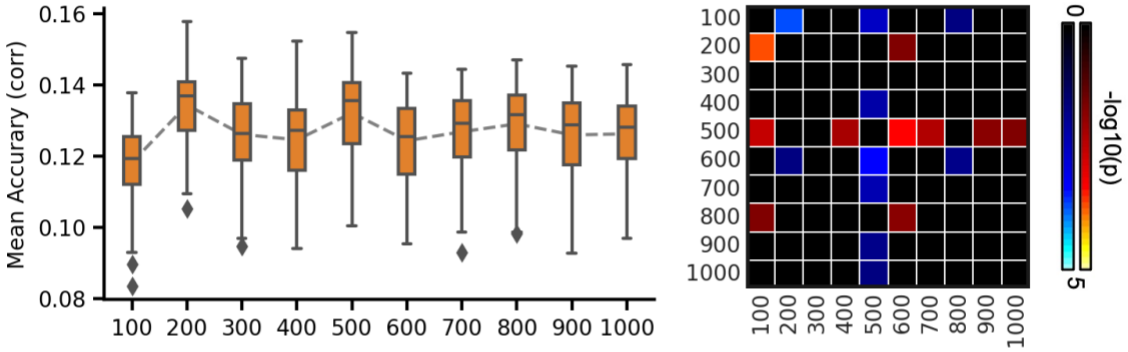

(C) sICA

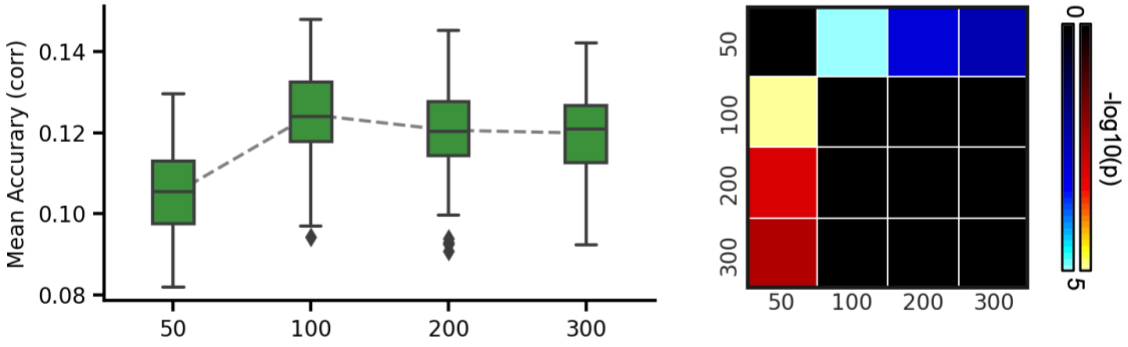

(D) PrincipalGrad

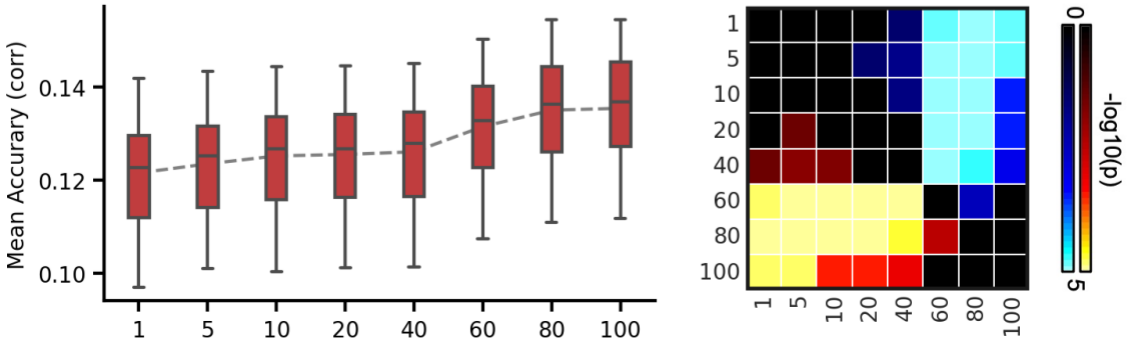

Figure S8. Average prediction accuracies (Pearson's correlation) of all 36 behavioral measures vary across resolutions for gradient and parcellation approaches using LRR in the ABCD dataset. (A) Prediction accuracies and p values of the hard-parcellation Schaefer2018 with 100 to 1000 ROIs. (B) Prediction accuracies and p values of the hard-parcellation Kong2021 with 100 to 1000 ROIs. (C) Prediction accuracies and p values of the soft-parcellation sICA with 50 to 300 components. (D) Prediction accuracies and p values of the principal gradient PrincipalGrad with 1 to 100 gradients. Boxplots utilized default Python seaborn parameters, that is, box shows median and interquartile range (IQR). Whiskers indicate 1.5 IQR. P values (-log10(p)) were computed between prediction accuracies of each pair of resolutions. Non-black colors denote significantly different prediction performances after correcting for multiple comparisons with FDR $q < 0.05$. Bright colors indicate small p values, dark colors indicate large p values. For each pair of comparisons, warm colors represent higher prediction accuracies of the "row" resolution than the "column" resolution.

(A) Schaefer2018

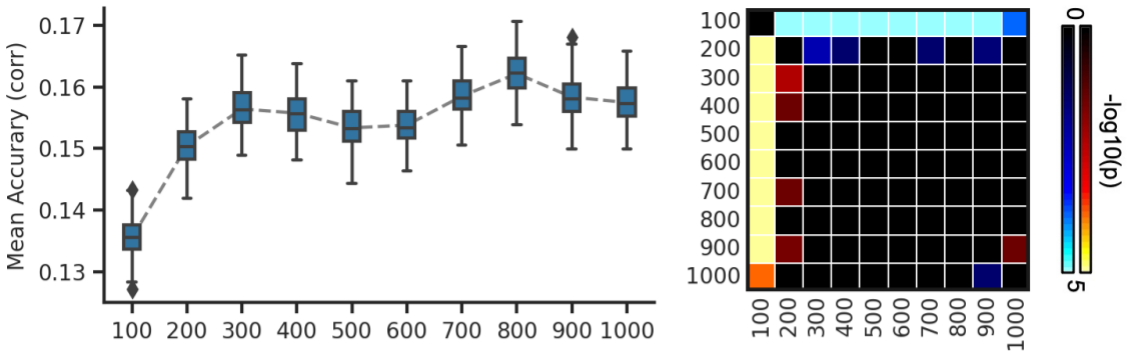

(B) Kong2021

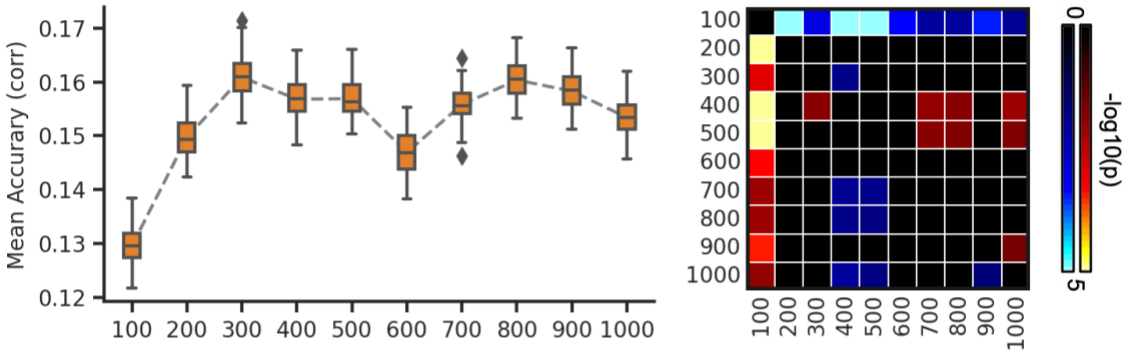

(C) sICA

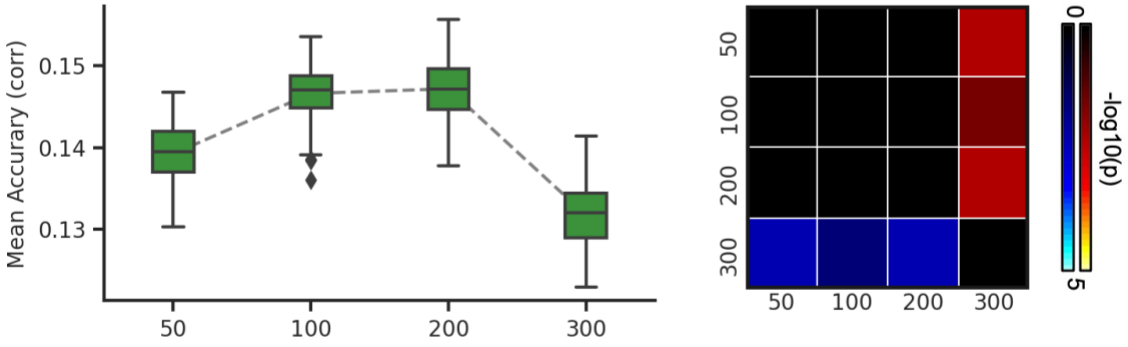

(D) PrincipalGrad

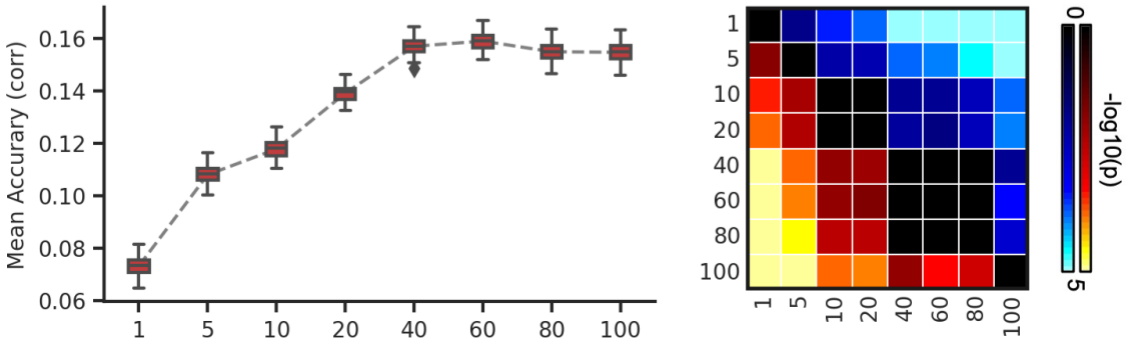

Figure S9. Average prediction accuracies (Pearson's correlation) of task performance measures vary across resolutions for gradient and parcellation approaches using KRR in the HCP dataset. (A) Prediction accuracies and p values of the hard-parcellation Schaefer2018 with 100 to 1000 ROIs. (B) Prediction accuracies and p values of the hard-parcellation Kong2021 with 100 to 1000 ROIs. (C) Prediction accuracies and p values of the soft-parcellation sICA with 50 to 300 components. (D) Prediction accuracies and p values of the principal gradient PrincipalGrad with 1 to 100 gradients. Boxplots utilized default Python seaborn parameters, that is, box shows median and interquartile range (IQR). Whiskers indicate 1.5 IQR. P values (-log10(p)) were computed between prediction accuracies of each pair of resolutions. Non-black colors denote significantly different prediction performances after correcting for multiple comparisons with FDR $q < 0.05$. Bright colors indicate small p values, dark colors indicate large p values. For each pair of comparisons, warm colors represent higher prediction accuracies of the "row" resolution than the "column" resolution.

(A) Schaefer2018

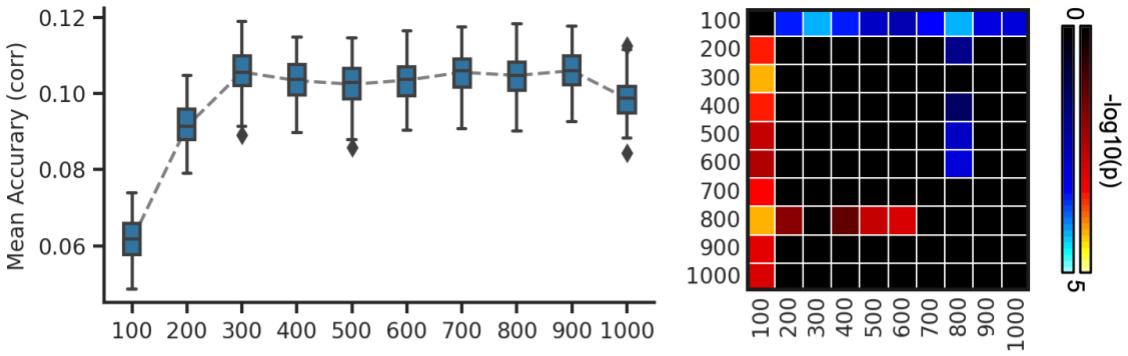

(B) Kong2021

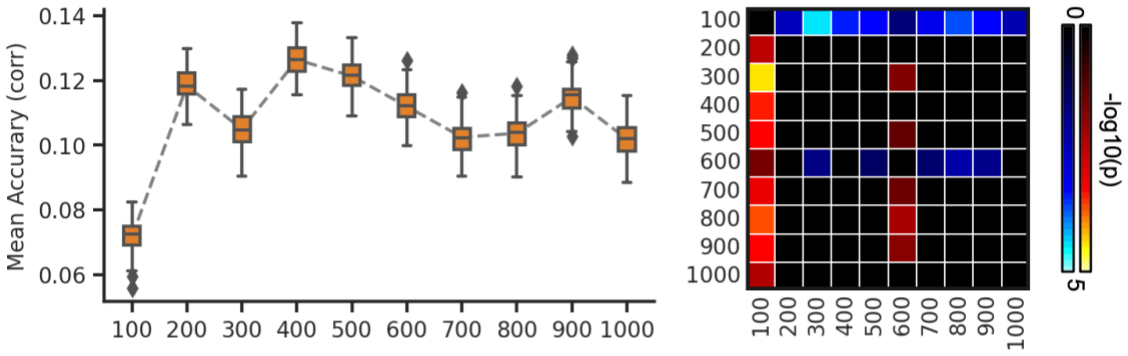

(C) sICA

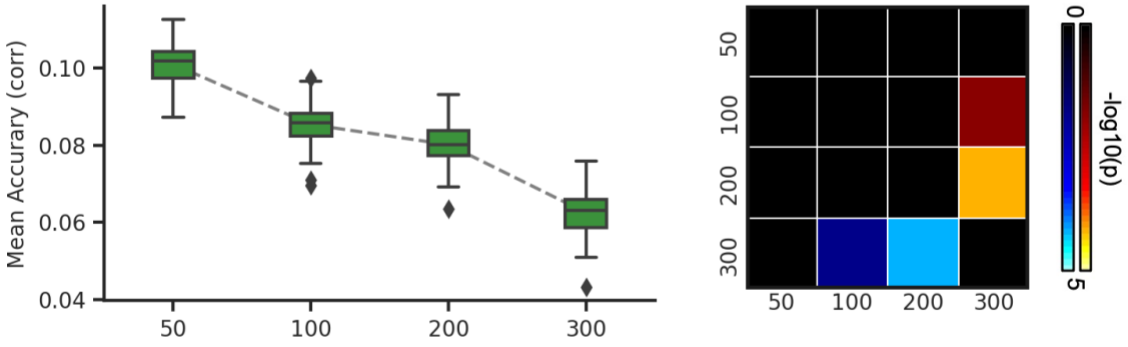

(D) PrincipalGrad

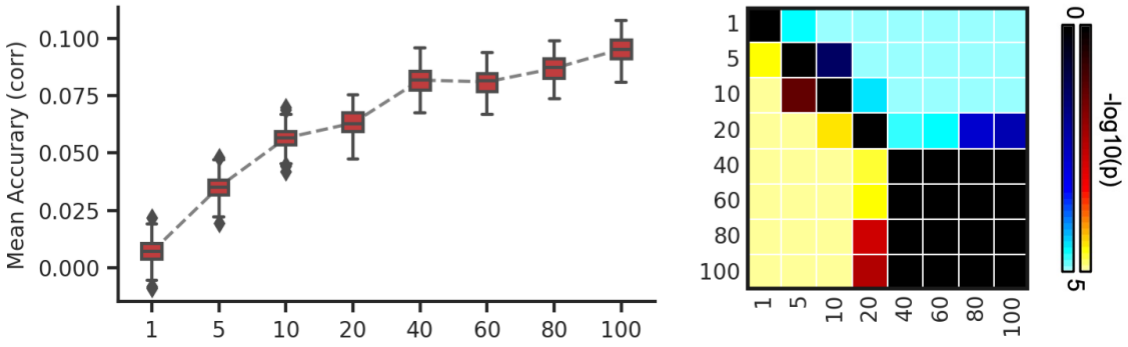

Figure S10. Average prediction accuracies (Pearson's correlation) of self-reported measures vary across resolutions for gradient and parcellation approaches using KRR in the HCP dataset. (A) Prediction accuracies and p values of the hard-parcellation Schaefer2018 with 100 to 1000 ROIs. (B) Prediction accuracies and p values of the hard-parcellation Kong2021 with 100 to 1000 ROIs. (C) Prediction accuracies and p values of the soft-parcellation sICA with 50 to 300 components. (D) Prediction accuracies and p values of the principal gradient PrincipalGrad with 1 to 100 gradients. Boxplots utilized default Python seaborn parameters, that is, box shows median and interquartile range (IQR). Whiskers indicate 1.5 IQR. P values (-log10(p)) were computed between prediction accuracies of each pair of resolutions. Non-black colors denote significantly different prediction performances after correcting for multiple comparisons with FDR $q < 0.05$. Bright colors indicate small p values, dark colors indicate large p values. For each pair of comparisons, warm colors represent higher prediction accuracies of the "row" resolution than the "column" resolution.

(A) Schaefer2018

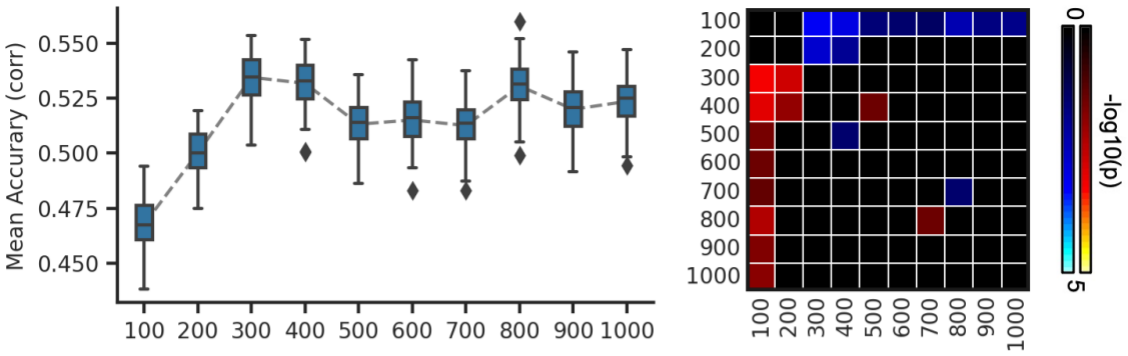

(B) Kong2021

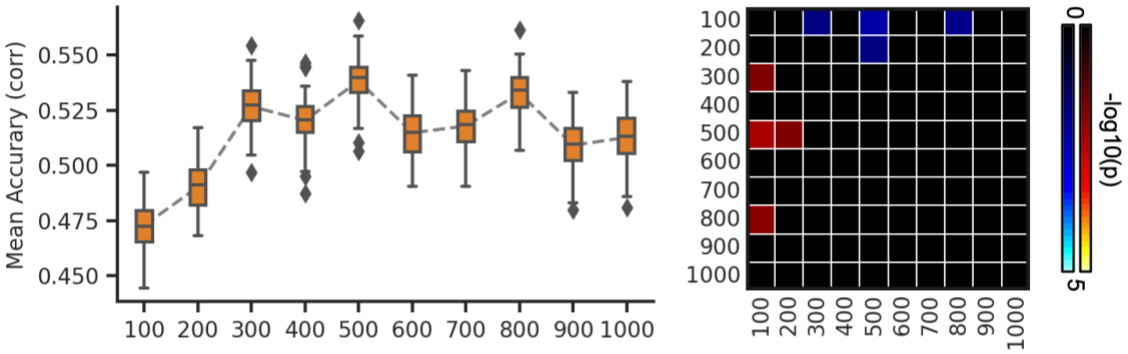

(C) sICA

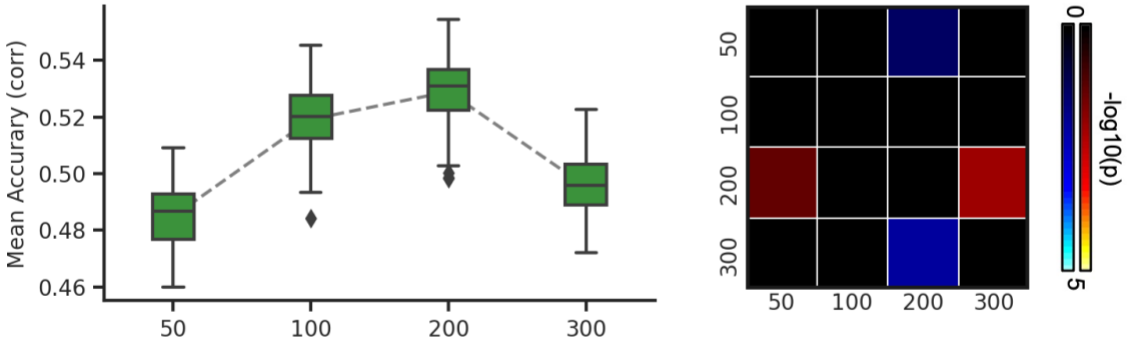

(D) PrincipalGrad

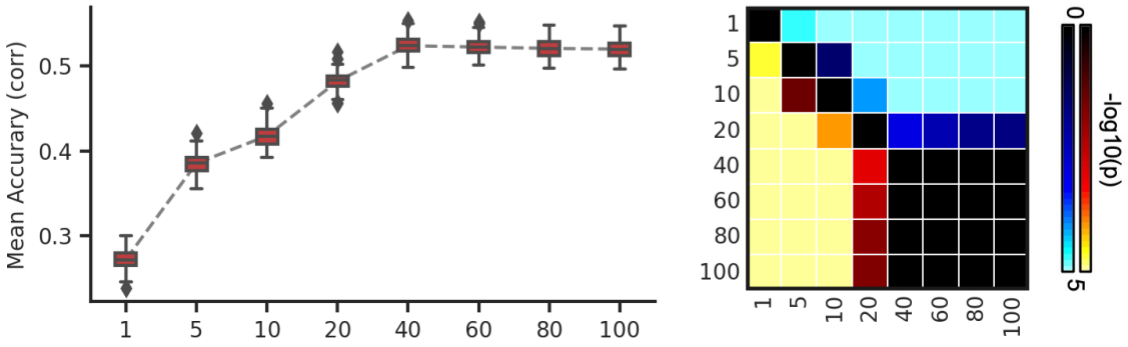

Figure S11. Prediction accuracies (Pearson's correlation) of cognition vary across resolutions for gradient and parcellation approaches using KRR in the HCP dataset. (A) Prediction accuracies and p values of the hard-parcellation Schaefer2018 with 100 to 1000 ROIs. (B) Prediction accuracies and p values of the hard-parcellation Kong2021 with 100 to 1000 ROIs. (C) Prediction accuracies and p values of the soft-parcellation sICA with 50 to 300 components. (D) Prediction accuracies and p values of the principal gradient PrincipalGrad with 1 to 100 gradients. Boxplots utilized default Python seaborn parameters, that is, box shows median and interquartile range (IQR). Whiskers indicate 1.5 IQR. P values (-log10(p)) were computed between prediction accuracies of each pair of resolutions. Non-black colors denote significantly different prediction performances after correcting for multiple comparisons with FDR $q < 0.05$. Bright colors indicate small p values, dark colors indicate large p values. For each pair of comparisons, warm colors represent higher prediction accuracies of the "row" resolution than the "column" resolution.

(A) Schaefer2018

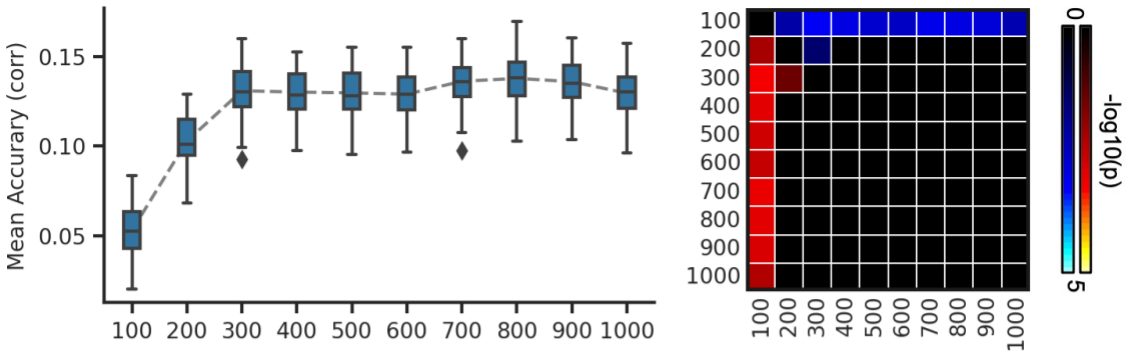

(B) Kong2021

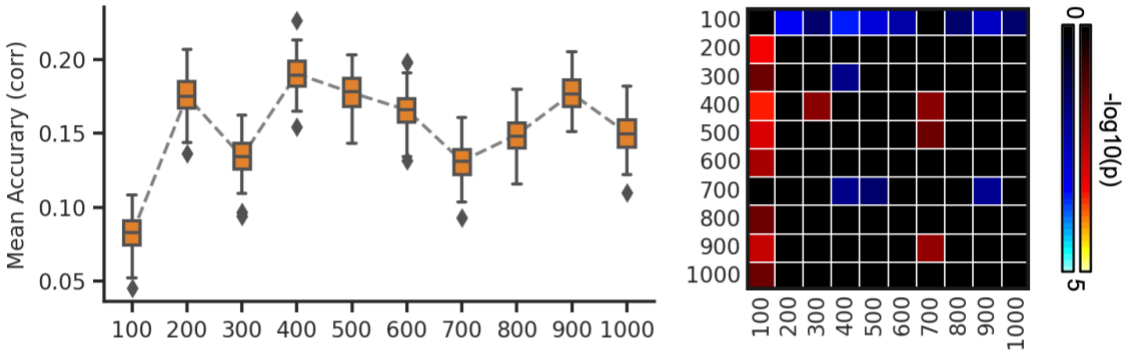

(C) sICA

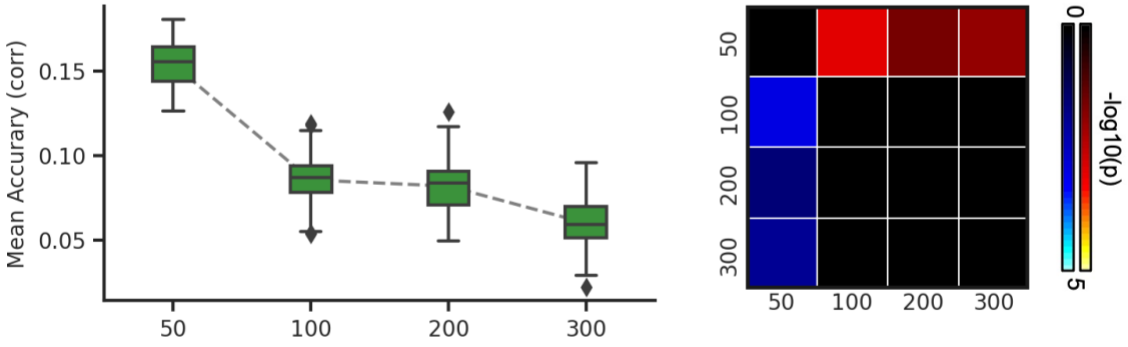

(D) PrincipalGrad

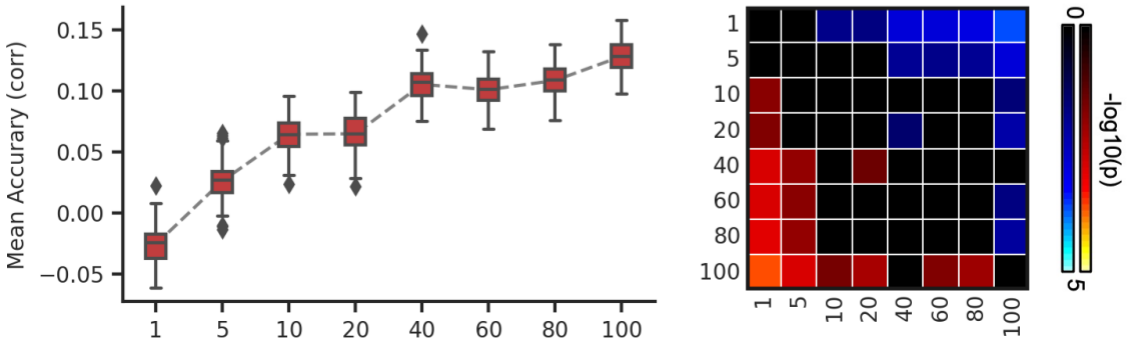

Figure S12. Prediction accuracies (Pearson's correlation) of dissatisfaction vary across resolutions for gradient and parcellation approaches using KRR in the HCP dataset. (A) Prediction accuracies and p values of the hard-parcellation Schaefer2018 with 100 to 1000 ROIs. (B) Prediction accuracies and p values of the hard-parcellation Kong2021 with 100 to 1000 ROIs. (C) Prediction accuracies and p values of the soft-parcellation sICA with 50 to 300 components. (D) Prediction accuracies and p values of the principal gradient PrincipalGrad with 1 to 100 gradients. Boxplots utilized default Python seaborn parameters, that is, box shows median and interquartile range (IQR). Whiskers indicate 1.5 IQR. P values (-log10(p)) were computed between prediction accuracies of each pair of resolutions. Non-black colors denote significantly different prediction performances after correcting for multiple comparisons with FDR $q < 0.05$. Bright colors indicate small p values, dark colors indicate large p values. For each pair of comparisons, warm colors represent higher prediction accuracies of the "row" resolution than the "column" resolution.

(A) Schaefer2018

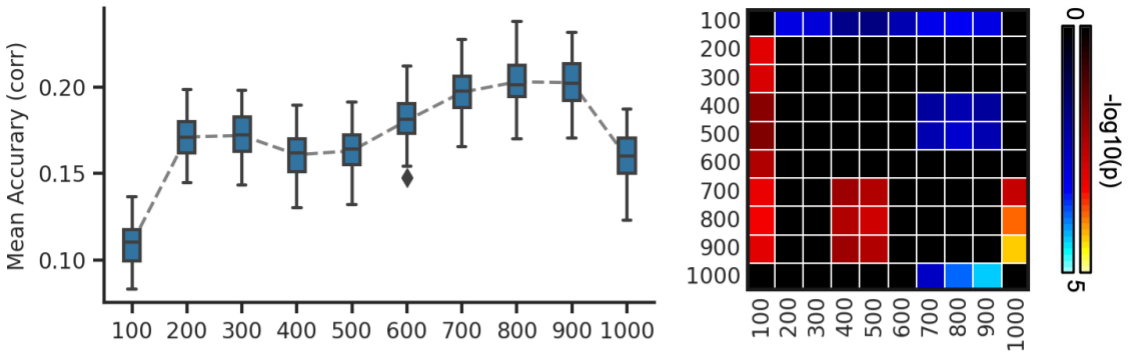

(B) Kong2021

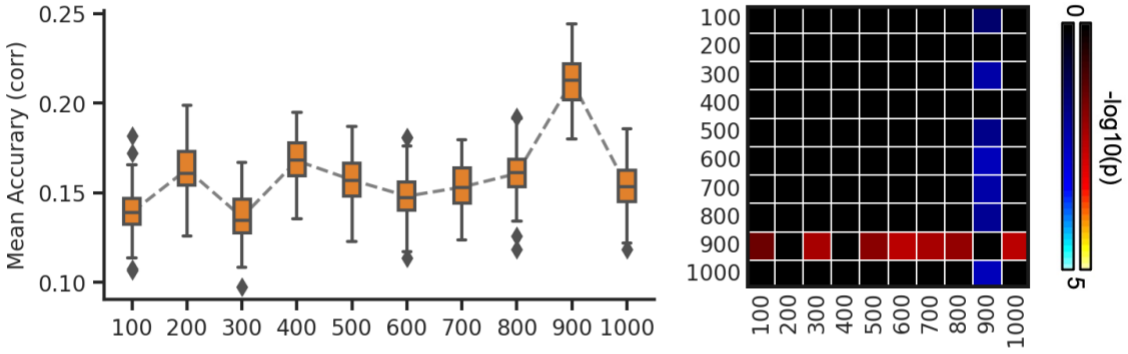

(C) sICA

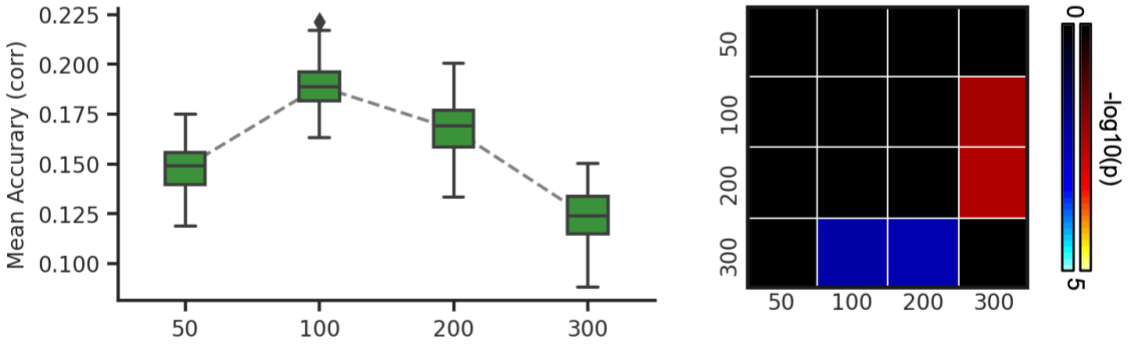

(D) PrincipalGrad

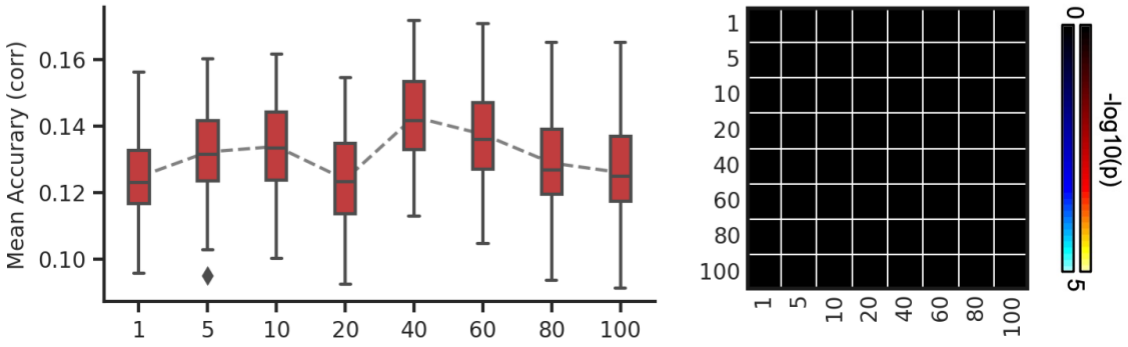

Figure S13. Prediction accuracies (Pearson's correlation) of emotion vary across resolutions for gradient and parcellation approaches using KRR in the HCP dataset. (A) Prediction accuracies and p values of the hard-parcellation Schaefer2018 with 100 to 1000 ROIs. (B) Prediction accuracies and p values of the hard-parcellation Kong2021 with 100 to 1000 ROIs. (C) Prediction accuracies and p values of the soft-parcellation sICA with 50 to 300 components. (D) Prediction accuracies and p values of the principal gradient PrincipalGrad with 1 to 100 gradients. Boxplots utilized default Python seaborn parameters, that is, box shows median and interquartile range (IQR). Whiskers indicate 1.5 IQR. P values (-log10(p)) were computed between prediction accuracies of each pair of resolutions. Non-black colors denote significantly different prediction performances after correcting for multiple comparisons with FDR $q < 0.05$. Bright colors indicate small p values, dark colors indicate large p values. For each pair of comparisons, warm colors represent higher prediction accuracies of the "row" resolution than the "column" resolution.

(A) Schaefer2018

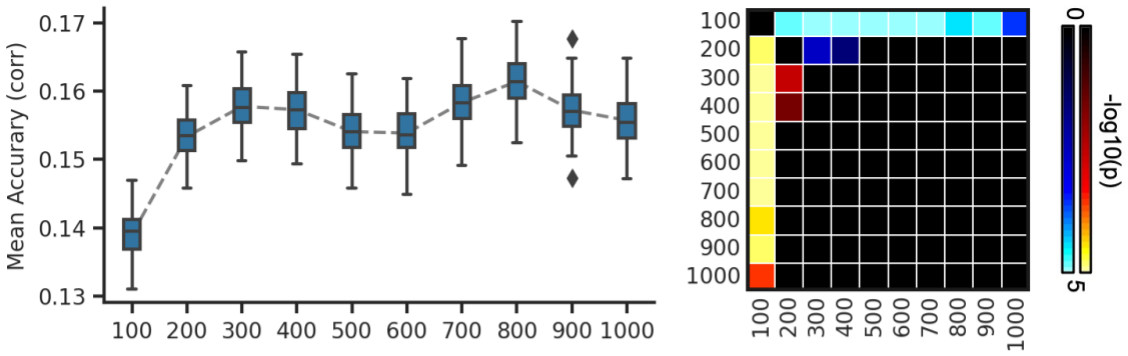

(B) Kong2021

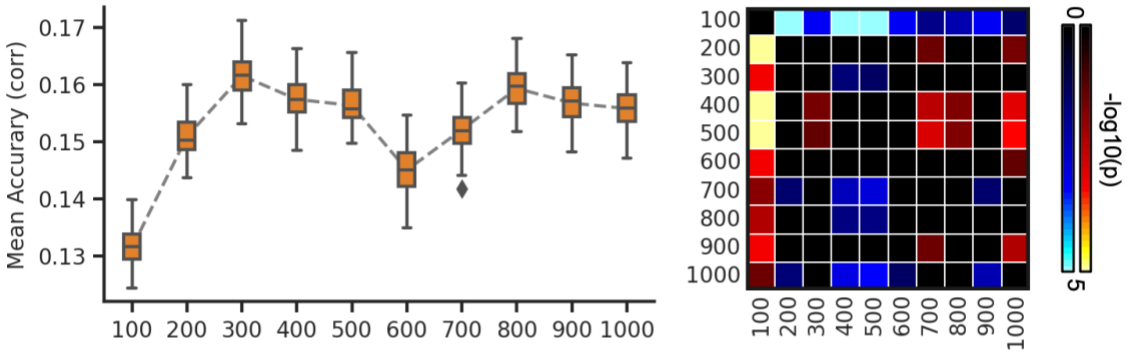

(C) sICA

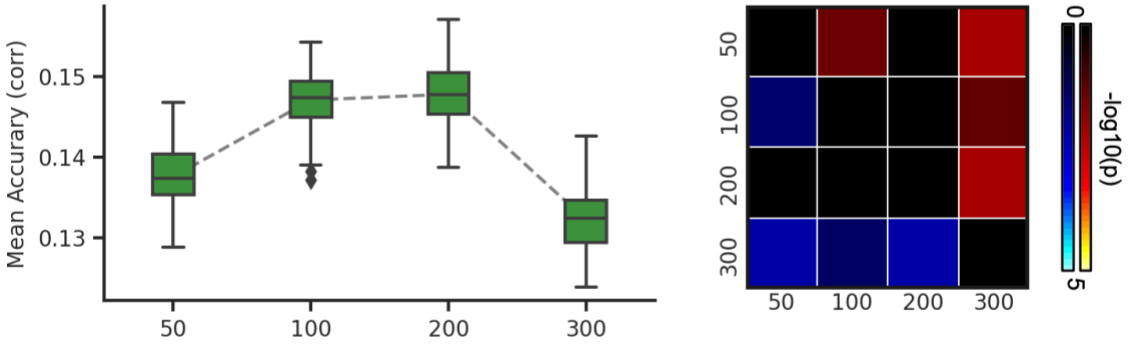

(D) PrincipalGrad

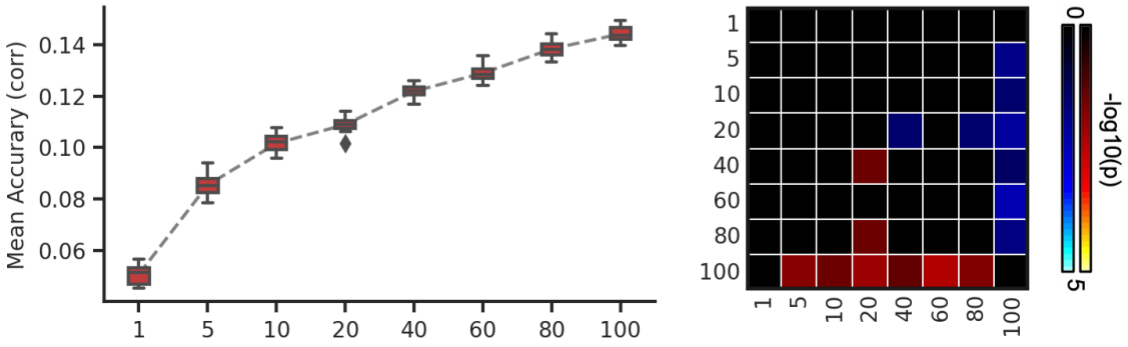

Figure S14. Average prediction accuracies (Pearson's correlation) of task performance measures vary across resolutions for gradient and parcellation approaches using LRR in the HCP dataset. (A) Prediction accuracies and p values of the hard-parcellation Schaefer2018 with 100 to 1000 ROIs. (B) Prediction accuracies and p values of the hard-parcellation Kong2021 with 100 to 1000 ROIs. (C) Prediction accuracies and p values of the soft-parcellation sICA with 50 to 300 components. (D) Prediction accuracies and p values of the principal gradient PrincipalGrad with 1 to 100 gradients. Boxplots utilized default Python seaborn parameters, that is, box shows median and interquartile range (IQR). Whiskers indicate 1.5 IQR. P values (-log10(p)) were computed between prediction accuracies of each pair of resolutions. Non-black colors denote significantly different prediction performances after correcting for multiple comparisons with FDR $q < 0.05$. Bright colors indicate small p values, dark colors indicate large p values. For each pair of comparisons, warm colors represent higher prediction accuracies of the "row" resolution than the "column" resolution.

(A) Schaefer2018

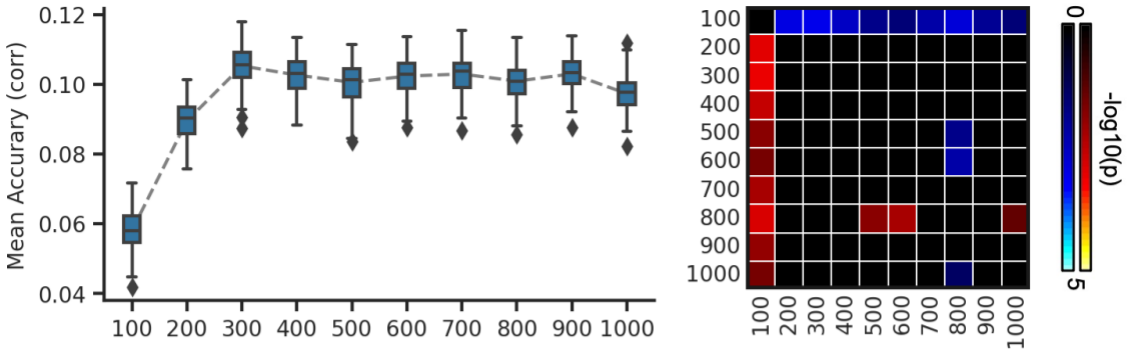

(B) Kong2021

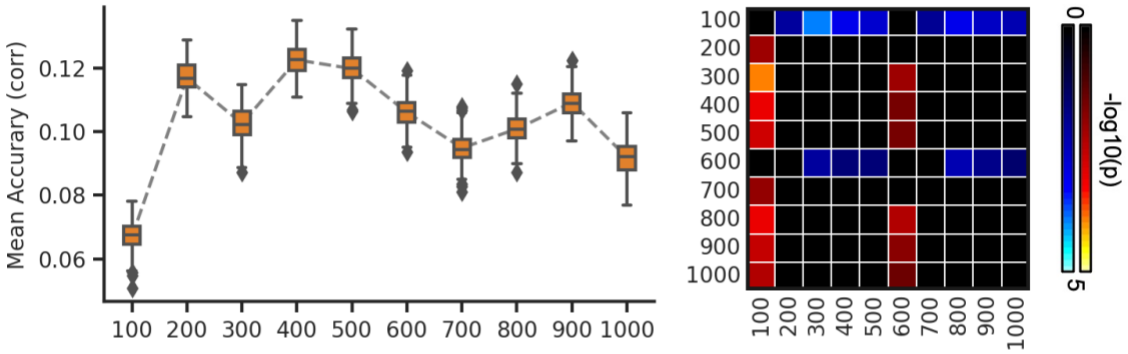

(C) sICA

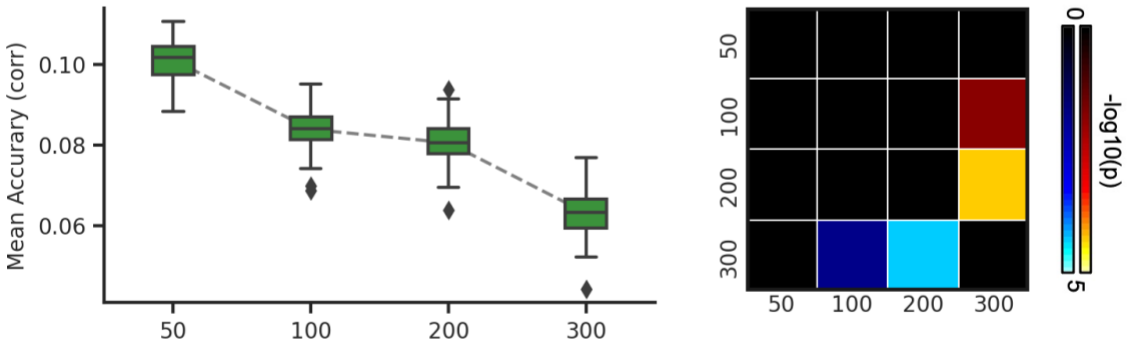

(D) PrincipalGrad

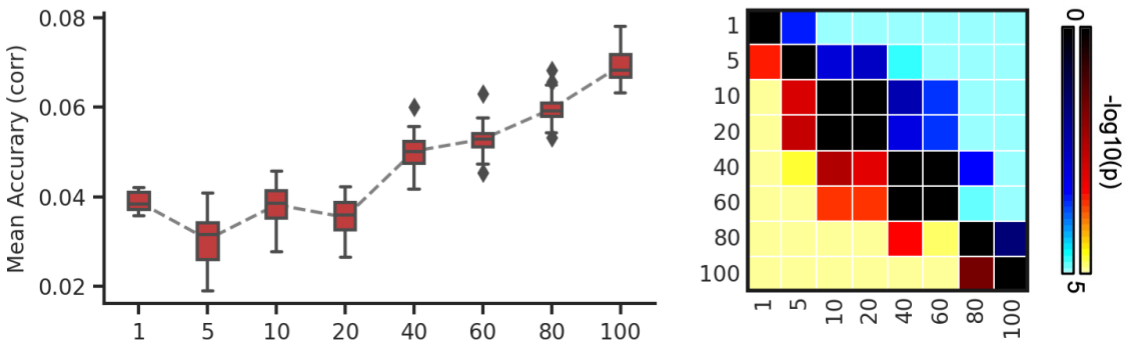

Figure S15. Average prediction accuracies (Pearson's correlation) of self-reported measures vary across resolutions for gradient and parcellation approaches using LRR in the HCP dataset. (A) Prediction accuracies and p values of the hard-parcellation Schaefer2018 with 100 to 1000 ROIs. (B) Prediction accuracies and p values of the hard-parcellation Kong2021 with 100 to 1000 ROIs. (C) Prediction accuracies and p values of the soft-parcellation sICA with 50 to 300 components. (D) Prediction accuracies and p values of the principal gradient PrincipalGrad with 1 to 100 gradients. Boxplots utilized default Python seaborn parameters, that is, box shows median and interquartile range (IQR). Whiskers indicate 1.5 IQR. P values (-log10(p)) were computed between prediction accuracies of each pair of resolutions. Non-black colors denote significantly different prediction performances after correcting for multiple comparisons with FDR $q < 0.05$. Bright colors indicate small p values, dark colors indicate large p values. For each pair of comparisons, warm colors represent higher prediction accuracies of the "row" resolution than the "column" resolution.

(A) Schaefer2018

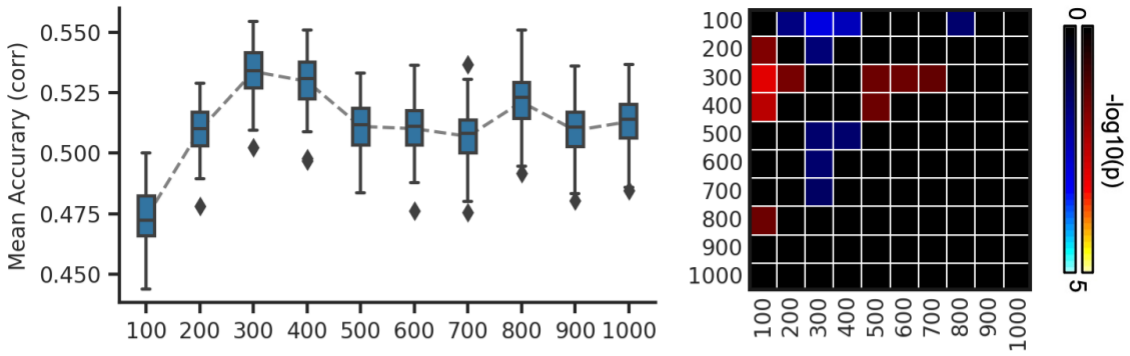

(B) Kong2021

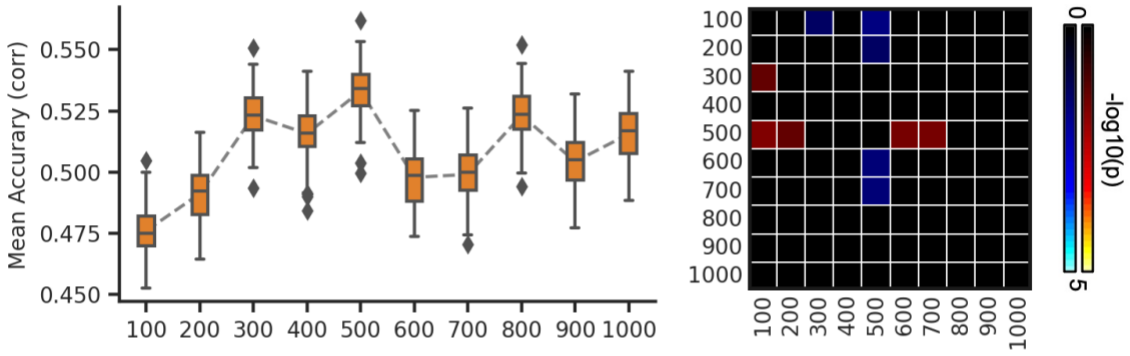

(C) sICA

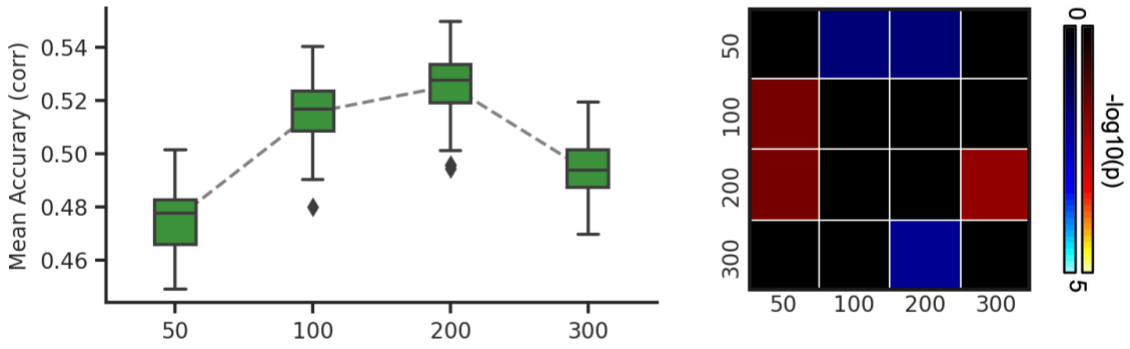

(D) PrincipalGrad

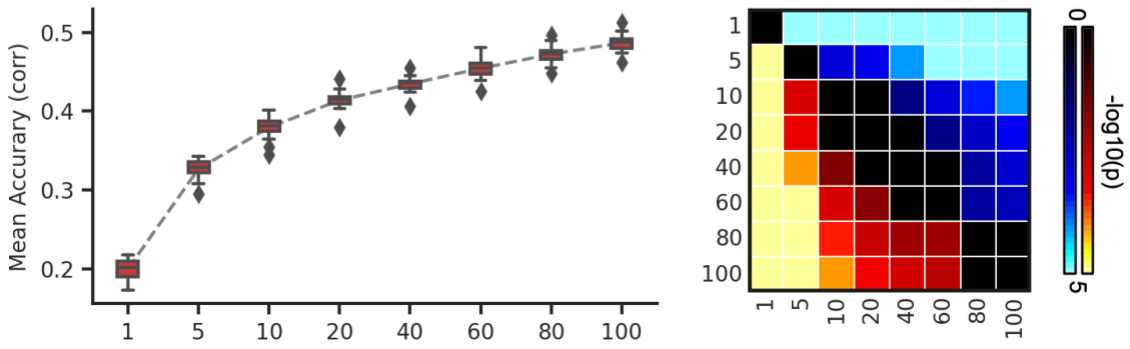

Figure S16. Prediction accuracies (Pearson's correlation) of cognition vary across resolutions for gradient and parcellation approaches using LRR in the HCP dataset. (A) Prediction accuracies and p values of the hard-parcellation Schaefer2018 with 100 to 1000 ROIs. (B) Prediction accuracies and p values of the hard-parcellation Kong2021 with 100 to 1000 ROIs. (C) Prediction accuracies and p values of the soft-parcellation sICA with 50 to 300 components. (D) Prediction accuracies and p values of the principal gradient PrincipalGrad with 1 to 100 gradients. Boxplots utilized default Python seaborn parameters, that is, box shows median and interquartile range (IQR). Whiskers indicate 1.5 IQR. P values (-log10(p)) were computed between prediction accuracies of each pair of resolutions. Non-black colors denote significantly different prediction performances after correcting for multiple comparisons with FDR $q < 0.05$. Bright colors indicate small p values, dark colors indicate large p values. For each pair of comparisons, warm colors represent higher prediction accuracies of the "row" resolution than the "column" resolution.

(A) Schaefer2018

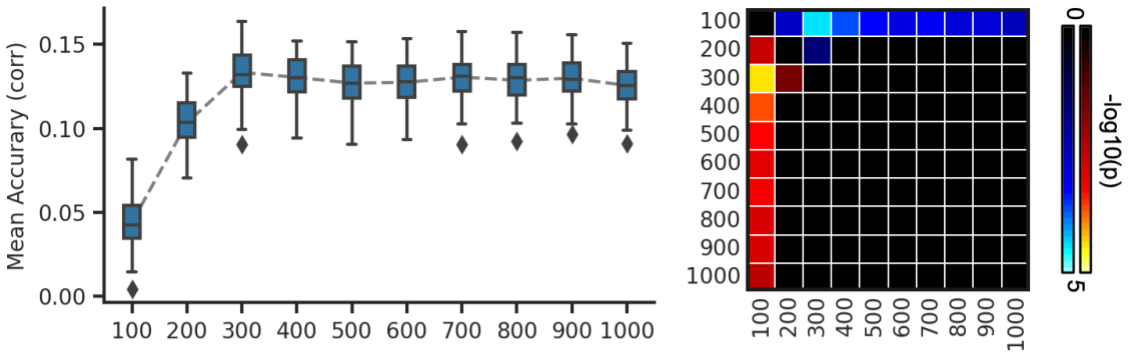

(B) Kong2021

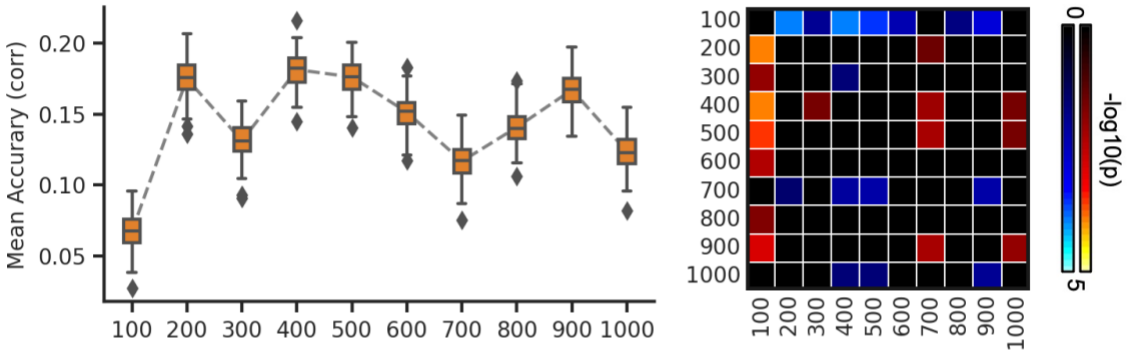

(C) sICA

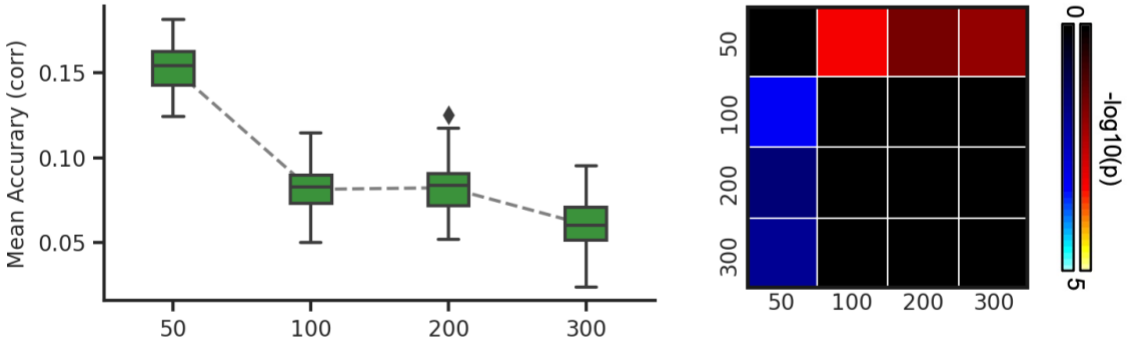

(D) PrincipalGrad

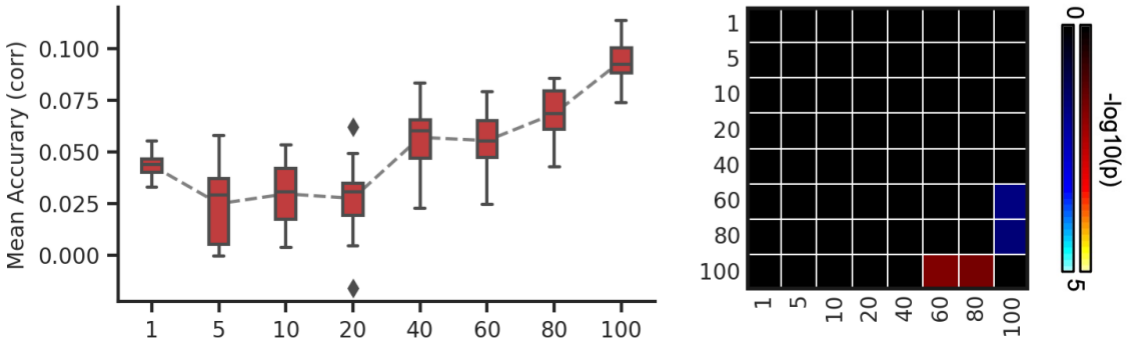

Figure S17. Prediction accuracies (Pearson's correlation) of dissatisfaction vary across resolutions for gradient and parcellation approaches using LRR in the HCP dataset. (A) Prediction accuracies and p values of the hard-parcellation Schaefer2018 with 100 to 1000 ROIs. (B) Prediction accuracies and p values of the hard-parcellation Kong2021 with 100 to 1000 ROIs. (C) Prediction accuracies and p values of the soft-parcellation sICA with 50 to 300 components. (D) Prediction accuracies and p values of the principal gradient PrincipalGrad with 1 to 100 gradients. Boxplots utilized default Python seaborn parameters, that is, box shows median and interquartile range (IQR). Whiskers indicate 1.5 IQR. P values (-log10(p)) were computed between prediction accuracies of each pair of resolutions. Non-black colors denote significantly different prediction performances after correcting for multiple comparisons with FDR $q < 0.05$. Bright colors indicate small p values, dark colors indicate large p values. For each pair of comparisons, warm colors represent higher prediction accuracies of the "row" resolution than the "column" resolution.

(A) Schaefer2018

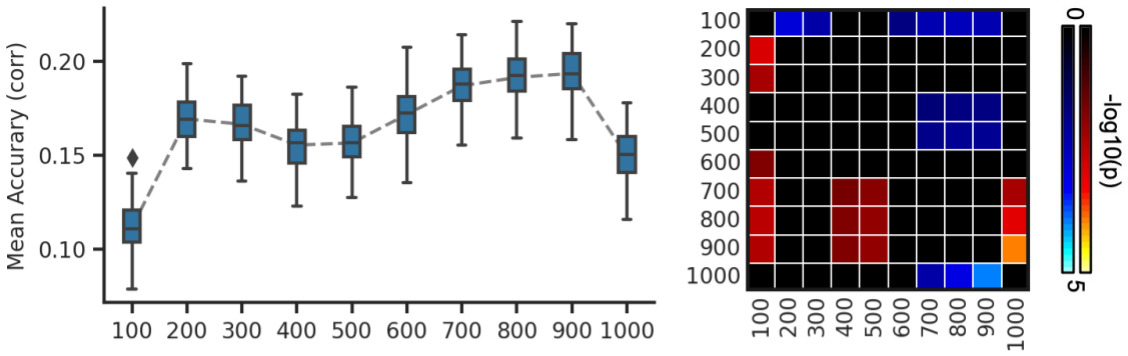

(B) Kong2021

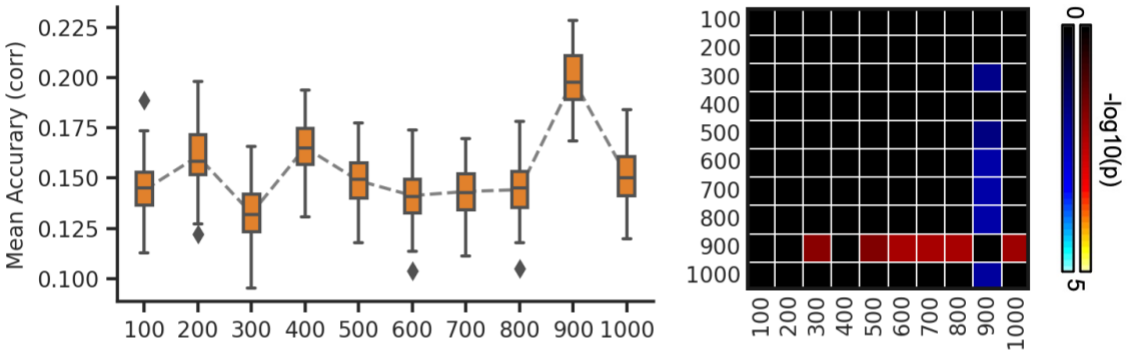

(C) sICA

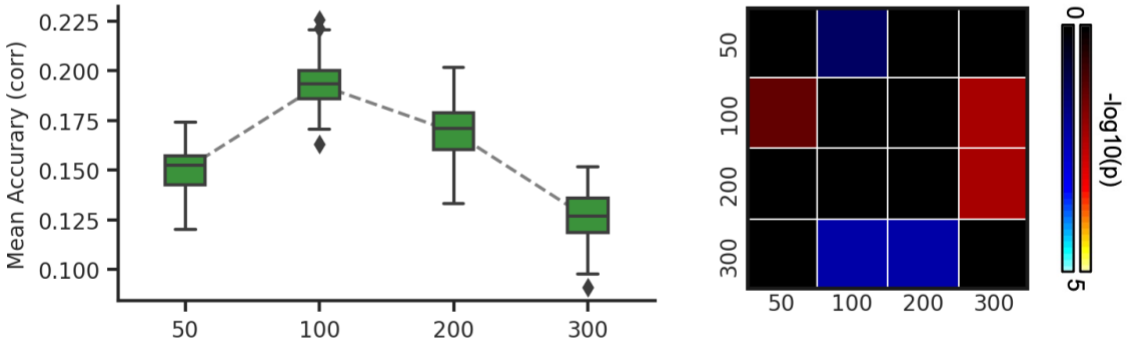

(D) PrincipalGrad

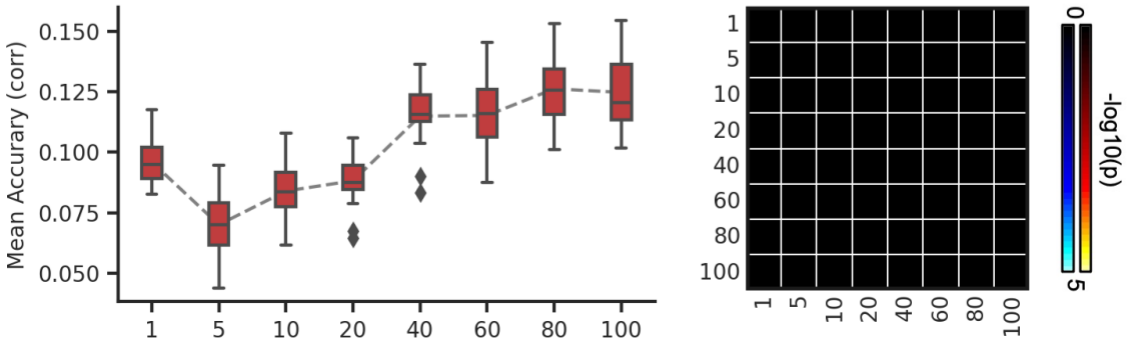

Figure S18. Prediction accuracies (Pearson's correlation) of emotion vary across resolutions for gradient and parcellation approaches using LRR in the HCP dataset. (A) Prediction accuracies and p values of the hard-parcellation Schaefer2018 with 100 to 1000 ROIs. (B) Prediction accuracies and p values of the hard-parcellation Kong2021 with 100 to 1000 ROIs. (C) Prediction accuracies and p values of the soft-parcellation sICA with 50 to 300 components. (D) Prediction accuracies and p values of the principal gradient PrincipalGrad with 1 to 100 gradients. Boxplots utilized default Python seaborn parameters, that is, box shows median and interquartile range (IQR). Whiskers indicate 1.5 IQR. P values (-log10(p)) were computed between prediction accuracies of each pair of resolutions. Non-black colors denote significantly different prediction performances after correcting for multiple comparisons with FDR $q < 0.05$. Bright colors indicate small p values, dark colors indicate large p values. For each pair of comparisons, warm colors represent higher prediction accuracies of the "row" resolution than the "column" resolution.

(A) Schaefer2018

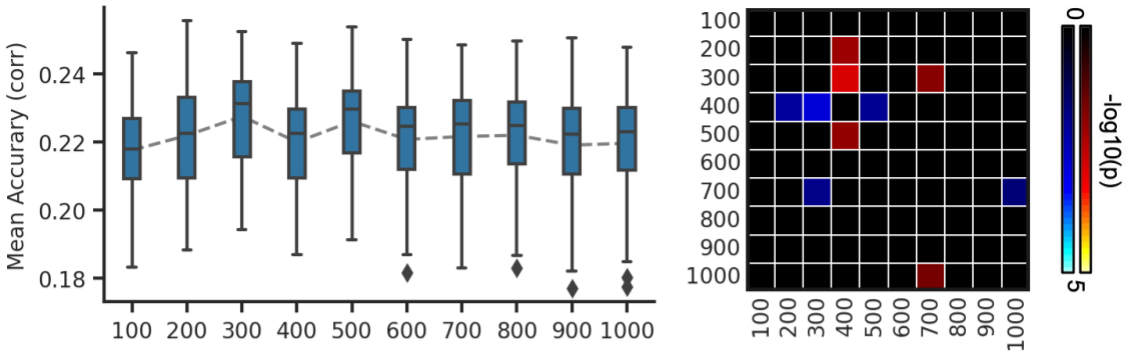

(B) Kong2021

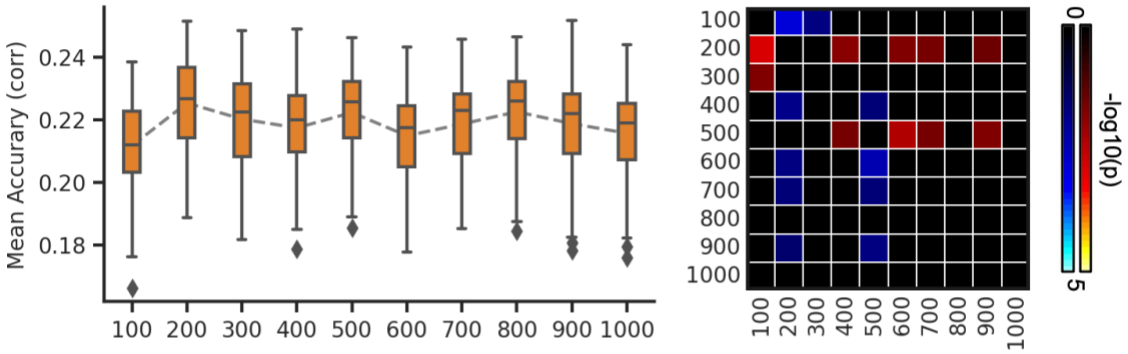

(C) sICA

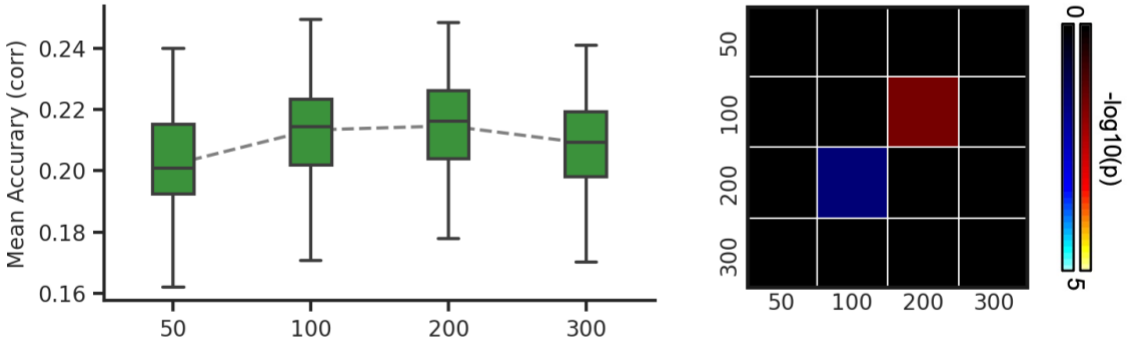

(D) PrincipalGrad

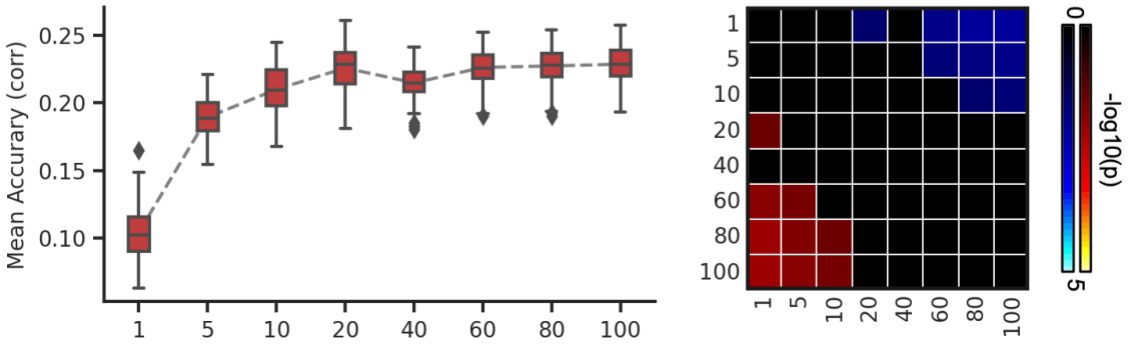

Figure S19. Average prediction accuracies (Pearson's correlation) of task performance measures vary across resolutions for gradient and parcellation approaches using KRR in the ABCD dataset. (A) Prediction accuracies and p values of the hard-parcellation Schaefer2018 with 100 to 1000 ROIs. (B) Prediction accuracies and p values of the hard-parcellation Kong2021 with 100 to 1000 ROIs. (C) Prediction accuracies and p values of the soft-parcellation sICA with 50 to 300 components. (D) Prediction accuracies and p values of the principal gradient PrincipalGrad with 1 to 100 gradients. Boxplots utilized default Python seaborn parameters, that is, box shows median and interquartile range (IQR). Whiskers indicate 1.5 IQR. P values (-log10(p)) were computed between prediction accuracies of each pair of resolutions. Non-black colors denote significantly different prediction performances after correcting for multiple comparisons with FDR $q < 0.05$. Bright colors indicate small p values, dark colors indicate large p values. For each pair of comparisons, warm colors represent higher prediction accuracies of the "row" resolution than the "column" resolution.

(A) Schaefer2018

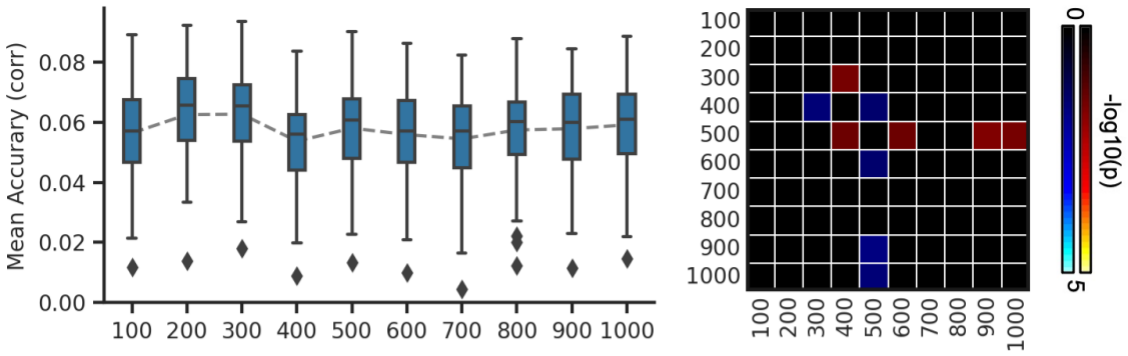

(B) Kong2021

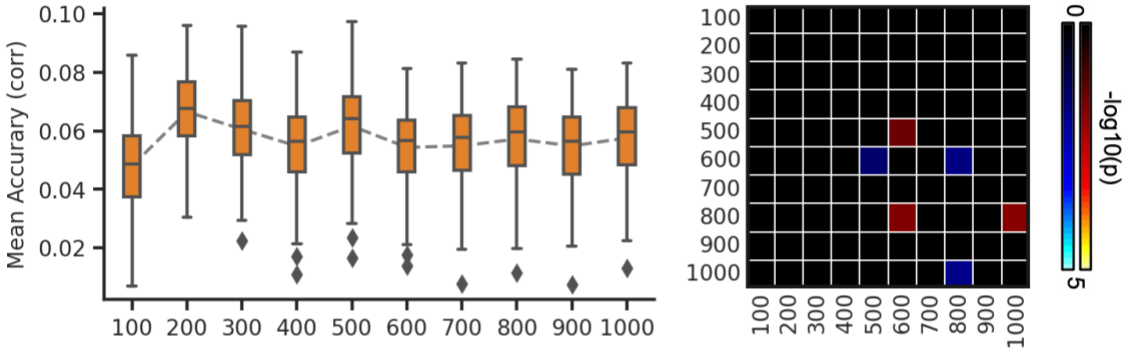

(C) sICA

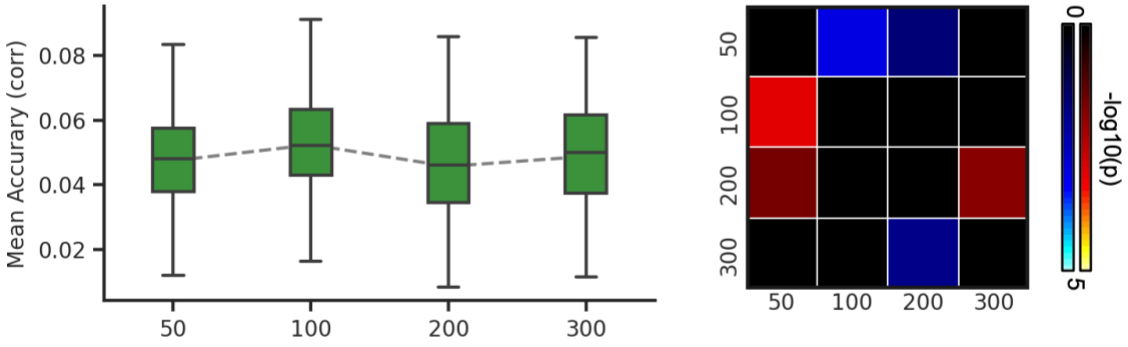

(D) PrincipalGrad

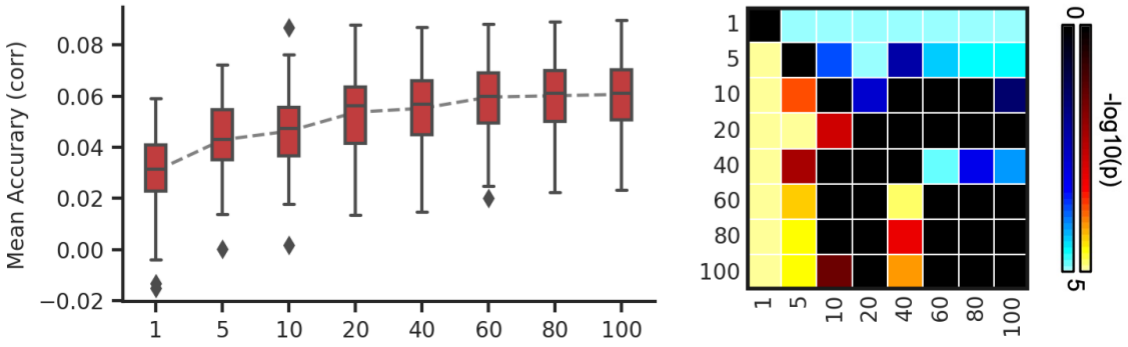

Figure S20. Average prediction accuracies (Pearson's correlation) of self-reported measures vary across resolutions for gradient and parcellation approaches using KRR in the ABCD dataset. (A) Prediction accuracies and p values of the hard-parcellation Schaefer2018 with 100 to 1000 ROIs. (B) Prediction accuracies and p values of the hard-parcellation Kong2021 with 100 to 1000 ROIs. (C) Prediction accuracies and p values of the soft-parcellation sICA with 50 to 300 components. (D) Prediction accuracies and p values of the principal gradient PrincipalGrad with 1 to 100 gradients. Boxplots utilized default Python seaborn parameters, that is, box shows median and interquartile range (IQR). Whiskers indicate 1.5 IQR. P values (-log10(p)) were computed between prediction accuracies of each pair of resolutions. Non-black colors denote significantly different prediction performances after correcting for multiple comparisons with FDR $q < 0.05$. Bright colors indicate small p values, dark colors indicate large p values. For each pair of comparisons, warm colors represent higher prediction accuracies of the "row" resolution than the "column" resolution.

(A) Schaefer2018

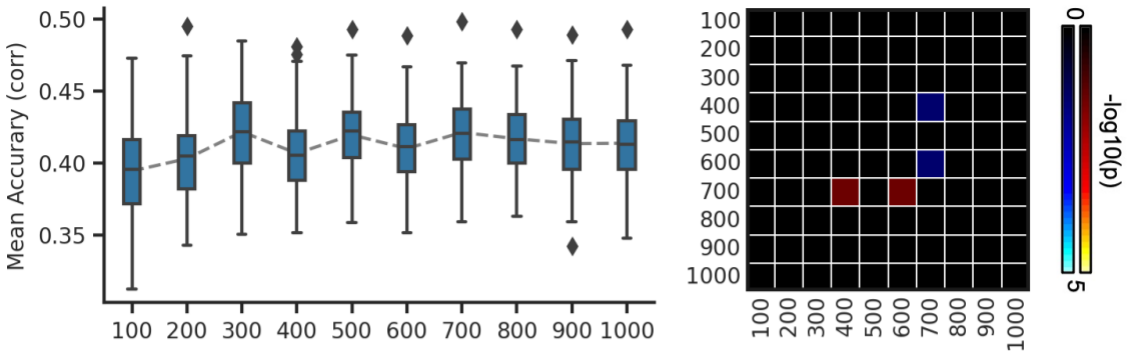

(B) Kong2021

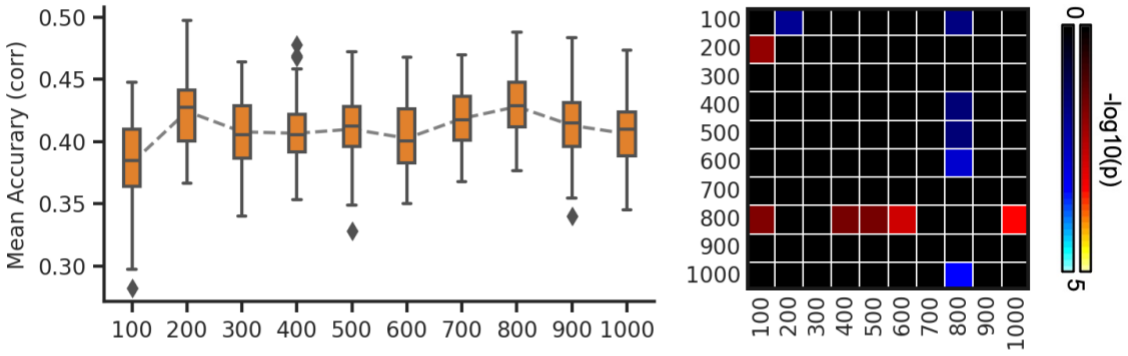

(C) sICA

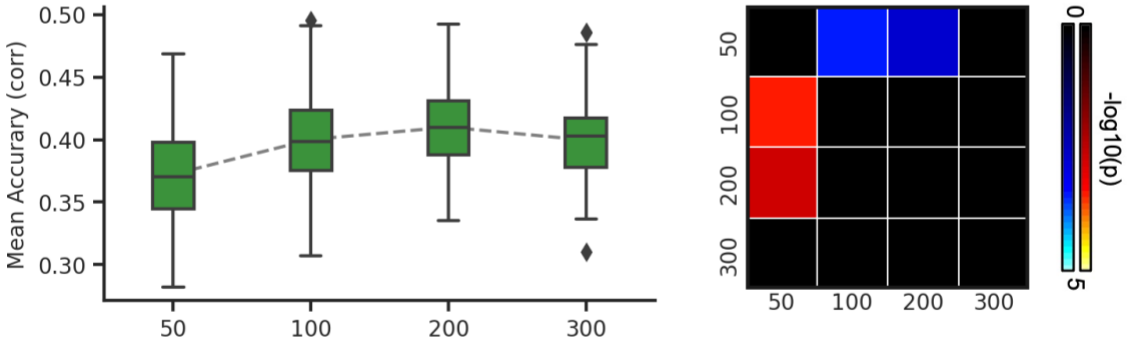

(D) PrincipalGrad

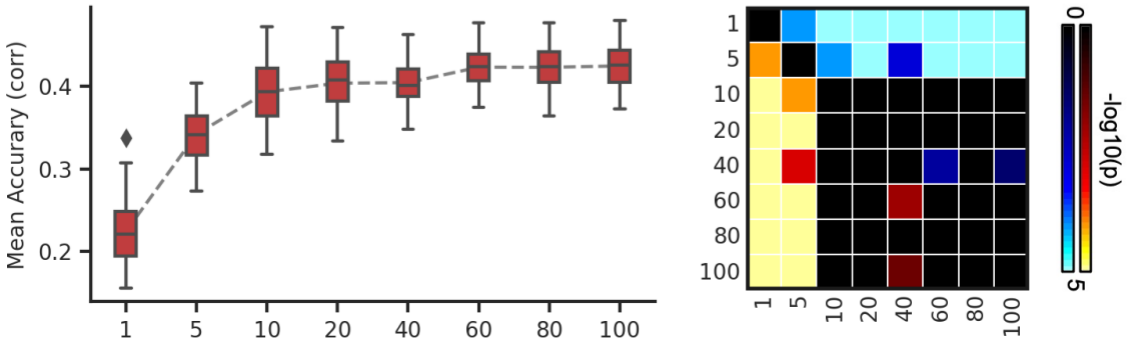

Figure S21. Prediction accuracies (Pearson's correlation) of cognition vary across resolutions for gradient and parcellation approaches using KRR in the ABCD dataset. (A) Prediction accuracies and p values of the hard-parcellation Schaefer2018 with 100 to 1000 ROIs. (B) Prediction accuracies and p values of the hard-parcellation Kong2021 with 100 to 1000 ROIs. (C) Prediction accuracies and p values of the soft-parcellation sICA with 50 to 300 components. (D) Prediction accuracies and p values of the principal gradient PrincipalGrad with 1 to 100 gradients. Boxplots utilized default Python seaborn parameters, that is, box shows median and interquartile range (IQR). Whiskers indicate 1.5 IQR. P values (-log10(p)) were computed between prediction accuracies of each pair of resolutions. Non-black colors denote significantly different prediction performances after correcting for multiple comparisons with FDR $q < 0.05$. Bright colors indicate small p values, dark colors indicate large p values. For each pair of comparisons, warm colors represent higher prediction accuracies of the "row" resolution than the "column" resolution.

(A) Schaefer2018

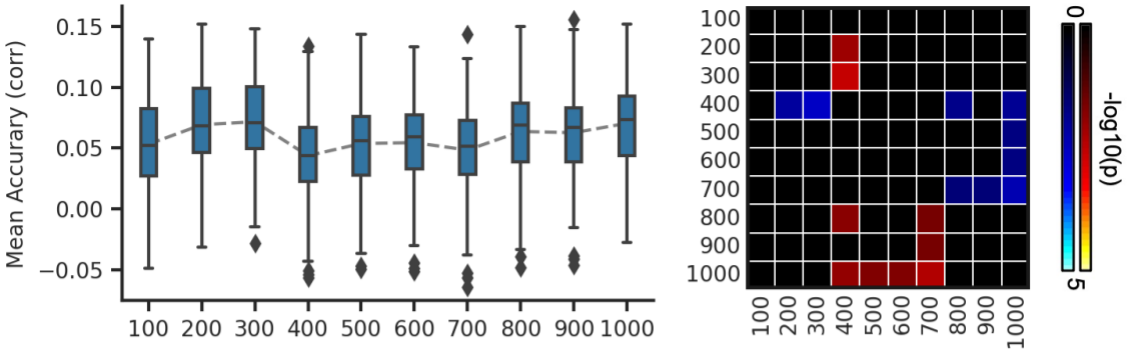

(B) Kong2021

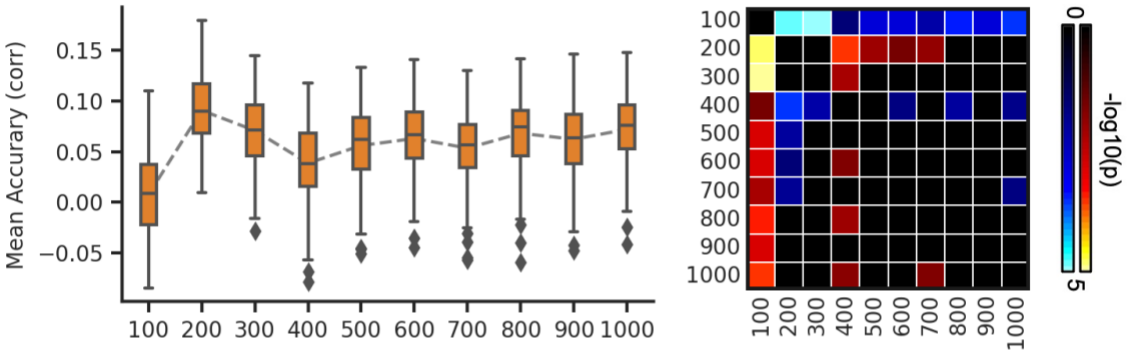

(C) sICA

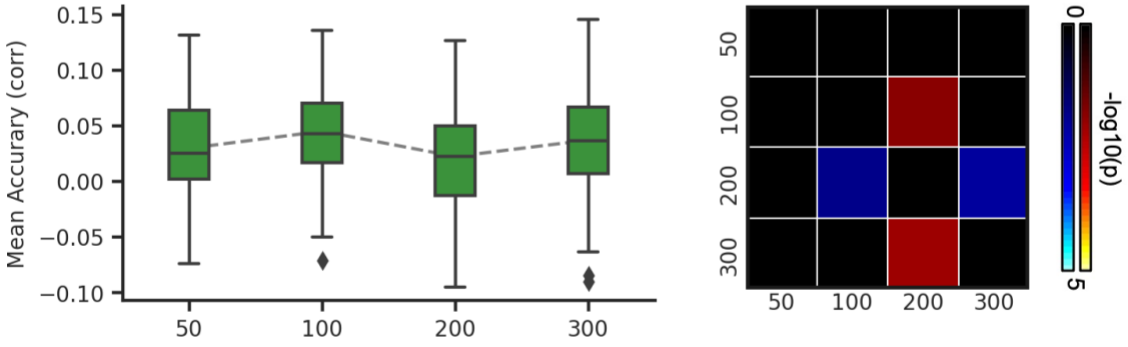

(D) PrincipalGrad

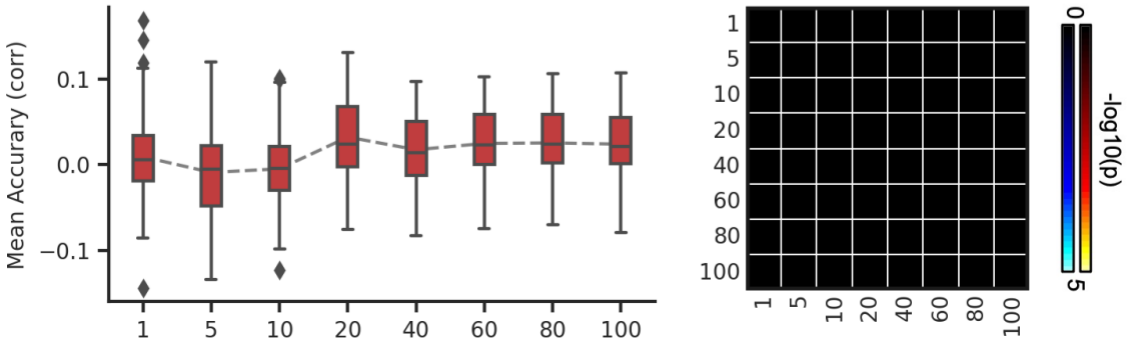

Figure S22. Prediction accuracies (Pearson's correlation) of mental health vary across resolutions for gradient and parcellation approaches using KRR in the ABCD dataset. (A) Prediction accuracies and p values of the hard-parcellation Schaefer2018 with 100 to 1000 ROIs. (B) Prediction accuracies and p values of the hard-parcellation Kong2021 with 100 to 1000 ROIs. (C) Prediction accuracies and p values of the soft-parcellation sICA with 50 to 300 components. (D) Prediction accuracies and p values of the principal gradient PrincipalGrad with 1 to 100 gradients. Boxplots utilized default Python seaborn parameters, that is, box shows median and interquartile range (IQR). Whiskers indicate 1.5 IQR. P values (-log10(p)) were computed between prediction accuracies of each pair of resolutions. Non-black colors denote significantly different prediction performances after correcting for multiple comparisons with FDR $q < 0.05$. Bright colors indicate small p values, dark colors indicate large p values. For each pair of comparisons, warm colors represent higher prediction accuracies of the "row" resolution than the "column" resolution.

(A) Schaefer2018

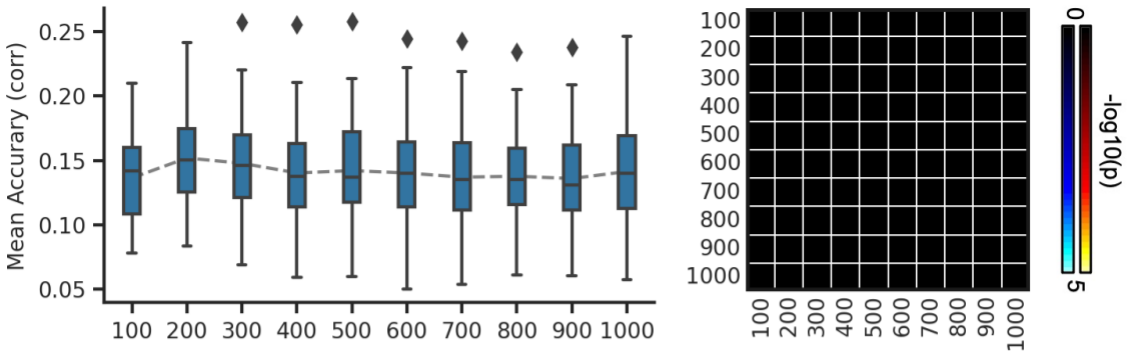

(B) Kong2021

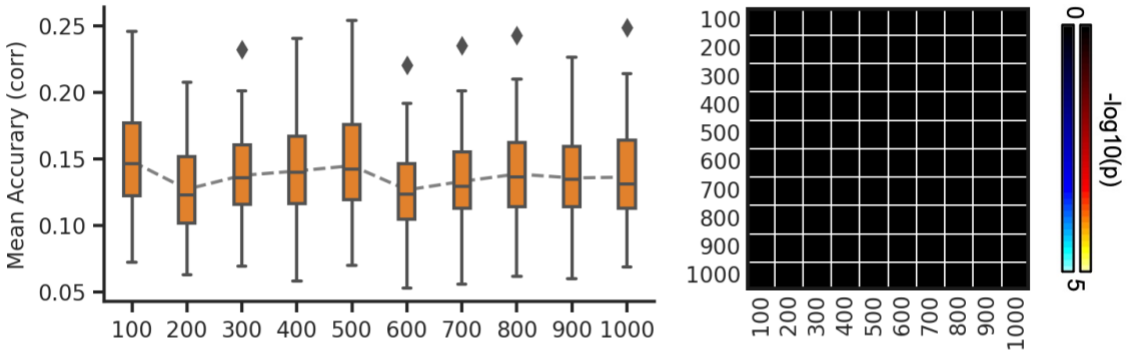

(C) sICA

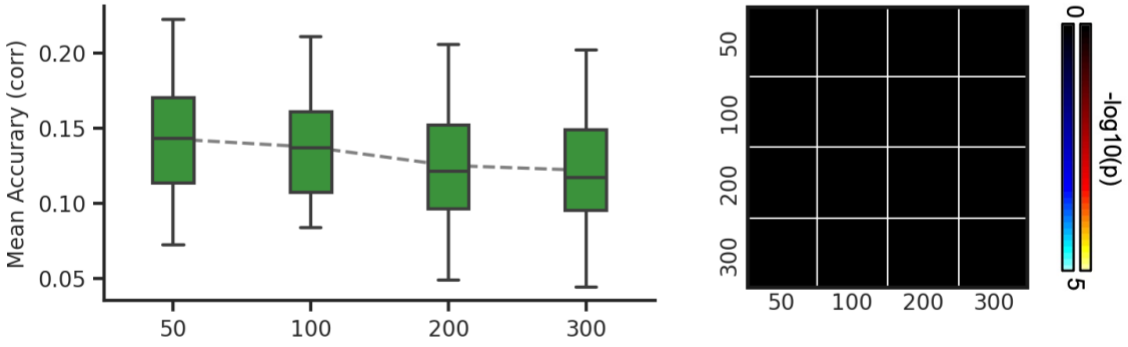

(D) PrincipalGrad

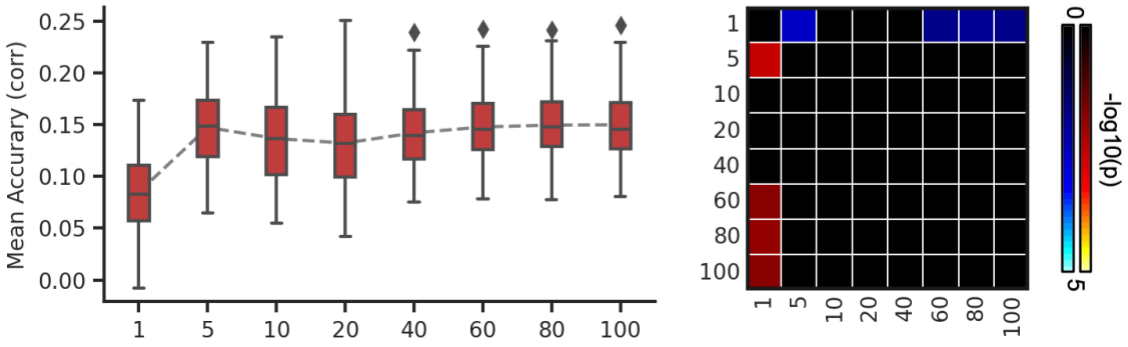

Figure S23. Prediction accuracies (Pearson's correlation) of personality vary across resolutions for gradient and parcellation approaches using KRR in the ABCD dataset. (A) Prediction accuracies and p values of the hard-parcellation Schaefer2018 with 100 to 1000 ROIs. (B) Prediction accuracies and p values of the hard-parcellation Kong2021 with 100 to 1000 ROIs. (C) Prediction accuracies and p values of the soft-parcellation sICA with 50 to 300 components. (D) Prediction accuracies and p values of the principal gradient PrincipalGrad with 1 to 100 gradients. Boxplots utilized default Python seaborn parameters, that is, box shows median and interquartile range (IQR). Whiskers indicate 1.5 IQR. P values (-log10(p)) were computed between prediction accuracies of each pair of resolutions. Non-black colors denote significantly different prediction performances after correcting for multiple comparisons with FDR $q < 0.05$. Bright colors indicate small p values, dark colors indicate large p values. For each pair of comparisons, warm colors represent higher prediction accuracies of the "row" resolution than the "column" resolution.

(A) Schaefer2018

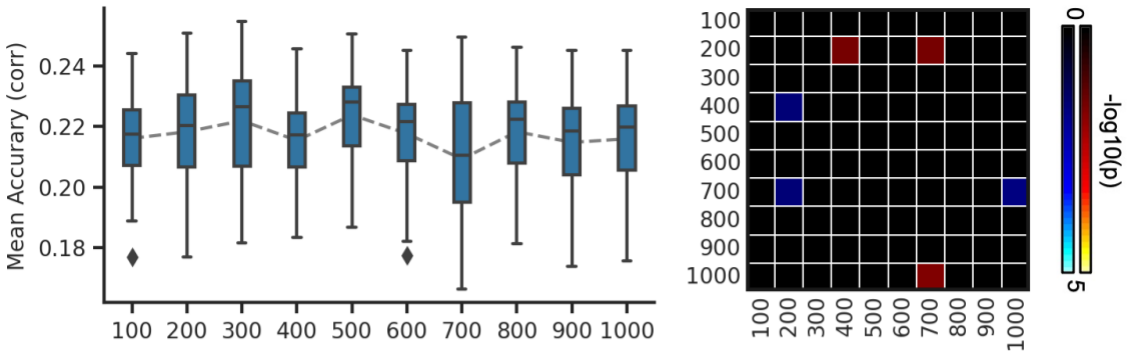

(B) Kong2021

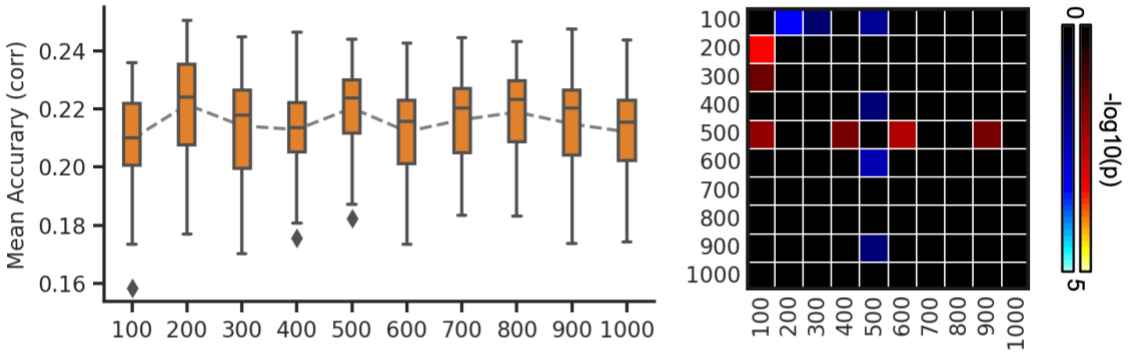

(C) sICA

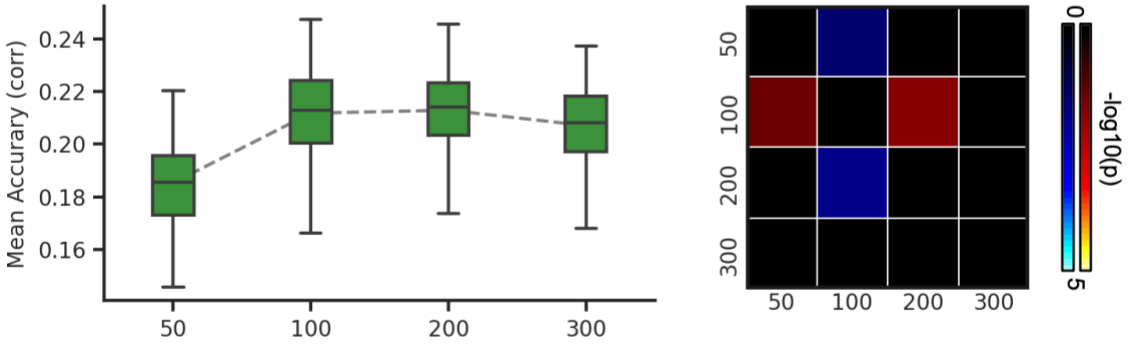

(D) PrincipalGrad

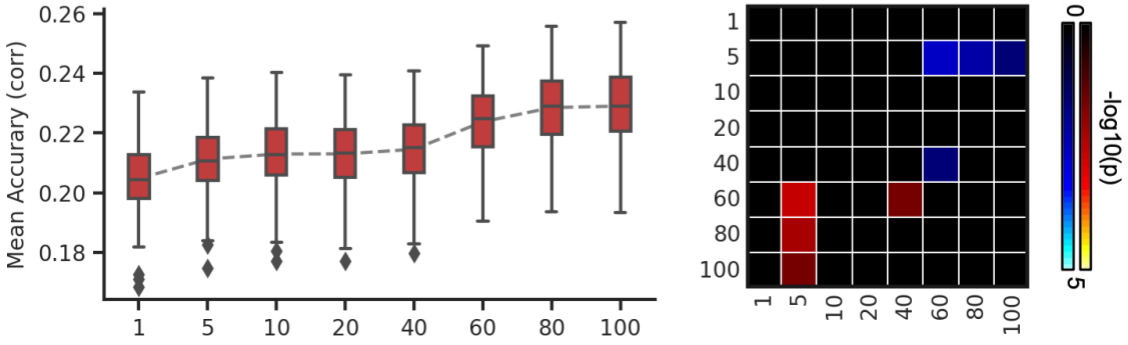

Figure S24. Average prediction accuracies (Pearson's correlation) of task performance measures vary across resolutions for gradient and parcellation approaches using LRR in the ABCD dataset. (A) Prediction accuracies and p values of the hard-parcellation Schaefer2018 with 100 to 1000 ROIs. (B) Prediction accuracies and p values of the hard-parcellation Kong2021 with 100 to 1000 ROIs. (C) Prediction accuracies and p values of the soft-parcellation sICA with 50 to 300 components. (D) Prediction accuracies and p values of the principal gradient PrincipalGrad with 1 to 100 gradients. Boxplots utilized default Python seaborn parameters, that is, box shows median and interquartile range (IQR). Whiskers indicate 1.5 IQR. P values (-log10(p)) were computed between prediction accuracies of each pair of resolutions. Non-black colors denote significantly different prediction performances after correcting for multiple comparisons with FDR $q < 0.05$. Bright colors indicate small p values, dark colors indicate large p values. For each pair of comparisons, warm colors represent higher prediction accuracies of the "row" resolution than the "column" resolution.

(A) Schaefer2018

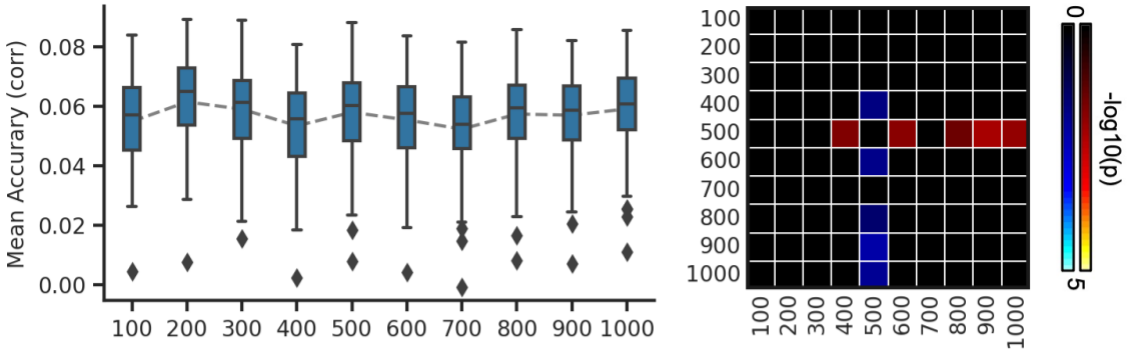

(B) Kong2021

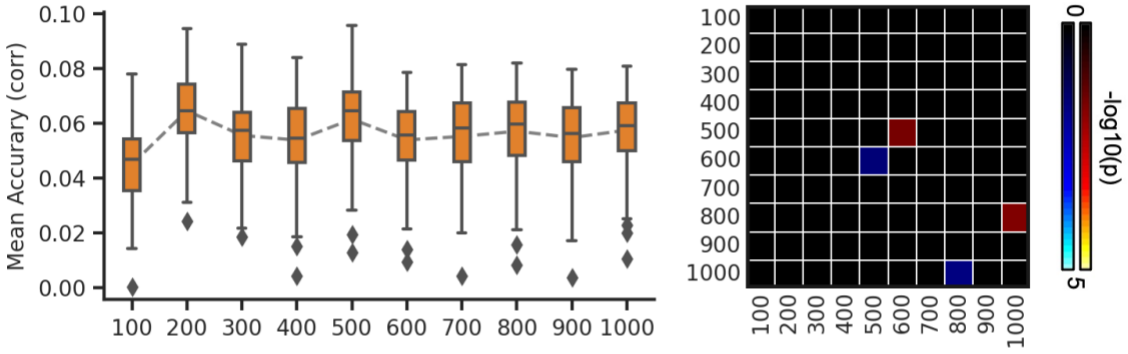

(C) sICA

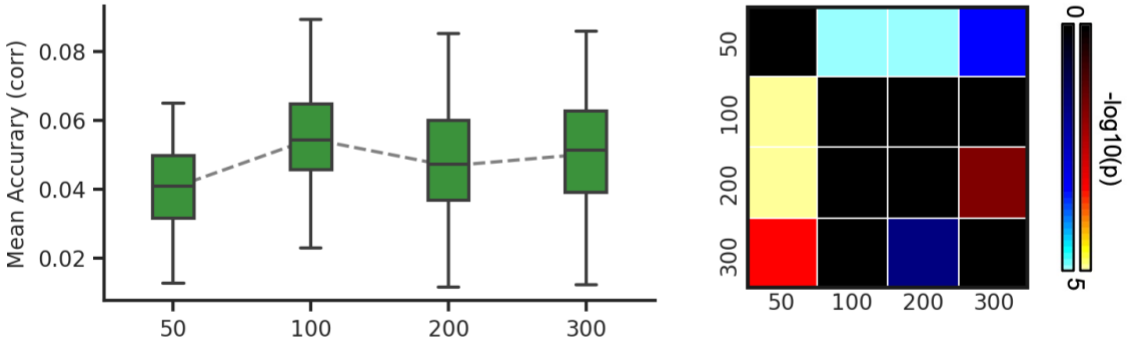

(D) PrincipalGrad

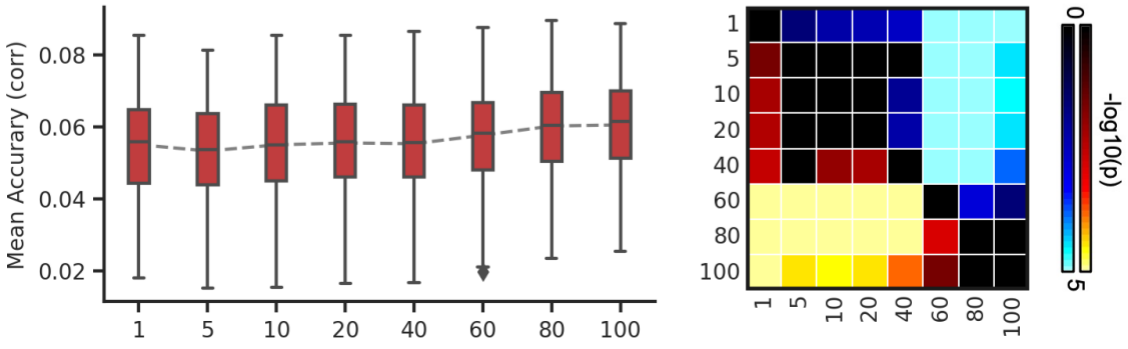

Figure S25. Average prediction accuracies (Pearson's correlation) of self-reported measures vary across resolutions for gradient and parcellation approaches using LRR in the ABCD dataset. (A) Prediction accuracies and p values of the hard-parcellation Schaefer2018 with 100 to 1000 ROIs. (B) Prediction accuracies and p values of the hard-parcellation Kong2021 with 100 to 1000 ROIs. (C) Prediction accuracies and p values of the soft-parcellation sICA with 50 to 300 components. (D) Prediction accuracies and p values of the principal gradient PrincipalGrad with 1 to 100 gradients. Boxplots utilized default Python seaborn parameters, that is, box shows median and interquartile range (IQR). Whiskers indicate 1.5 IQR. P values (-log10(p)) were computed between prediction accuracies of each pair of resolutions. Non-black colors denote significantly different prediction performances after correcting for multiple comparisons with FDR $q < 0.05$. Bright colors indicate small p values, dark colors indicate large p values. For each pair of comparisons, warm colors represent higher prediction accuracies of the "row" resolution than the "column" resolution.

(A) Schaefer2018

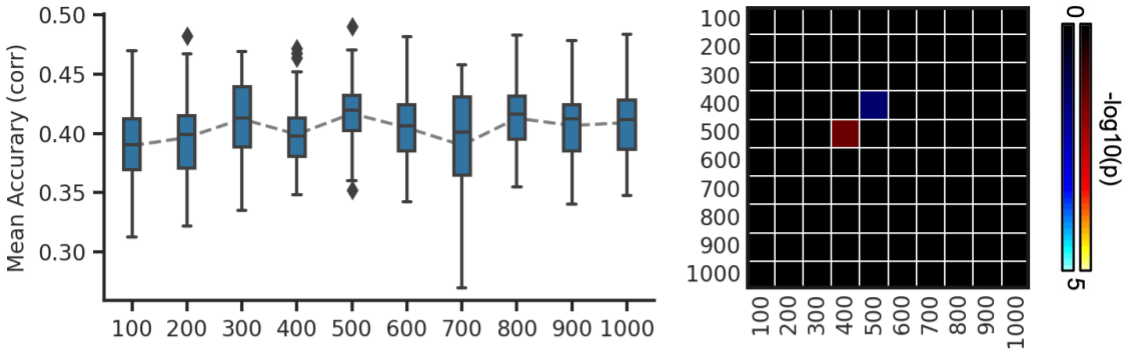

(B) Kong2021

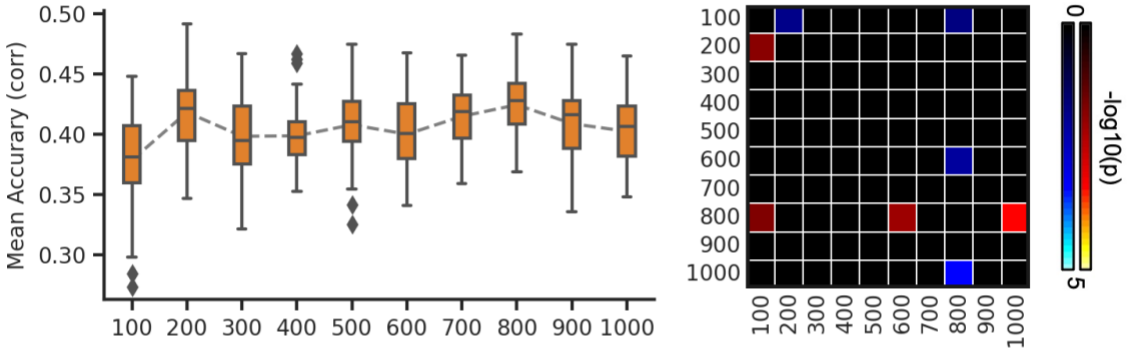

(C) sICA

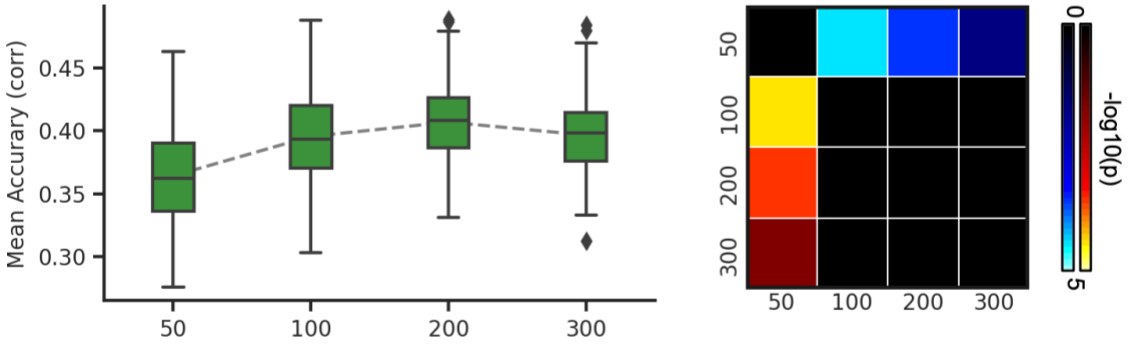

(D) PrincipalGrad

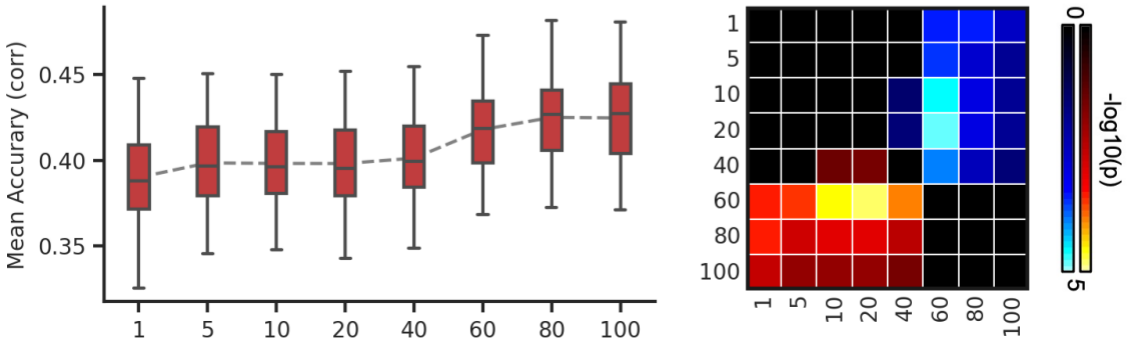

Figure S26. Prediction accuracies (Pearson's correlation) of cognition vary across resolutions for gradient and parcellation approaches using LRR in the ABCD dataset. (A) Prediction accuracies and p values of the hard-parcellation Schaefer2018 with 100 to 1000 ROIs. (B) Prediction accuracies and p values of the hard-parcellation Kong2021 with 100 to 1000 ROIs. (C) Prediction accuracies and p values of the soft-parcellation sICA with 50 to 300 components. (D) Prediction accuracies and p values of the principal gradient PrincipalGrad with 1 to 100 gradients. Boxplots utilized default Python seaborn parameters, that is, box shows median and interquartile range (IQR). Whiskers indicate 1.5 IQR. P values (-log10(p)) were computed between prediction accuracies of each pair of resolutions. Non-black colors denote significantly different prediction performances after correcting for multiple comparisons with FDR $q < 0.05$. Bright colors indicate small p values, dark colors indicate large p values. For each pair of comparisons, warm colors represent higher prediction accuracies of the "row" resolution than the "column" resolution.

(A) Schaefer2018

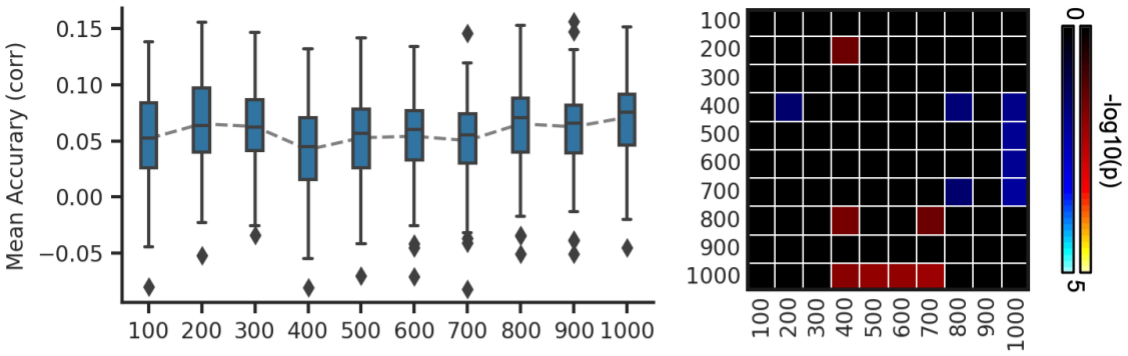

(B) Kong2021

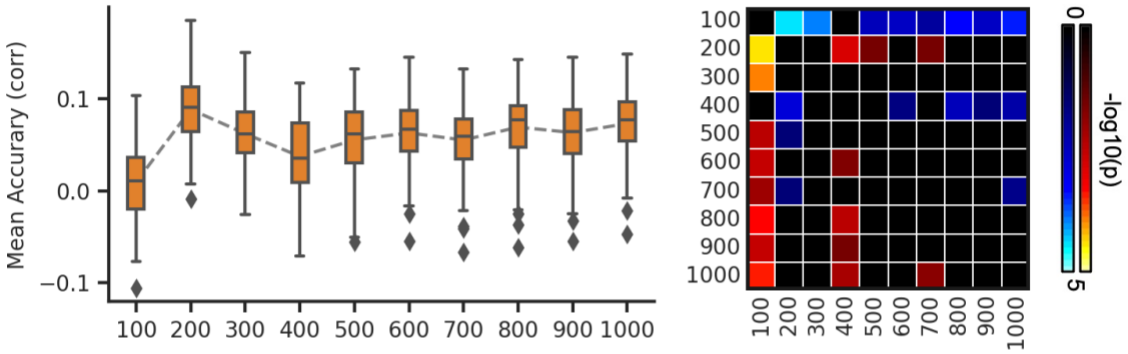

(C) sICA

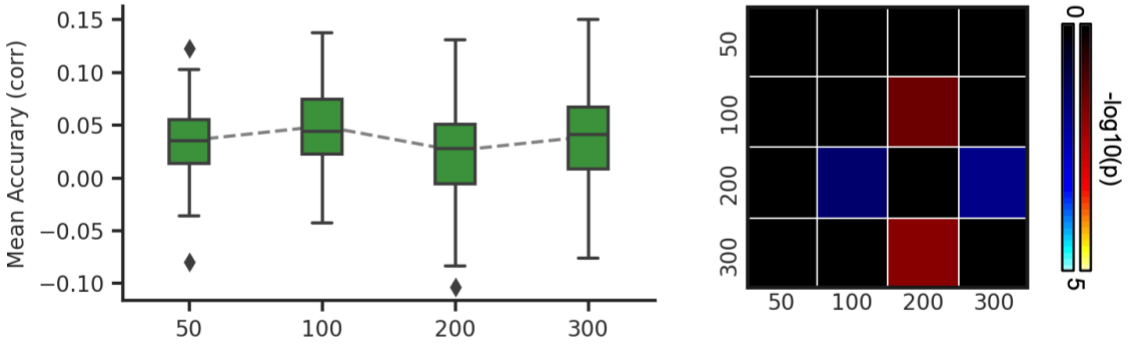

(D) PrincipalGrad

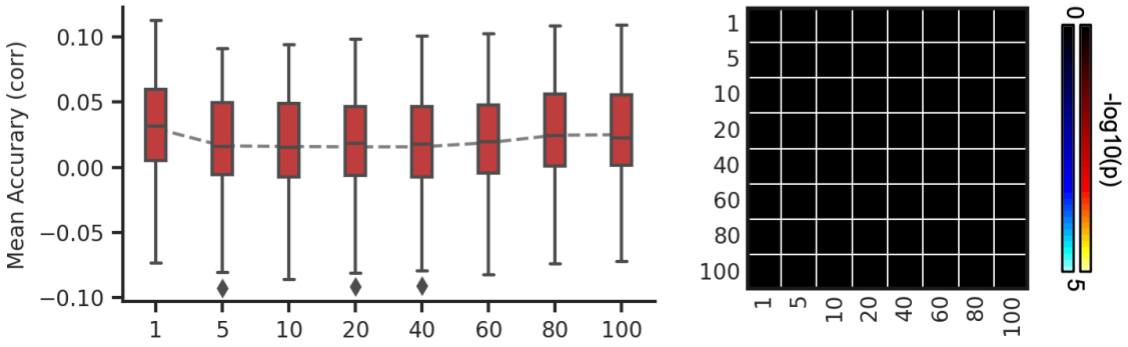

Figure S27. Prediction accuracies (Pearson's correlation) of mental health vary across resolutions for gradient and parcellation approaches using LRR in the ABCD dataset. (A) Prediction accuracies and p values of the hard-parcellation Schaefer2018 with 100 to 1000 ROIs. (B) Prediction accuracies and p values of the hard-parcellation Kong2021 with 100 to 1000 ROIs. (C) Prediction accuracies and p values of the soft-parcellation sICA with 50 to 300 components. (D) Prediction accuracies and p values of the principal gradient PrincipalGrad with 1 to 100 gradients. Boxplots utilized default Python seaborn parameters, that is, box shows median and interquartile range (IQR). Whiskers indicate 1.5 IQR. P values (-log10(p)) were computed between prediction accuracies of each pair of resolutions. Non-black colors denote significantly different prediction performances after correcting for multiple comparisons with FDR $q < 0.05$. Bright colors indicate small p values, dark colors indicate large p values. For each pair of comparisons, warm colors represent higher prediction accuracies of the "row" resolution than the "column" resolution.

(A) Schaefer2018

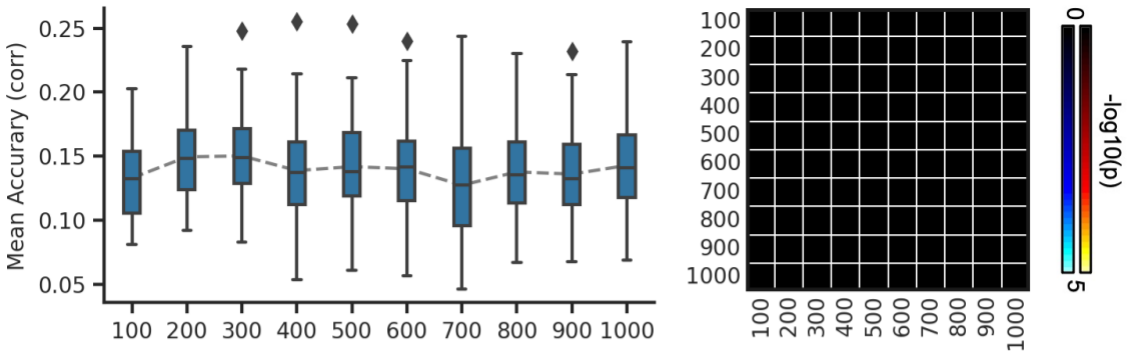

(B) Kong2021

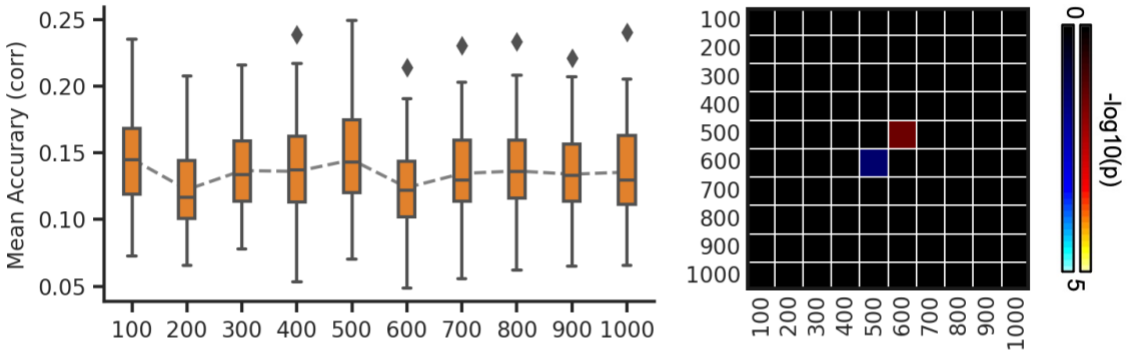

(C) sICA

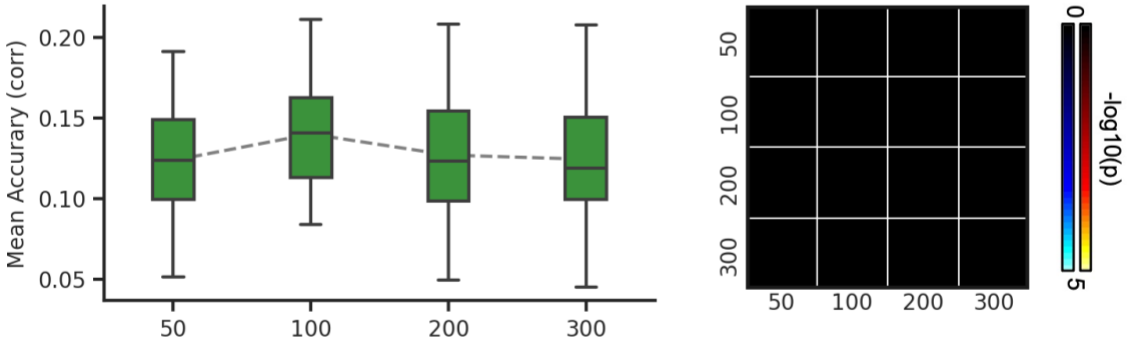

(D) PrincipalGrad

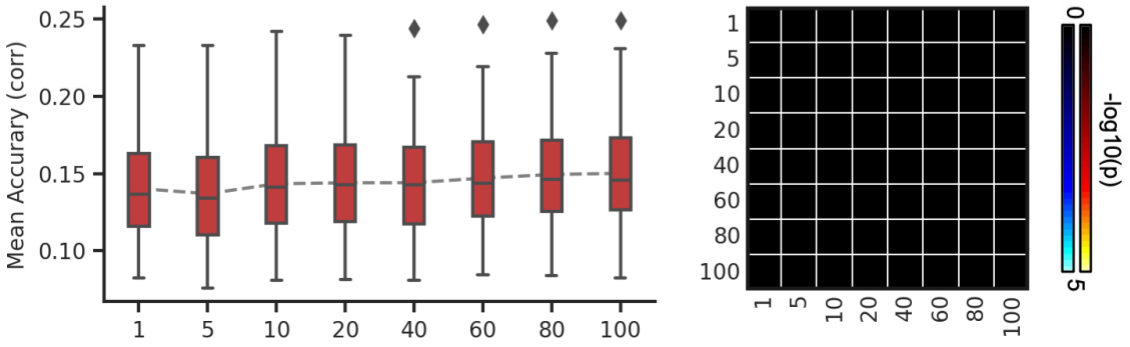

Figure S28. Prediction accuracies (Pearson's correlation) of emotion vary across resolutions for gradient and parcellation approaches using LRR in the ABCD dataset. (A) Prediction accuracies and p values of the hard-parcellation Schaefer2018 with 100 to 1000 ROIs. (B) Prediction accuracies and p values of the hard-parcellation Kong2021 with 100 to 1000 ROIs. (C) Prediction accuracies and p values of the soft-parcellation sICA with 50 to 300 components. (D) Prediction accuracies and p values of the principal gradient PrincipalGrad with 1 to 100 gradients. Boxplots utilized default Python seaborn parameters, that is, box shows median and interquartile range (IQR). Whiskers indicate 1.5 IQR. P values (-log10(p)) were computed between prediction accuracies of each pair of resolutions. Non-black colors denote significantly different prediction performances after correcting for multiple comparisons with FDR $q < 0.05$. Bright colors indicate small p values, dark colors indicate large p values. For each pair of comparisons, warm colors represent higher prediction accuracies of the "row" resolution than the "column" resolution.

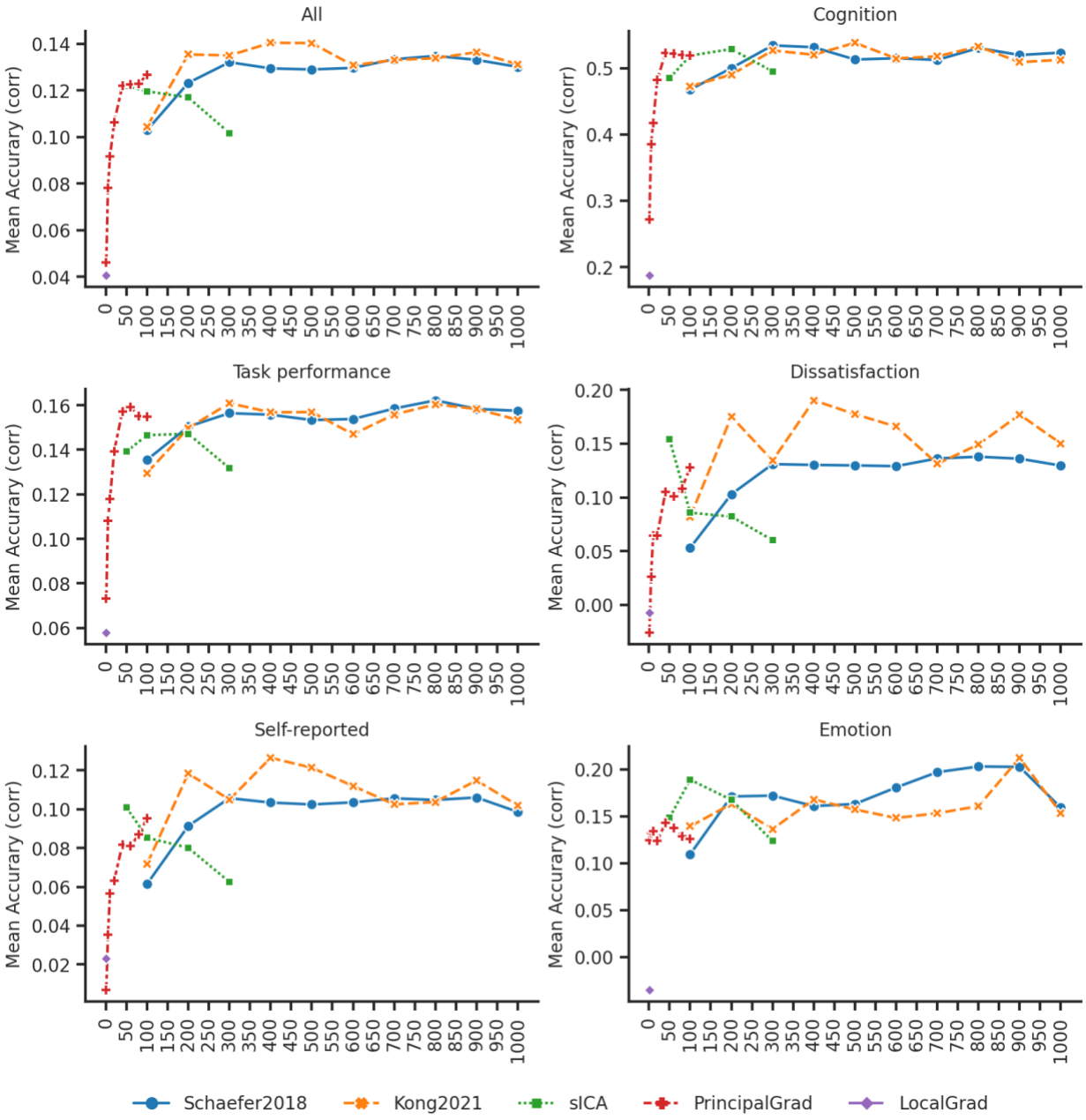

Figure S29. Prediction accuracies (Pearson's correlation) vary across resolutions for gradient and parcellation approaches using KRR in the HCP dataset.

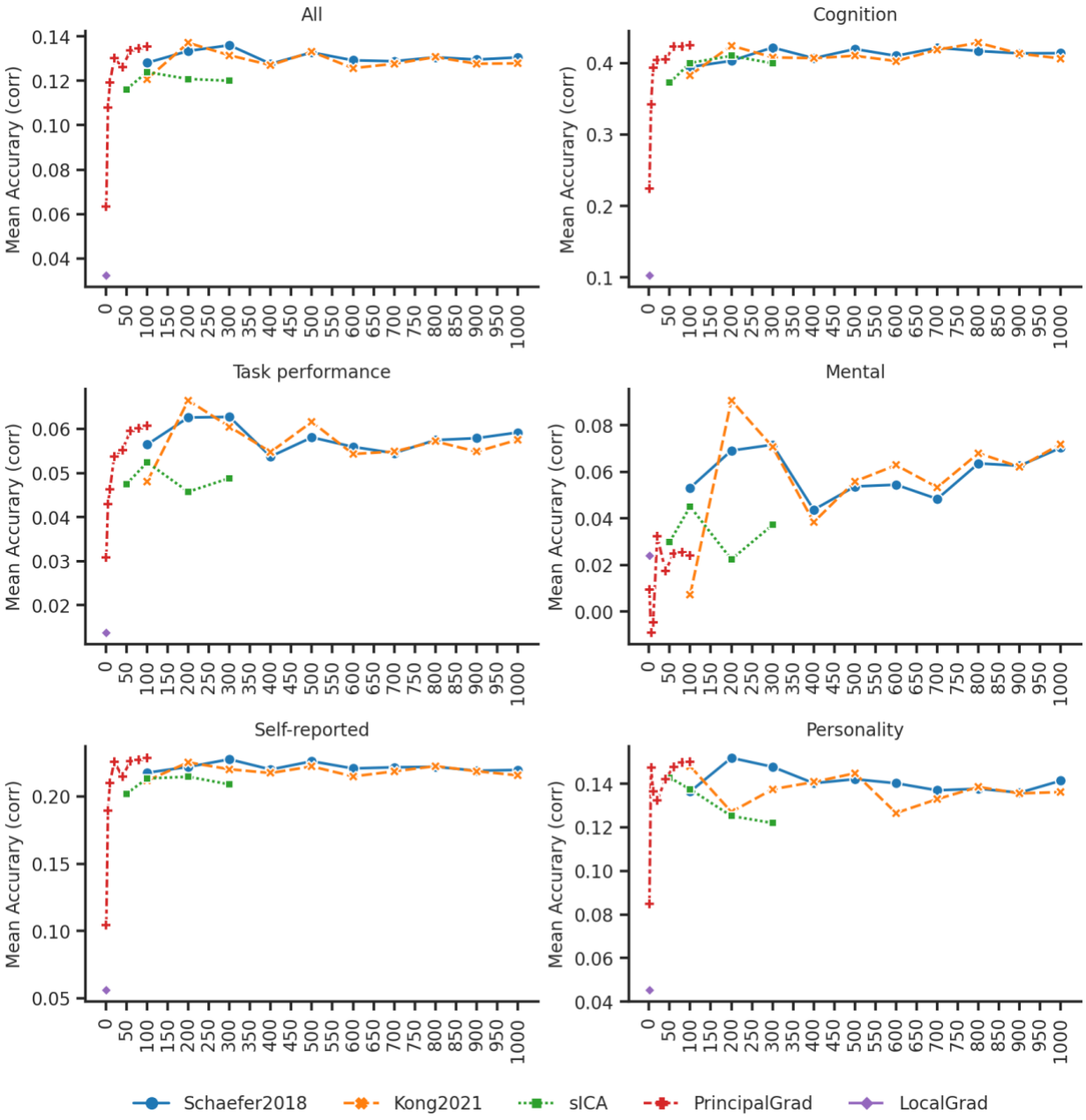

Figure S30. Prediction accuracies (Pearson's correlation) vary across resolutions for gradient and parcellation approaches using KRR in the ABCD dataset.

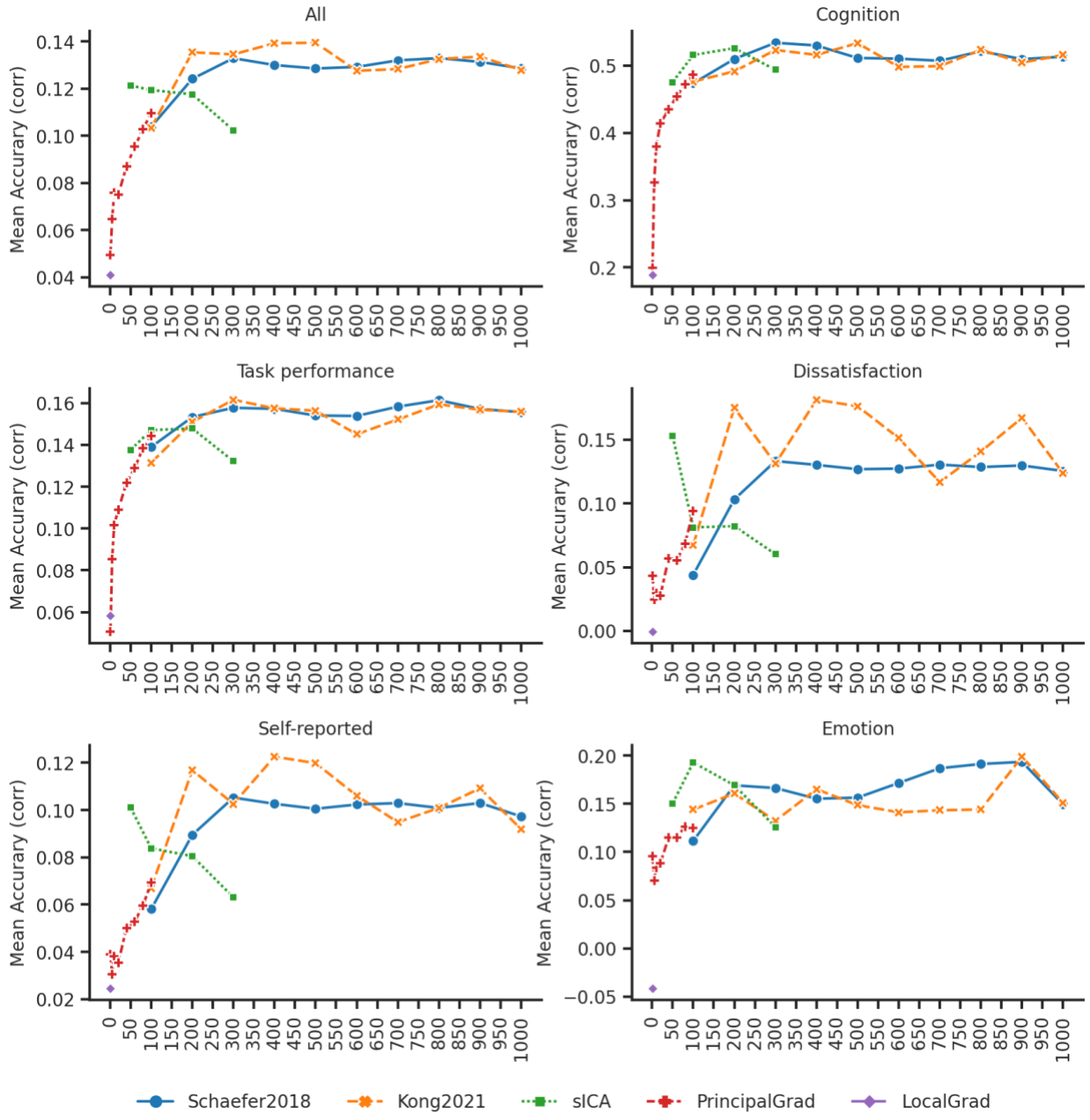

Figure S31. Prediction accuracies (Pearson's correlation) vary across resolutions for gradient and parcellation approaches using LRR in the HCP dataset.

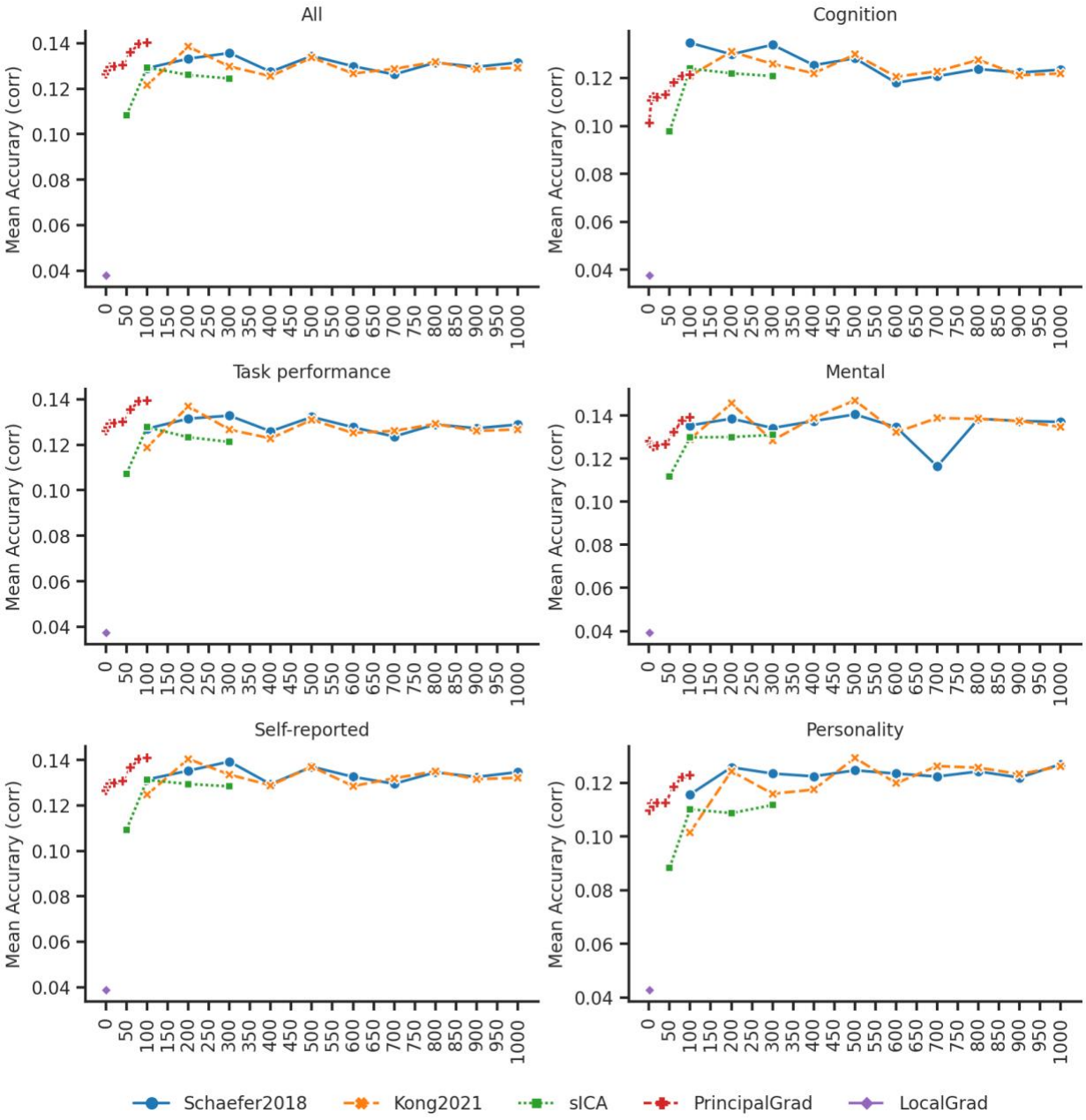

Figure S32. Prediction accuracies (Pearson's correlation) vary across resolutions for gradient and parcellation approaches using LRR in the ABCD dataset.